

ENGINEERING DELIVERY VEHICLES FOR SIRNA THERAPEUTICS

By

Daniel Burton Vocelle

A DISSERTATION

Submitted to
Michigan State University
in partial fulfillment of the requirements
for the degree of

Chemical Engineering - Doctor of Philosophy
Quantitative Biology – Dual Major

2020

ABSTRACT

ENGINEERING DELIVERY VEHICLES FOR siRNA THERAPEUTICS

By

Daniel Burton Vocelle

Small molecule and protein-based drugs, while critically important therapies, cannot treat all diseases. As such, alternative treatment modalities must be developed to complement existing strategies. One potential alternative is small interfering RNA (siRNA) therapeutics, which are capable of specific inhibition of a wide range of intracellular, membrane, and extracellular proteins. siRNAs are hydrophilic due to their anionic backbone and do not readily diffuse across cellular membranes. During systemic delivery, naked siRNAs are rapidly filtered by the kidneys or degraded by serum nucleases and can often initiate an immune response. Thus, for siRNAs to be useful as therapeutics, they must be complexed with delivery vehicles for protection during extracellular transport and cellular internalization.

Once delivered to the cytoplasm, siRNAs act through RNA interference (RNAi) to degrade messenger RNAs (mRNAs) in a sequence-specific manner, thereby reducing target protein expression. Despite the recent clinical success, development of siRNA therapeutics is limited due to the inefficiency, toxicity, and immunogenicity of current delivery vehicles. To overcome these hurdles, this research aimed to understand the role of delivery vehicle characteristics in influencing the cellular uptake and processing of siRNA-containing complexes.

While many types of delivery vehicles have been developed for siRNAs, the characteristics that are essential for success are still not well understood. To address this issue, we synthesized a variety of silica nanoparticles (sNPs), and assessed their ability to effectively deliver siRNAs to human lung carcinoma cells (H1299). By varying the concentration of amines and dextran during sNP synthesis, we defined chemical/physical characteristics important for active siRNA delivery.

Another roadblock in the development of siRNA therapeutics is a limited understanding of the intracellular processing of siRNA-containing complexes leading to initiation of RNAi. With recent evidence showing that the intracellular fate of endocytosed material was influenced by the endocytic pathway used for internalization, we developed a novel assay capable of differentiating uptake among the different endocytic pathways and assessing their functionality in initiating RNAi. Our results showed that Lipofectamine 2000 (LF2K) was internalized by Graf1-, Arf6-, or flotillin-mediated endocytosis for the initiation of RNAi, depending on cell type. Additionally, our study identified functional differences among endocytic pathways in a cell, indicating that uptake alone was not sufficient to initiate silencing. In a mixed cell population, we found that targeted inhibition of the non-functional pathways in some cells enhanced silencing in the uninhibited cells. These findings suggest that designing delivery vehicles for specific endocytic pathways may enhance the activity of the delivered siRNAs by directing them preferentially to the intended target cells.

Finally, due to the limitations of current techniques, the intracellular pathways used in processing siRNA-containing complexes are not well defined. As a result, it is unclear how delivery vehicle characteristics affect the intracellular trafficking of siRNAs. To address this issue, we developed a novel microscopy-based assay that uses automated multi-well live-cell imaging to track the intracellular location of siRNAs over time. Through this assay we determined the intracellular pathways utilized in sNP-mediated siRNA delivery and identified how dextran functionalization of sNPs altered the intracellular trafficking of siRNAs. This assay provides a new analytical technique to assess intracellular pathways and could aid in the development of more efficient siRNA delivery vehicles.

TABLE OF CONTENTS

LIST OF TABLES	vi
LIST OF FIGURES	vii
KEY TO ABBREVIATIONS	ix
CHAPTER 1: INTRODUCTION	1
1.1 Significance	1
1.2 Background	1
1.3 Delivery Vehicle Design	2
1.4 Endocytosis	5
1.5 Intracellular Trafficking	9
1.6 Clinical Challenges and Successes	10
1.7 Approach and Specific Aims	13
CHAPTER 2: SILICA NANOPARTICLE CHARACTERISTICS ASSOCIATED WITH ACTIVE SIRNA DELIVERY	15
2.1 Abstract	15
2.2 Introduction	15
2.3 Results	17
2.3.1 Effect of Amine and Dextran Content on siRNA Silencing Efficiency	17
2.3.2 Inhibition of siRNA Endocytosis and Silencing	20
2.3.3 Intracellular Trafficking of sNPs	23
2.3.4 Acidic Degradation of sNPs	24
2.3.5 siRNA Binding under Acidic Conditions	25
2.4 Discussion	26
CHAPTER 3: ENDOCYTOSIS CONTROLS SIRNA EFFICIENCY: IMPLICATIONS FOR SIRNA THERAPEUTIC DESIGN AND CELL SPECIFIC TARGETING	31
3.1 Abstract	31
3.2 Introduction	31
3.3 Results	33
3.3.1 Silencing Efficiency in Different Cell Lines	33
3.3.2 Inhibition of siRNA Accumulation and Silencing	34
3.3.3 Overexpression of Endocytic Proteins	38
3.3.4 Targeted Inhibition in a Co-cultured Population	40
3.4 Discussion	43
CHAPTER 4: KINETIC ANALYSIS OF THE INTRACELLULAR PROCESSING OF siRNAs BY CONFOCAL MICROSCOPY	49
4.1 Abstract	49
4.2 Introduction	49
4.3 Discussion	56
CHAPTER 5: CONCLUSIONS AND FUTURE WORK	58

5.1 Conclusions	58
5.2 Future Work	59
5.2.1 Silica Nanoparticle Optimization	59
5.2.2 Predicting Optimal Endocytic Pathways	60
5.2.3 Additional Intracellular Pathways	60
APPENDICES	62
APPENDIX A: Materials and Methods for Chapter 2	63
APPENDIX B: Materials and Methods for Chapter 3	77
APPENDIX C: Materials and Methods for Chapter 4	91
BIBLIOGRAPHY	94

LIST OF TABLES

Table 1-1 siRNA therapeutics in clinical trial	12
Table 2-1 Target and mechanism of action for endocytosis inhibitors [53,195].	22
Table 3-1 Chemical inhibitors of endocytic proteins	35
Table 3-2 Chemical inhibitor vs endocytic pathway matrix	35
Table A-1 Statistical analysis for Figures 2-2 and 2-3	75
Table A-2 Statistical analysis for Figure A-6	76
Table A-3 Statistical analysis for Figure 2-7	76
Table A-4 Inhibitor toxicity	83
Table A-5 Statistical analysis for Figures 3-2, 3-3, and 3-4	90
Table A-6 Gene expression	90

LIST OF FIGURES

Figure 1-1 RNAi pathway	2
Figure 1-2 Endocytic pathways	6
Figure 2-1 Effect of dextran and amine content on silencing	19
Figure 2-2 Role of sNP zeta potential (mV) on silencing	20
Figure 2-3 Influence of endocytotic inhibitors on the uptake of siRNAs	22
Figure 2-4 EGFP silencing in the presence of endocytotic inhibitors	23
Figure 2-5 TEM analysis of sNP-siRNA complex endocytosis and trafficking	24
Figure 2-6 sNP degradation under acidic conditions	25
Figure 2-7 Nucleic acid release under acidic conditions	26
Figure 3-1 EGFP silencing and siRNA accumulation	34
Figure 3-2 Influence of endocytic inhibitors on EGFP silencing and siRNA accumulation	36
Figure 3-3 Influence of endocytic protein overexpression on the intracellular accumulation of siRNAs	39
Figure 3-4 Influence of endocytic inhibitors on EGFP silencing and siRNA accumulation in co-cultured and mono-cultured populations	42
Figure 4-1 Intracellular trafficking flowchart	51
Figure 4-2 Intracellular trafficking pathways in eukaryotic cells	53
Figure 4-3 Kinetic colocalization profiles of siRNA with Rab4, Rab5, and Rab7	54
Figure 4-4 Kinetic colocalization profiles of siRNA with Rab11, Lysosome, and ER	55
Figure 4-5 Kinetic colocalization heat maps	56
Figure A-1 Plasmid transfection efficiency of sNPs	70
Figure A-2 Confocal microscopy of non-inhibited silencing – 24 h post-transfection	71
Figure A-3 Confocal microscopy of inhibited silencing - 4 h post-transfection	72

Figure A-4 Confocal microscopy of inhibited silencing – 24 h post-transfection	73
Figure A-5 EGFP silencing in the presence of endocytotic inhibitors (HeLa)	74
Figure A-6 Inhibitor dose response	84
Figure A-7 Inhibitor microscopy experiments	87
Figure A-8 Flow cytometry fluorescence distribution	88
Figure A-9 Flow cytometry fluorescence distribution	88
Figure A-10 Overexpression microscopy experiment	89

KEY TO ABBREVIATIONS

AAV	adeno-associated virus
ADE	Arf6-dependent endocytosis
Ago2	argonaute 2
AP2	AP2 adapter complex
APTES	3-(triethoxysilyl)-propyl amine
AS	antisense strand
ASGPR	asialoglycoprotein receptors
CCIE	clathrin/caveolin-independent endocytosis
CDC42	cell division cycle 42
CME	clathrin-mediated endocytosis
CNS	central nerve system
CNT	carbon nanotubes
CvME	caveolin-mediated endocytosis
DNM1	dynamin-1
DNM2	dynamin-2
EDS	energy-dispersive X-ray spectroscopy
EE	early endosome
EGF	epidermal growth factor
EGFP	enhanced green fluorescent protein
ER	endoplasmic reticulum
FACS	fluorescence-activated cell sorting

FME	flotillin-mediated endocytosis
FWHM	full width at half max
GEEC	GPI- enriched endocytic compartments
GFP	green fluorescent protein
GME	Graf1-mediated endocytosis
H1299	human lung carcinoma
HEK293	human embryonic kidney
HepG2	hepatocellular carcinoma
Hsc70	heat shock cognate 71 kDa protein
HSPG	heparan sulfate proteoglycan
HSV	herpes simplex virus
LAMP1	lysosomal associated membrane protein 1
LDL	low density lipoprotein
LE	late endosome
LF2K	Lipofectamine 2000
MHCI	major histocompatibility complex class I proteins
miRNA	microRNA
MP	macropinocytosis
mRNA	messenger RNA
MWCNT	multi-walled carbon nanotube
M β CD	methyl- β -cyclodextrin
NSCLC	non-small cell lung cancers
PAK1	P21 Activated Kinase 1

PFS	perfect focus system
PI3K	phosphatidylinositol-3-kinase
PIP3K	phosphoinositide 3-kinase
PM	plasma membrane
RAC1	Rac family small GTPase 1
RE	recycling endosome
RISC	RNA induced silencing complex
RLC	RISC loading complex
RNAi	RNA interference
shRNA	short hairpin RNA
siRNA	small interfering RNA
sNP	silica nanoparticle
SS	sense strand
SWCNT	single walled carbon nanotube
TEM	transmission electron microscopy
TRBP	TAR RNA binding protein

CHAPTER 1: INTRODUCTION

Note: This chapter has been modified from previously published work [1]

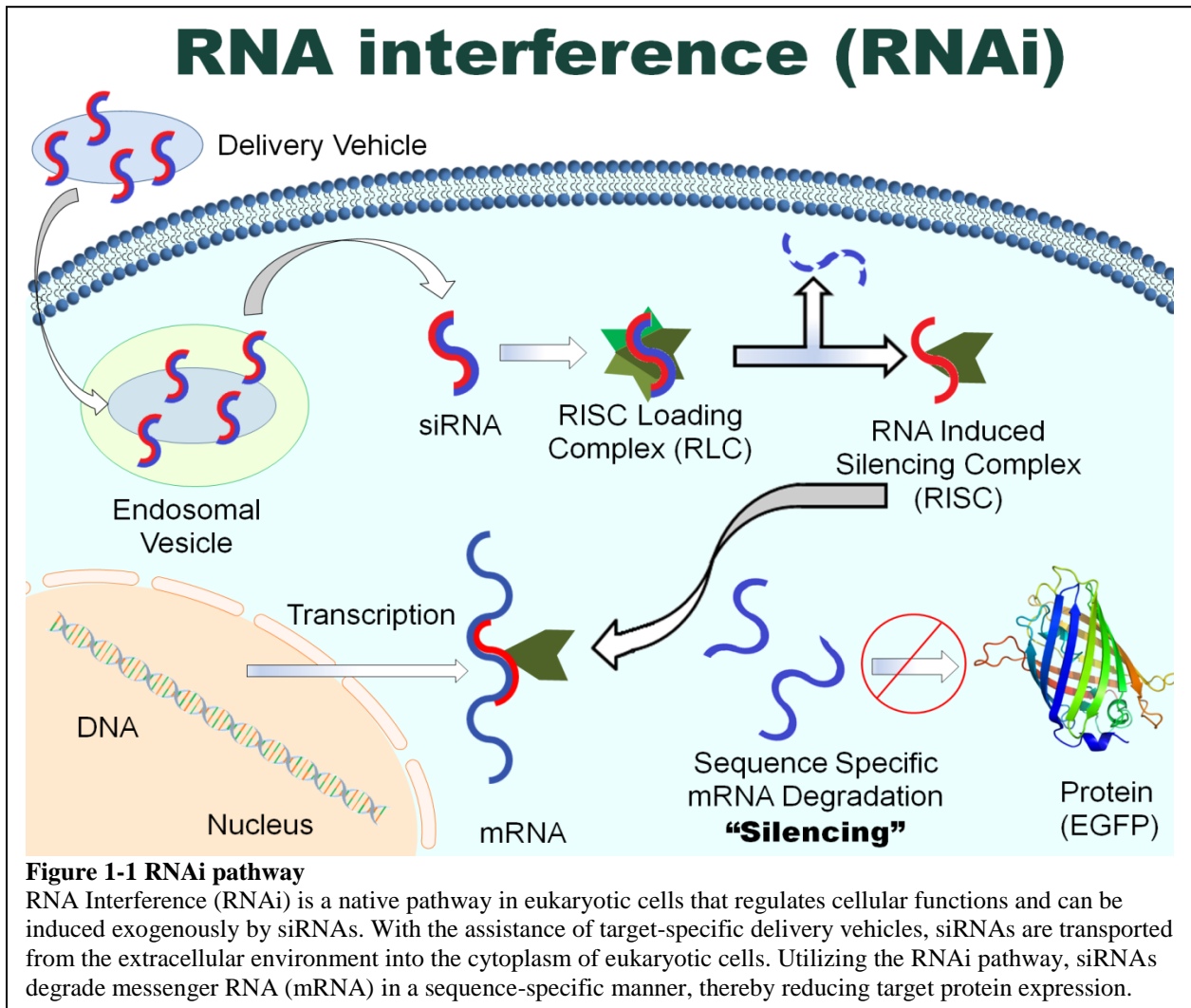
1.1 Significance

Small molecule and protein-based drugs, while critically important therapies, have limited therapeutic potential [2]. In some cases, the drugs cannot access or interact with proteins that are causing the disease phenotype. As such, alternative treatment modalities must be developed to complement existing strategies. One potential alternative is siRNA therapeutics, that are capable of targeted inhibition for a wide range of intracellular, membrane, and extracellular proteins [3]. siRNA therapeutics are being developed as treatments for a variety of targets, including cancers and infectious diseases, with one therapeutic recently approved for clinical use [4–6]. Despite the recent clinical success, the continued development of siRNA therapeutics is limited by poor delivery efficiency that stems from an incomplete understanding of the intracellular pathways associated with RNAi [7–9].

1.2 Background

RNAi is a native pathway in eukaryotic cells that regulates cellular functions through miRNAs and can be induced exogenously by siRNAs (Figure 1-1) [10]. Once delivered to the cytoplasm, siRNAs are identified by the RISC loading complex (RLC), a ribonucleoprotein complex minimally composed of Argonaute 2 (Ago2), Dicer, and TAR RNA binding protein (TRBP) [11–14]. The RLC preferentially selects one of the siRNA strands as the guide strand (antisense strand) loading it into Ago2, forming the active RNA induced silencing complex (RISC) [11,12,14,15]. The other strand, the passenger strand (sense strand), is subsequently removed from the pathway and degraded [12]. Active RISC cleaves target mRNA at the center

region complementary to the guide strand, causing the mRNA to be degraded and halting production of the protein it encodes [12,16,17].



1.3 Delivery Vehicle Design

Previously, siRNA therapeutics were limited by the ability to design and predict active siRNA sequences but are currently hindered by poor delivery [18,19]. siRNAs are hydrophilic due to their anionic backbone, and do not readily diffuse across cellular membranes [3]. During systemic delivery, naked siRNAs are rapidly filtered by the kidneys, degraded by serum nucleases, and stimulate an immune response [20,21]. Thus, siRNAs require delivery vehicles for protection/concealment during transport until delivered to the cytoplasm of a target cell.

siRNA delivery vehicles are classified as being either viral or non-viral. Viral approaches loaded genetic material into inactive viral envelopes, capitalizing upon a highly efficient natural mechanism. However, these viral approaches were generally limited to a single treatment due to an adaptive immune response [22]. Viral vectors are now primarily used in the treatment of chronic disorders, where a short hairpin RNA (shRNA) is incorporated into the genome of a target cell resulting in the constitutive expression of siRNAs [23]. Non-viral vehicles were initially inefficient at delivering active siRNAs, but were considered non-immunogenic. In the last decade, considerable strides have been made at improving non-viral delivery efficiencies making them the preferred choice for development of siRNA therapeutics [24]. There are many sub-types of non-viral delivery vehicles used by researchers, each categorized according to their composition.

Lipid-based delivery vehicles are commonly referred to as lipoplexes and in general, have achieved the greatest clinical and commercial success among types of siRNA delivery vehicles [24,25]. Lipoplexes are principally comprised of cationic lipids roughly 100 nm in diameter, and during self-assembly form spherical lipid bilayers that encapsulate siRNAs [26]. While effective at delivering siRNAs, lipoplexes are generally toxic at concentrations required for therapeutic effect [27]. Lipoplexes have been shown to use multiple endocytic pathways depending on cell type and lipid composition [28,29]. *In vivo*, lipoplexes are primarily used to target diseases in the liver due to the high concentration of lipoprotein receptors [30].

Polyplexes are comprised of biocompatible cationic polymers derived from both natural and synthetic sources [31,32]. Depending on the polymer formulation, polyplexes can range from 10-400 nm in size [33]. Additionally, chemical modification to the polymer backbone can produce spherical, rod, or globular particles [33]. Given their geometric variability, polyplexes can be

used to either encapsulate siRNAs in a micelle-like structure, or bind them electrostatically to a cationic surface [34]. The mechanism of endocytosis used by polyplexes varies given the diversity in their physical/chemical characteristics [35–37]. Polyplexes have been used to target the widest variety of diseases, most commonly targeting the liver, kidney, and lungs. Polyplexes are considered non-toxic and bio-degradable, but have poor delivery efficiency due to aggregation and inefficient siRNA release in the cytoplasm [38,39].

Carbon nanotubes (CNTs) are hollow graphene based nano-cylinders containing a single wall (SWCNTs) or multiple walls (MWCNTs) [40]. Their length varies between 50 and 100 nm with a diameter of 0.4-2 nm for SWCNTs and 2-100 nm for MWCNTs [8,41]. Using surface functionalized cations; CNTs use electrostatics to bind siRNAs to their surface [42]. Instead of being endocytosed, CNTs pass through the cell membrane through a spontaneous and non-destructive mechanism [41]. While this process makes CNTs ideal for treating delivery resistant cells and bypassing biological barriers, it poses significant challenges for systemic delivery. *In vivo*, CNTs are rapidly filtered by the kidney due to their small diameter, sequestered by phagocytic cells due to their rod shape, or indiscriminately deliver siRNAs [43]. While short-term data suggests CNTs are safe, many researchers have expressed concerns over their accumulation and long-term toxicity [44].

Ceramic nanoparticles are porous inorganic spheres roughly, 50 nm in diameter, commonly composed of silica, titania, or alumina due to their biological inertness [45]. Additionally, silver oxides have been used for their anti-bacterial properties, as CeO₂ and Y₂O₃ have for their antioxidant properties. Generally, ceramic nanoparticles use amine functionalized surfaces to bind siRNAs through electrostatics [46]. No specific endocytic pathway has been identified for ceramic nanoparticles or their various compositions [47]. While ceramic nanoparticles have been

used to target filtering organs *in vivo*, they are considered inefficient at delivery and toxic due to long-term accumulation [48,49].

Metallic nanoparticles are highly modifiable solid core particles most commonly synthesized using colloidal gold [50]. Typically 1-150 nm in size, metallic nanoparticles can form rods and spheres that electrostatically bind siRNAs to their surface via functionalized amines [50].

Metallic nanoparticles have been reported to use multiple endocytic pathways to successfully deliver siRNAs. *In vivo*, metallic nanoparticles have been used to target filtering organs with limited success due to rapid opsonization and toxic accumulation in the liver and spleen [51,52].

1.4 Endocytosis

To reach the cytoplasm, vehicle-siRNA complexes must first be endocytosed. Until recently, cellular endocytic pathways were classified as macropinocytosis (MP), clathrin-mediated endocytosis (CME), caveolin-mediated endocytosis (CvME), or clathrin/caveolin-independent endocytosis (CCIE) [53]. Researchers have since characterized three distinct types of CCIE, flotillin-mediated endocytosis (FME), Arf6-dependent endocytosis (ADE), and Graf1-mediated endocytosis (GME) (Figure 1-2) [54–56]. Currently, there is no consensus regarding the optimal endocytic pathway for active siRNA delivery, as multiple endocytic pathways have been found to result in successful delivery of siRNAs and initiation of silencing [57]. Further, it is difficult to correlate the characteristics of a delivery vehicle with a specific pathway as most studies are limited to a single cell type or cannot distinguish among the current endocytic pathways.

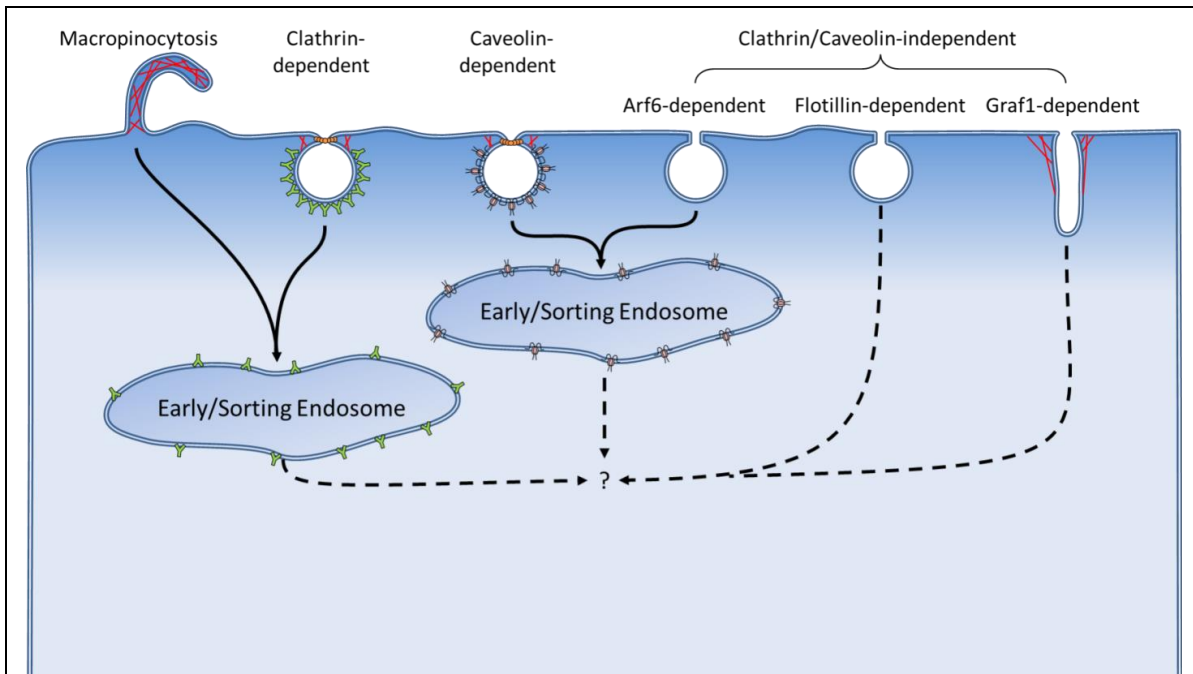


Figure 1-2 Endocytic pathways

Different endocytic pathways used by mammalian cells for the internalization of cargo. At present the following pathways have been identified: macropinocytosis (actin, Cdc42, and Rac1 dependent), clathrin-mediated (clathrin, actin, AP2, Arf6, and dynamin dependent), caveolin-mediated (caveolin, actin, Src, dynamin, and lipid-raft dependent), Arf6-dependent (Arf6, actin, PIP3K, and lipid-raft dependent), flotillin-mediated (flotillin, dynamin, and lipid-raft dependent), and Graf1-mediated (Graf1, dynamin, Cdc42, actin, and lipid-raft dependent).

MP is traditionally associated with the bulk uptake of extracellular fluid and nutrients. Unlike the other endocytic pathways, macropinocytosis is characterized by membrane ruffles at the cell surface that envelop extracellular fluid [58]. This process is driven by actin polymerization, and regulated at the plasma membrane by phosphatidylinositol-3-kinase (PI3K) and the GTPases rac family small GTPase 1 (Rac1), cell division cycle 42 (Cdc42), and p21 activated kinase 1 (PAK1) [59]. Additionally, while other endocytic pathways are initiated by ligand binding with surface receptors, macropinocytosis is transiently induced by growth factors such as epidermal growth factor (EGF) [60]. Macropinocytosis leads to the intracellular formation of macropinosomes, that range from 150-5000 nm in diameter, and undergo acidification during vesicular transport to the lysosome [59]. The use of macropinocytosis by delivery vehicles is

primarily associated with the non-specific uptake of macroparticles and nanoparticle aggregates [61].

CME is the pathway most often associated with receptor mediated endocytosis, and is considered to be a “universal” endocytic pathway among eukaryotic cells [62]. CME is characterized by the formation of a clathrin coated pit at the plasma membrane that internalizes receptor bound cargo. This process is dependent on both dynamin and actin, but regulated by the AP2 adapter complex (AP2) that recruits clathrin to the plasma membrane and catalyzes formation of the clathrin triskelion lattice. In the cell, heat shock cognate 71 kDa protein (Hsc70) mediates disassembly of the clathrin coat, allowing the endocytic vesicle to fuse with the early endosome [63]. Endocytic vesicles formed during CME are typically 100 – 150 nm in diameter, although they have been shown to encapsulate larger cargo. It has been reported that CME is used by cells to internalize a variety of drug delivery complexes (polyplexes, lipoplexes, metallic, etc) with varying degrees of success [35,64]. Using endocytic targeting motifs to target specific receptors associated with CME, such as the transferrin and low density lipoprotein (LDL) receptor, researchers have enhanced both target specificity and delivery efficiency [65,66].

All other forms of endocytosis are differentiated from MP and CME by their dependence on lipid-rafts, hydrophobic subdomains of the plasma membrane rich in cholesterol and glycosphingolipids [67]. The first of these is CvME, which upon activation of a surface receptor, forms caveolar-coated pits through the recruitment of caveolin proteins to lipid rafts. Src-dependent phosphorylation of the caveolins initiates coat disassembly and dynamin/actin-dependent vesiculation [68]. The resulting vesicles, roughly 50-60 nm in diameter, are trafficked to the early endosome through a process that inhibits vesicle acidification [69]. Similar to CME,

multiple delivery platforms have reported using CvME, with varying degrees of success [35,61]. It is unclear what receptors and cargo utilize CvME, as those previously assigned to other pathways (e.g., albumin and cholera toxin B), are now known to use other lipid-raft dependent pathways [70,71].

ADE is a relatively recently-identified type of endocytosis regulated by the GTP cycle of Arf6 [55]. Internalization through ADE leads to the formation of Arf6-containing endosomes that are either recycled to the plasma membrane or trafficked to early endosomes, a process dependent upon the hydrolysis of Arf6-GTP, actin polymerization, and activation of Phosphoinositide 3-kinase (PIP3K). Vesicles that result from ADE have been shown to form intermediate endosomal compartments, that are capable of sorting cargo before reaching the early endosome [55]. It also has been shown that compared to CME, vesicles from ADE take roughly 6 times longer to reach the early endosome [55]. ADE has currently been implicated in the internalization of IL-2 receptor α subunit Tac [72], major histocompatibility complex class I proteins (MHCI) [73], β -integrin [74], and the herpes simplex virus (HSV) [75]. As Arf6 has been shown to regulate AP2, it is likely that some uptake by ADE has been mistaken for CME, which is also dependent on AP2.

GME is commonly characterized by tubulovesicular invaginations rich in Graf1 and an intracellular association with GPI- Enriched Endocytic Compartments (GEECs). In GME, Graf1 and dynamin form a stable complex that regulates the scission and stability of the tubulovesicular structures, through a process also dependent on actin and Cdc42. Interestingly, Graf1 has a higher affinity for dynamin-1 (DNM1), thought to be exclusive to neurons, than dynamin-2 (DNM2), which has ubiquitous expression [56,76]. Similar to ADE, GME forms unique endosomal compartments capable of sorting cargo before reaching the early endosomes. Since its

discovery, GME has been implicated in the uptake of GPI-linked proteins [56], adeno-associated virus (AAV) [77], dextran [78], and extracellular fluid [56]. It is likely that uptake by GME has been mistaken for macropinocytosis, as they both facilitate uptake of dextran and are dependent upon Cdc42.

FME was first characterized as the endocytic pathway associated with CD59 [54] and cholera toxin B [54]. It has since been implicated in the uptake of lipids [79], silica nanoparticles [80], and cationic polyplexes [79]. In FME, flotillin-1 and flotillin-2 co-assemble into plasma membrane microdomains in lipid-rafts and are internalized after phosphorylation by FYN [81]. Interestingly, the role of dynamin in this process is, as of yet, undefined and possibly dependent on cell type or cargo [82]. Upon internalization, flotillin endosomal vesicles are trafficked directly to the Golgi, bypassing the early endosome.

At present, multiple endocytic pathways have been found to result in successful delivery of siRNAs and initiation of silencing. As a result, researchers have focused on the intracellular hurdles of siRNA delivery instead of exploring alternate endocytic pathways. However, due to the discovery and characterization of the CCIE pathways, it has become evident that the pathway of endocytosis greatly impacts the subsequent trafficking of cargo [66,83]. This suggests that the role of endocytosis in siRNA delivery is worth reinvestigating, and may provide an alternative means to enhancing the effectiveness of siRNAs.

1.5 Intracellular Trafficking

For siRNA to be incorporated into the RNAi pathway they must reach the cytoplasm of a target cell, however the optimal intracellular pathway for achieving this goal is unclear [84]. Studies have shown that only a small portion of internalized siRNAs reach the cytoplasm, whereas the majority are exocytosed through endosomal recycling or retained within endolysosomal vesicles [85]. While the exact mechanism for cytoplasmic delivery is unknown,

the prevailing theories suggest membrane fusion or the proton sponge effect [86,87]. In membrane fusion, amphipathic functional groups on the surface of a delivery vehicle interact with the cholesterol rich regions of the endosomal membrane; destabilizing the integrity of the endosomal membrane and allowing the delivery vehicle to “leak” into the cytoplasm [88]. According to the proton sponge effect, once particles are internalized via endocytosis, the endosome begins to acidify. However, because nucleic acid delivery vehicles are often polycationic to allow for self-assembly with the polyanionic nucleic acids, they possess a basic pKa and significant buffering capacity [24]. As such, the cell continues to acidify the vesicle, resulting in an accumulation of Cl⁻. The excess of Cl⁻ causes osmotic swelling to the point that the endosome eventually bursts, releasing its contents into the cytoplasm [89].

1.6 Clinical Challenges and Successes

siRNA therapeutics in clinical trials have predominately used variations of lipoplexes and polyplexes, although with the recent success of Onpattro™, GalNAc-conjugated siRNAs now represent ~50% of RNAi drugs in clinical trials (Table 1-1). In lieu of a delivery vehicle, siRNA conjugates use a chemically modified siRNA backbone to enhance their overall potency and attenuate activation of the immune system. By conjugating these siRNAs to a receptor targeting ligand, they achieve cell specific targeting. So far the success of siRNA conjugates has been limited to GalNAc, a sugar derivative of galactose, that targets the asialoglycoprotein receptors (ASGPRs) found in the liver [6]. While a promising delivery method for siRNA therapeutics, the development of additional ligands that are non-toxic, metabolically stable, and potent has proved challenging [90]. In addition to a greater diversity among the delivery platforms represented in clinical trials, the number of disease targets has also expanded in recent years. Presently there are

promising siRNA therapies that target ocular [91], renal [92], central nerve system (CNS) [93], and solid tumor [84] diseases.

Despite these successes, there is considerable room for further advancement of siRNA therapeutics. *In vivo*, delivery methods favor subcutaneous injection over IV infusions to limit systemic toxicity [94,95]. On a cellular level, siRNA therapeutics are limited by endolysosomal retention and rapid recycling to the plasma membrane [85]. Additionally, studies have shown a passive escape rate of <0.01% for internalized siRNAs [96]. Researchers are actively exploring the use of endosomolytic motifs [97] and retrograde intracellular transport [98] to overcome these hurdles, however progress is limited due to an incomplete understanding of the biological pathways involved in cargo transport.

Table 1-1 siRNA therapeutics in clinical trial

Delivery system	Disease Target	NCT ID
Cardio-metabolic and endocrinological disease		
Conjugated siRNAs	Primary Hyperoxaluria	NCT03681184
Conjugated siRNAs	Amyloidosis	NCT03759379
Conjugated siRNAs	Acute hepatic porphyrias	NCT03338816
Conjugated siRNAs	Hypercholesterolemia	NCT03814187
Conjugated siRNAs	Amyloidosis	NCT02319005
Conjugated siRNAs	Alpha-1 liver disease	NCT03767829
Conjugated siRNAs	Cardiovascular disease	NCT03626662
Conjugated siRNAs	Primary Hyperoxaluria	NCT03392896
Conjugated siRNAs	Hypertriglyceridemia	NCT03747224
Conjugated siRNAs	Hypertriglyceridemia	NCT03783377
Conjugated siRNAs	Alpha-1 antitrypsin deficiency	NCT03362242
Lipoplex	Amyloidosis	NCT01960348
Lipoplex	Hypercholesterolemia	NCT00927459
Lipoplex	Primary Hyperoxaluria	NCT02795325
Polyplex	Alpha-1 antitrypsin deficiency	NCT02900183
Infectious disease		
Conjugated siRNAs	Hepatitis B	NCT03365947
Conjugated siRNAs	Hepatitis B	NCT03772249
Conjugated siRNAs	Hepatitis B	NCT02826018
Lipoplex	Hepatitis B	NCT02631096
Lipoplex	Ebola	NCT02041715
Polyplex	Hepatitis B	NCT02535416
Polyplex	Hepatitis B	NCT02797522
Cancer		
Exosome	Pancreatic cancer	NCT03608631
Gold nanoparticle	Gliosarcoma	NCT03020017
Lipoplex	Hepatocellular carcinoma	NCT02191878
Lipoplex	Carcinoma, pancreatic ductal	NCT01808638
Lipoplex	Hepatocellular carcinoma	NCT02314052
Lipoplex	Solid tumors	NCT00882180
Lipoplex	Advanced cancers	NCT01591356
Polyplex	Pancreatic cancer	NCT01676259
Polyplex	Cancer, solid tumor	NCT00689065
Viral Vector	Chronic myeloid leukemia	NCT00257647
Others		
Conjugated siRNAs	Hemophilia	NCT03549871
Conjugated siRNAs	Hemolytic uremic syndrome	NCT03303313
Conjugated siRNAs	Hypertrophic scar	NCT03133130
Conjugated siRNAs	Hypertrophic cicatrix	NCT03569267
Lipoplex	Idiopathic pulmonary fibrosis	NCT03538301

1.7 Approach and Specific Aims

The work described here aimed to improve the design criteria for siRNA delivery vehicles with the ultimate goal of improving their therapeutic efficacy. This research explored the characteristics of delivery vehicles that optimized active siRNA delivery and developed assays to assess the impacts of these characteristics on endocytosis and intracellular trafficking. This dissertation details three approaches taken towards understanding characteristics and intracellular pathways used by delivery vehicles for active siRNA delivery.

The specific aims of this dissertation were to:

1. Identify vehicle characteristics that promote active siRNA delivery

While many types of delivery vehicles have been developed for siRNA delivery, there is relatively little information to guide the design of a delivery system *de novo*. Here, we used silica nanoparticles (sNPs) that varied by charge and functionalized surface, to assess the role of each characteristic among the following design criteria: siRNA binding, membrane translocation, and silencing. Our results suggest an optimal binding affinity facilitates active siRNA delivery. Additionally, we showed that dextran functionalization enhanced the efficacy of sNPs for delivering siRNAs, by facilitating their uptake through a scavenger receptor-mediated endocytic pathway that is clathrin/caveolin-independent. Going forward, the generality of these findings can be further evaluated in other delivery systems.

2. Determine the preferential endocytic pathway for active siRNA delivery

The discovery of new clathrin/caveolin-independent endocytic pathways has resulted in the reclassification of the endocytic pathways associated with many species. As a result of these findings, it has also become evident that the intracellular trafficking of cargo is highly influenced by the endocytic pathway used during internalization. In this study, our work explores

endocytosis (whether by clathrin, caveolin, Arf6, Graf1, flotillin, or macropinocytosis) across multiple cell types (human cervical cancer (HeLa), human lung carcinoma (H1299) (lung), human embryonic kidney (HEK293), and hepatocellular carcinoma (HepG2)). Our results showed that active siRNA delivery occurs via Graf1 (GME) -, Arf6 (ADE), or flotillin-mediated (FME) endocytosis depending on cell type. Additionally, we determined that a portion of siRNA-containing complexes are internalized by pathways that do not initiate silencing. In a mixed cell population, we found that inhibition of a cell specific endocytic pathway enhanced siRNA delivery in the remaining cell populations. In the field of siRNA therapeutics, these findings suggest that delivery vehicles should be designed to utilize specific endocytic pathways when targeting a particular cell type.

3. Characterize the intracellular pathways associated with siRNA delivery

While understanding the intercellular pathways associated with cargo trafficking is critical to the design of a siRNA delivery vehicle, it is unclear how the specific characteristics of a nanoparticle affect intracellular trafficking. In part, the techniques used to track the intracellular location of cargo limit additional study in the field due to high operating costs and low throughput associated with data acquisition. Herein, we developed a new method that uses automated multi-well imaging of stable cell lines, to detect the intracellular pathways used by target molecules and is capable of measuring kinetic variations in target localization as a result of external stimuli. Using this assay, we characterized how dextran functionalization of sNPs affected the intracellular trafficking of siRNAs. Our results indicate that dextran enhances siRNA retention in the early endosome, reduces fast endosomal recycling, and enhances association with the ER.

CHAPTER 2: SILICA NANOPARTICLE CHARACTERISTICS ASSOCIATED WITH ACTIVE siRNA DELIVERY.

Note: This chapter is adapted from previously published work [1]

2.1 Abstract

Understanding the endocytosis and intracellular trafficking of siRNA-delivery vehicle complexes remains a critical bottleneck in designing siRNA delivery vehicles for highly-active RNAi-based therapeutics. In this study, we show that dextran functionalization of silica nanoparticles enhanced uptake and intracellular delivery of siRNAs in cultured cells. Using pharmacological inhibitors for endocytotic pathways, we determined that our complexes are endocytosed via a previously unreported mechanism for siRNA delivery in which dextran initiates scavenger receptor-mediated endocytosis through a clathrin/caveolin-independent process. Our findings suggest that siRNA delivery efficiency could be enhanced by incorporating dextran into existing delivery platforms to activate scavenger receptor activity across a variety of target cell types.

2.2 Introduction

New therapeutic approaches are continually needed for targeting disease-associated proteins. Short interfering RNA (siRNA) therapeutics are a potential approach capable of highly specific targeting of a wide range of proteins through the activation of RNA interference (RNAi) [2]. With the assistance of delivery vehicles, siRNAs are transported from the extracellular environment into the cytoplasm of eukaryotic cells. After processing by the RNAi pathway proteins [11–14,99], siRNAs guide degradation of target messenger RNAs (mRNAs) in a sequence-specific manner, resulting in a decrease in target protein levels. siRNA therapeutics are being developed for the treatment of cancers, genetic disorders, and infectious diseases [4].

While siRNA technology is well-established in the laboratory environment, continued progress on the *in vivo* use of siRNAs will depend on the development of improved delivery vehicles.

Delivery vehicles are required to prevent degradation of siRNAs by serum nucleases, rapid filtration of siRNAs by the kidneys, or siRNA-initiated immunogenic responses [100–102]. Moreover, if designed correctly, delivery vehicles can maximize delivery of the siRNAs to the target cells/tissues of interest [3]. Currently, lipoplexes (complexes of siRNAs with lipids) and polyplexes (complexes of siRNAs with polymers) are the most prevalent among ongoing clinical trials with some *in vivo* successes [2,4,7,18,37,48,103]. However, most existing delivery vehicles cannot be used clinically due to *in vivo* toxicity, immunogenicity, or inactivity [7–9,49,50]. One means to address these limitations is through functional modifications [104–106]. One modification, dextran, has demonstrated success in enhancing the activity of multiple delivery vehicles [37,39,107–109]. Functionally, dextran has been used to reduce toxicity, prevent opsonization, and block non-specific binding [110–112]. Furthermore, functionalization with dextran polymers has been used for targeted delivery to various tissues [113–115].

While progress has been made on enhancing the systemic and extracellular trafficking of delivery vehicles, transfection efficiencies among delivery vehicles remain low relative to viral vectors, due in part to an incomplete understanding of siRNA-vehicle complex endocytosis and intracellular trafficking [4,116]. It remains unclear if RNAi is associated with a particular mechanism of endocytosis or if the mechanism of cytoplasmic delivery is specific to a certain cell type or delivery vehicle. Lipid and polymer based vehicles have been reported to use clathrin-mediated endocytosis, caveolin-mediated endocytosis, macropinocytosis, and phagocytosis [35,53,117], though endocytosed material typically remains in endosomal compartments rather than entering the cytoplasm [87,116]. siRNAs that cannot escape early

endosomes are exocytosed or degraded [118]. It has been postulated that siRNAs and complexes escape the endosomes via lipid fusion with the membrane, endosomal swelling (proton sponge effect), leaky membranes, or, for vehicles with the appropriate functional groups, photochemical disruption [87]. However, these escape mechanisms are not used in all cases [119,120]. Recent reports suggest that activation of RNAi may not even require endosomal escape [121], as the RNAi machinery has been found to be associated with early endosomes. Developing a better understanding of the intracellular trafficking events associated with RNAi remains a significant hurdle towards improving the efficacy of siRNA delivery vehicles.

The aim of this study was to investigate the impacts of chemical characteristics of delivery vehicles, specifically the inclusion of dextran, in influencing the endocytosis and intracellular trafficking of siRNA-silica nanoparticle (sNP) complexes. sNPs were chosen as a delivery platform for their highly tunable synthesis, consistent physical conformation, low cytotoxicity, and delivery efficacy [48,122,123]. Our results showed that dextran significantly enhanced the utility of sNPs for delivering siRNAs to cultured cells, by initiating their uptake through a scavenger receptor-mediated endocytosis mechanism that is clathrin/caveolin-independent. Subsequent degradation of the sNPs, attributed in part to the acidic conditions of intracellular vesicles, suggested a means for activating release of the siRNAs from the sNPs and initiation of the silencing cascade.

2.3 Results

2.3.1 Effect of Amine and Dextran Content on siRNA Silencing Efficiency

sNPs were synthesized with varying concentrations of the primary amine-containing moiety 3-(triethoxysilyl)-propyl amine (APTES), with and without dextran, to determine if these variables (amine content and the presence of dextran) influenced the delivery or silencing of the siRNA cargo (Figure 2-1). At 24 h post transfection, seven of the nine dextran-containing sNPs

achieved significant silencing compared to the nanoparticle only controls. Six achieved > 50% reduction in enhanced green fluorescent protein (EGFP) levels and were statistically equivalent to LF2K. Increasing amines resulted in increased silencing, with maximal silencing achieved at 40% APTES, with little gain and perhaps some loss of activity at higher amine contents. Only one non-dextran sNP achieved statistically significant reduction in EGFP levels, again at 40% APTES. sNPs were characterized for their potential to bind siRNAs using zeta potential (Figure 2-2). Both the silencing data (~40% APTES) and ζ potential (~27 mV) results suggest that there may be an ideal amine content/charge density for siRNA delivery vehicles, though further characterization would be required to establish this concretely. As our objective was to understand better the uptake and trafficking mechanism for sNPs that yield active silencing, we focused our subsequent analyses on our best performing sNP (40% APTES with dextran).

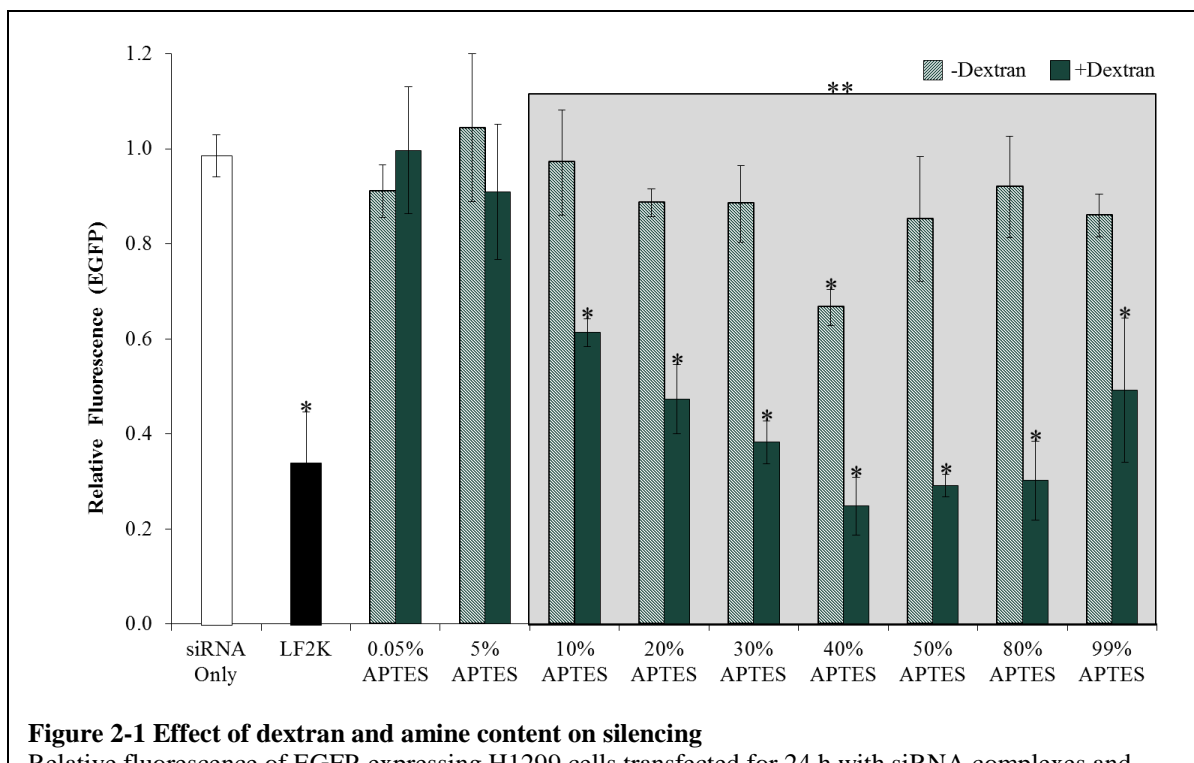
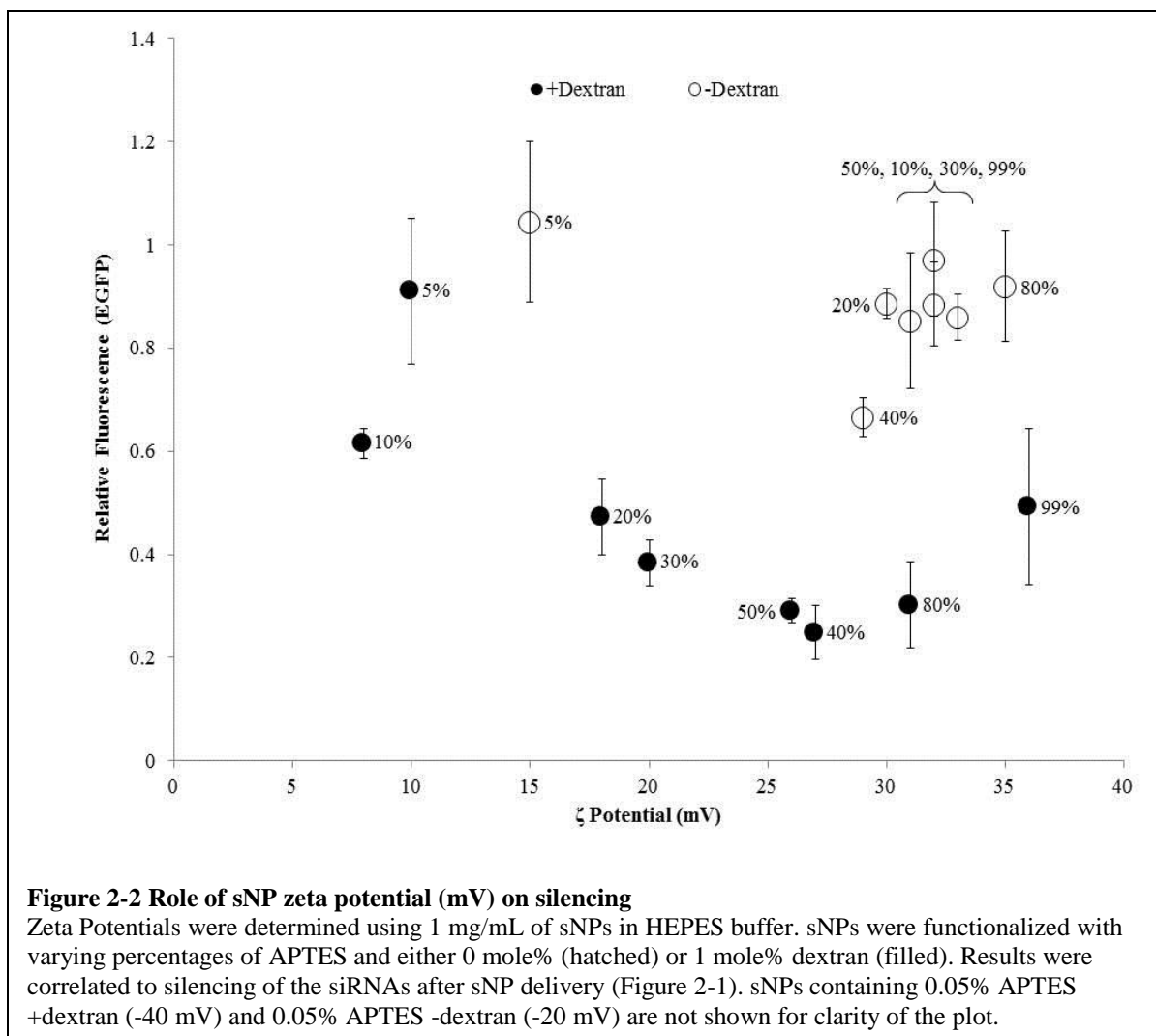


Figure 2-1 Effect of dextran and amine content on silencing

Relative fluorescence of EGFP-expressing H1299 cells transfected for 24 h with siRNA complexes and normalized to the EGFP fluorescence of vehicle-only control cells. The complexes contain either 2.3 $\mu\text{g/ml}$ of LF2K or 200 $\mu\text{g/ml}$ of sNPs functionalized with varying percentages of APTES and either 0 mole% (hatched) or 1 mole% dextran (filled), and 100 nM of siRNAs. Error bars represent + 1 standard deviation; $n = 3$. Statistical analysis was performed using two-way ANOVA, followed by Tukey's HSD post-hoc analysis. *Significant difference ($p < 0.05$) as compared to vector-only treatments. **Significant difference ($p < 0.05$) of non-dextran sNPs to dextran-containing sNPs.



2.3.2 Inhibition of siRNA Endocytosis and Silencing

Having confirmed the ability of our sNPs to deliver siRNAs that then silence the EGFP target, we wanted to evaluate the mechanism of uptake for our sNP-siRNA complexes as compared to LF2K lipoplexes and naked siRNAs. From the literature, we selected a number of chemical inhibitors for individual endocytosis pathways (Table 2-1) and investigated the quantity of siRNAs delivered (Figure 2-3) and the silencing achieved (Figure 2-4) following delivery of siRNAs using our most effective sNP (40% APTES +dextran), LF2K, or no vehicle.

As expected, intracellular levels of siRNA were significantly increased using LF2K (5x increase) and sNPs (40x increase), compared to naked siRNA (Figure 2-2, see insets). Delivery

by LF2K was significantly reduced by the combination of chlorpromazine and filipin, low temperature (4°C), and dextran sulfate. For sNP delivery, the active inhibitors were chlorpromazine, cytochalasin D, low temperatures (4°C), and dextran sulfate. The differential effects of the inhibitors indicate that the sNPs were delivered through a mechanism distinct from that of LF2K. Moreover, plasmid DNA delivered with our sNPs (Figure A-1) did not result in significant overexpression whereas plasmid delivery with LF2K resulted in significant gene overexpression, further suggesting that sNPs and LF2K utilize different delivery pathways. However, the strong impact of dextran sulfate suggests that both sNP and LF2K complexes used scavenger receptor-mediated uptake in delivering siRNAs. Our Fluorescence-activated cell sorting (FACS) analyses were corroborated using confocal microscopy at 4 h and 24 h after transfection (Figures A-2, A-3, and A-4). Likewise, to examine the generality of our results across cell types, replicate experiments were performed in HeLa cells, producing similar results (Figure A-5).

In examining the resulting silencing in the presence of inhibitors (Figure 2-4), low temperature and dextran sulfate significantly reduced silencing following delivery by both LF2K and our sNP. This is a direct reflection of the inhibition observed for siRNA delivery (Figure 2-3). This suggests that both sNP-siRNA complexes and LF2K-siRNA lipoplexes are effectively endocytosed and processed by the scavenger receptor pathway. However, there are discrepancies between the inhibition of delivery and the reduction in silencing activity. Cytochalasin D also significantly inhibited silencing by sNP delivery, indicating that the processing of endocytotic vesicles on actin networks may be essential for silencing, regardless of the pathway of endocytosis.

Table 2-1 Target and mechanism of action for endocytosis inhibitors [53,195].

Inhibitor	Target	Mechanism of Action
Chlorpromazine	Clathrin-mediated endocytosis	Inhibits formation of clathrin coated pits
Filipin	Caveolae-mediated endocytosis	Removes cholesterol from caveolae
Cytochalasin D	Actin dependent processes	Depolymerizes actin and disrupts actin filament formation
Temperature	Energy dependent processes	Reduces membrane fluidity and available ATP
Dextran Sulfate	Scavenger Receptors	Competitive inhibitor for acetyl-LDL receptors

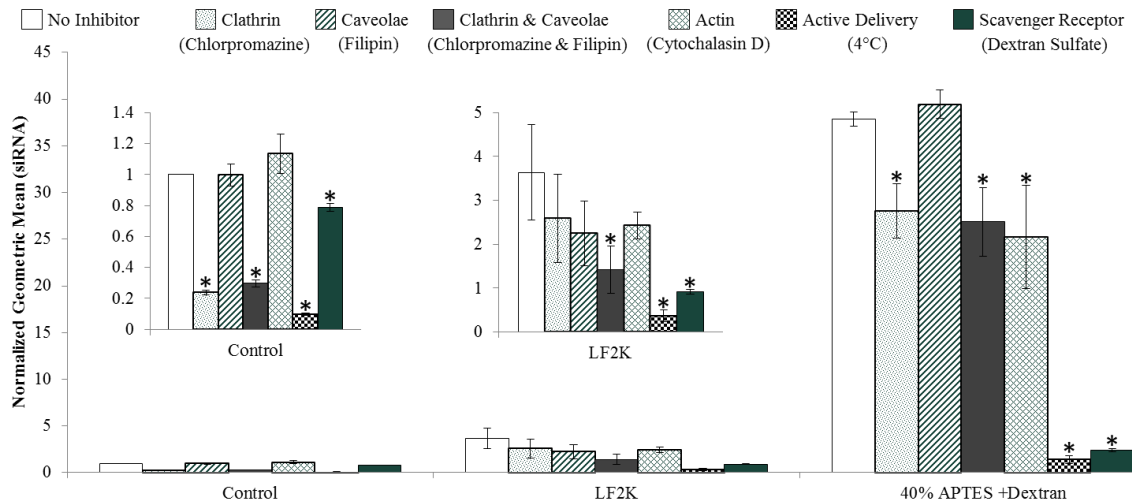
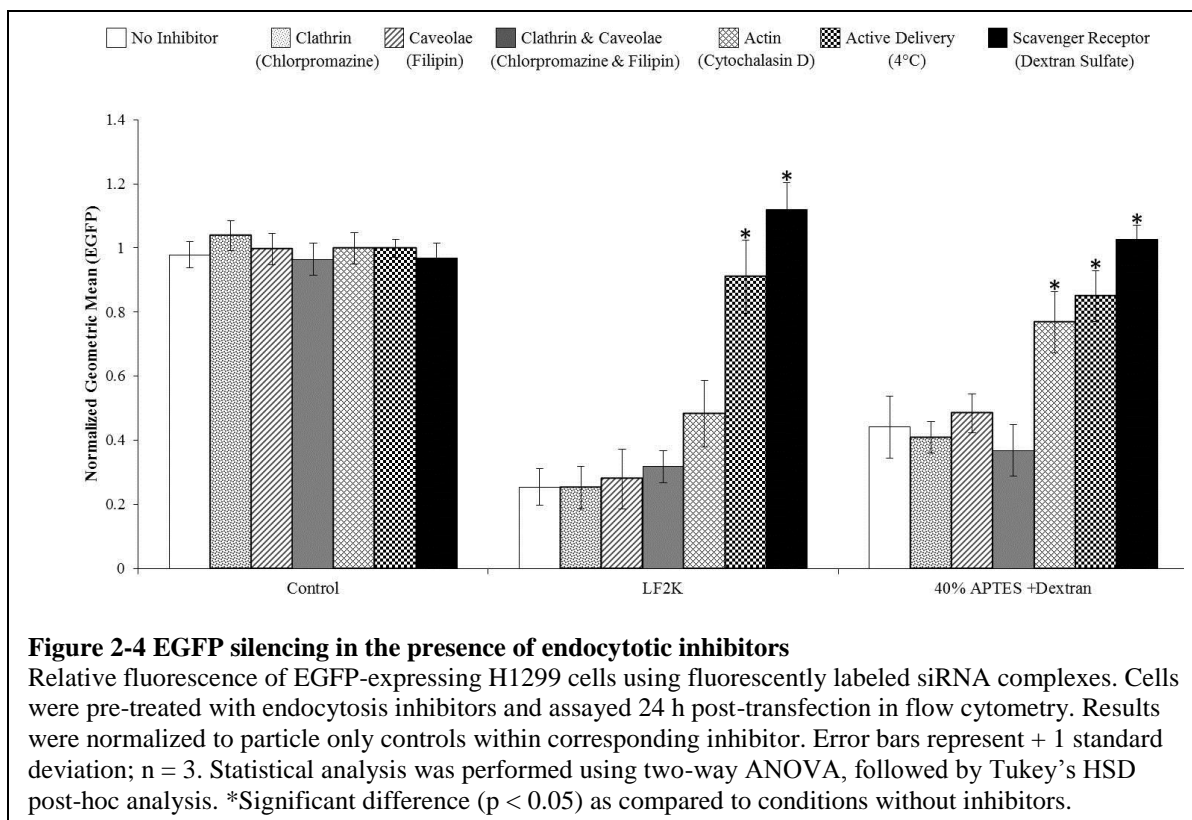


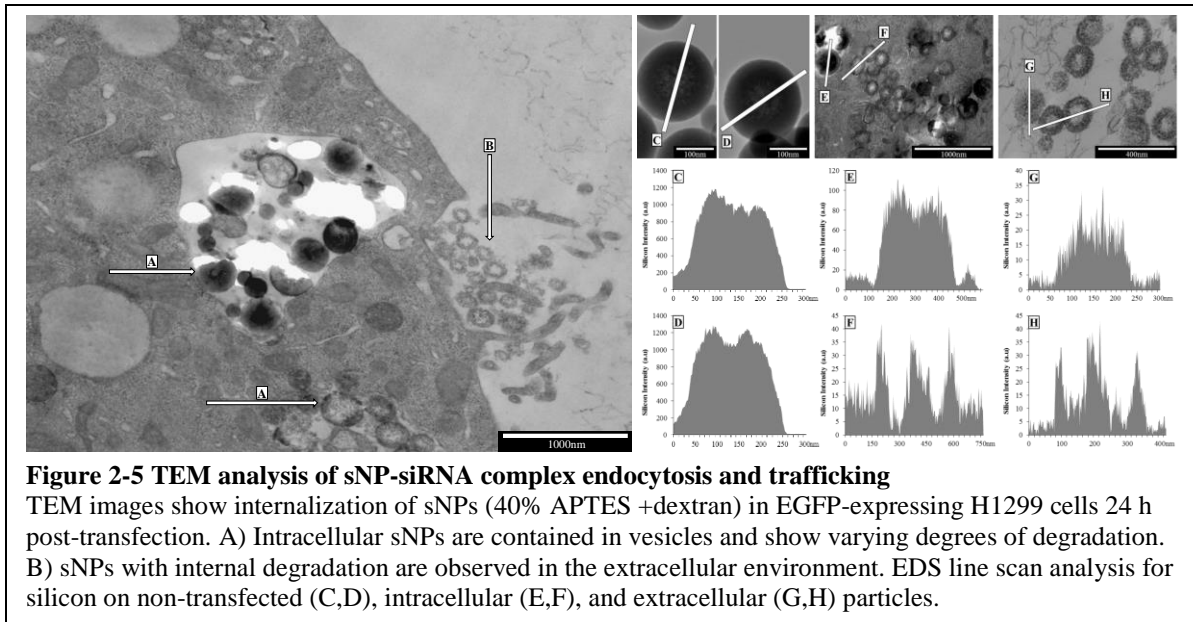
Figure 2-3 Influence of endocytotic inhibitors on the uptake of siRNAs

Relative fluorescence of labeled siRNA complexes delivered to EGFP expressing H1299 cells. Cells were pre-treated with endocytosis inhibitors and assayed 24 h post-transfection using flow cytometry. Results are normalized to uptake of siRNA only controls. Error bars represent + 1 standard deviation; n = 3. Statistical analysis was performed using two-way ANOVA, followed by Tukey's HSD post-hoc analysis. *Significant difference ($p < 0.05$) as compared to delivery in the absence of an inhibitor.



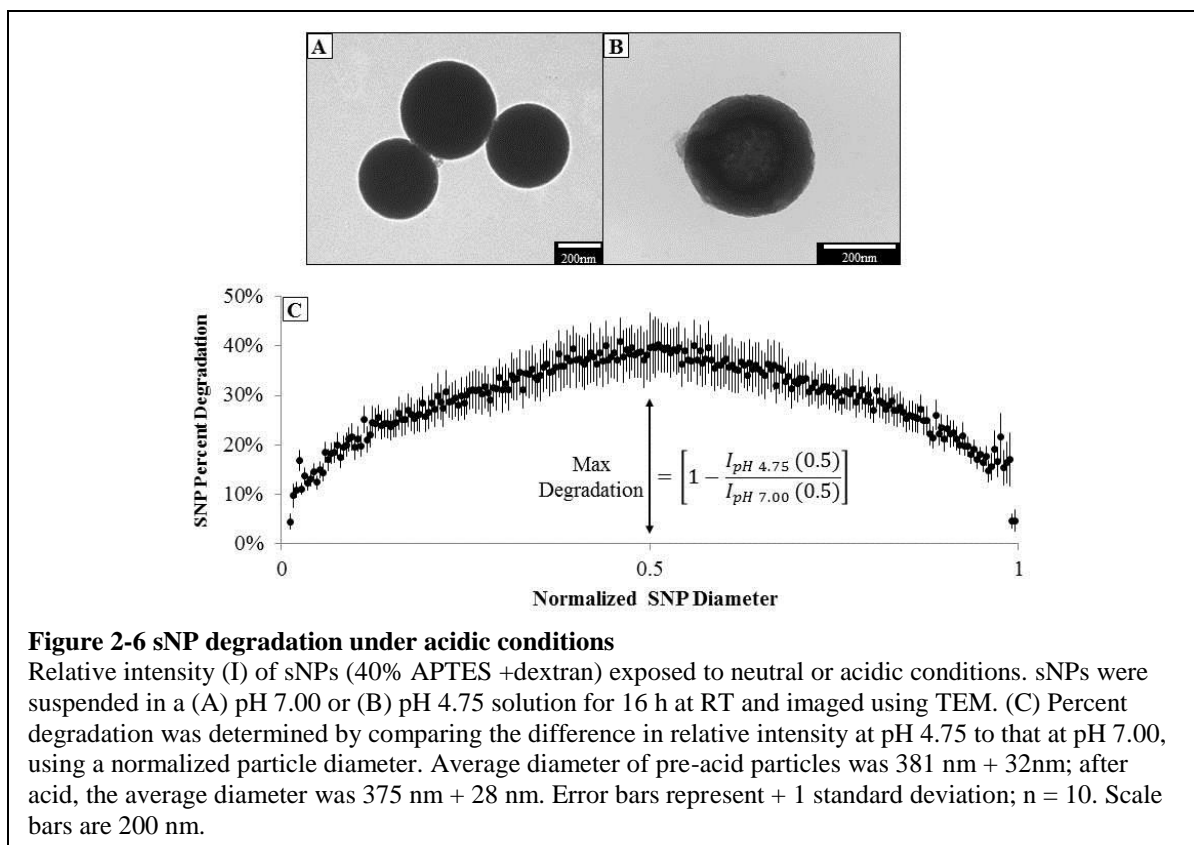
2.3.3 Intracellular Trafficking of sNPs

Using TEM, we confirmed the uptake of our sNP-siRNA complexes and identified the subcellular locations that sNPs were trafficked (Figure 2-5). In all cases, we confirmed the presence of our sNPs using energy-dispersive X-ray spectroscopy (EDS) line scans to detect silicon, that should not be present at significant levels endogenously (Figures 2-5C-F). The images showed sNPs localized in membrane-bound endocytotic vesicles. Visual inspection of the signal intensity for the endocytosed particles suggested that the density of the interiors of the particles was decreased relative to particles before endocytosis. This observation was further supported by the appearance of degraded sNPs adjacent to the cell membrane, suggesting that they had been recently exocytosed from the cells.



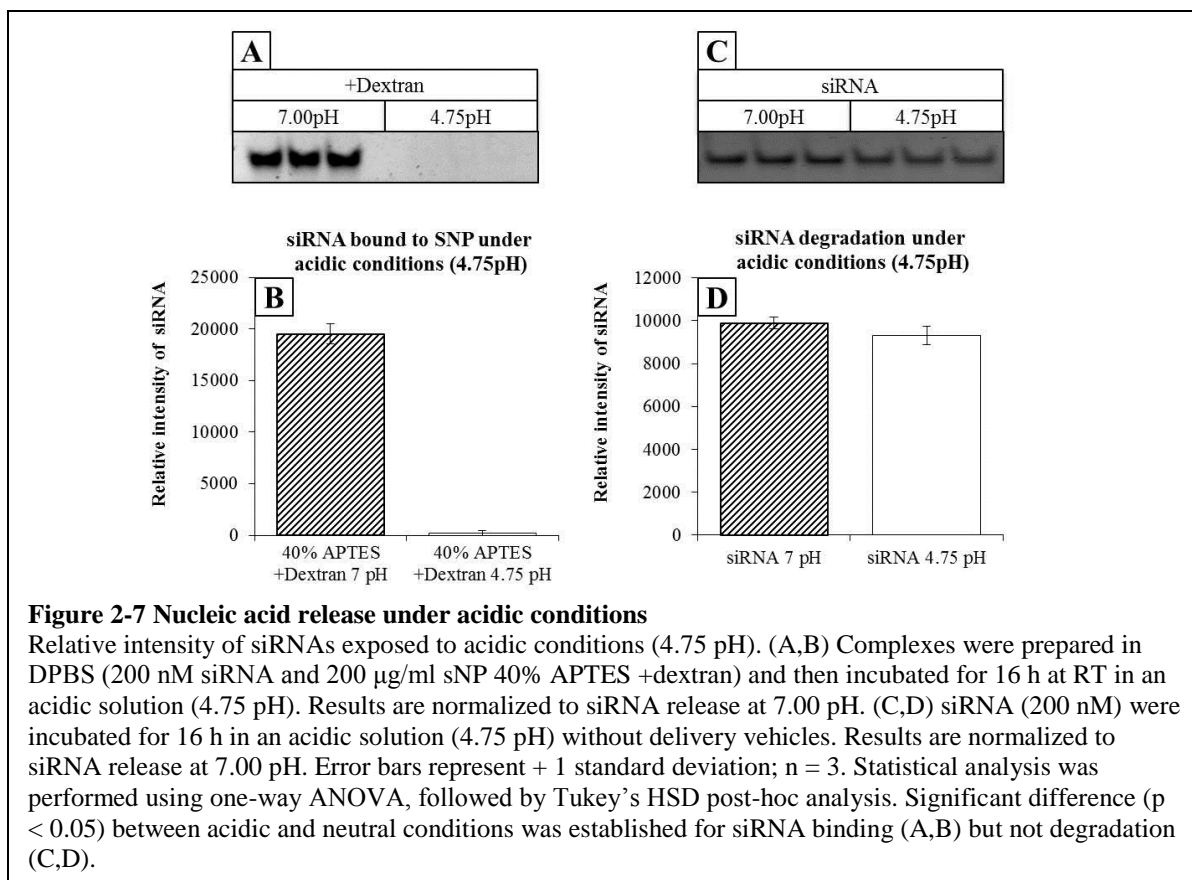
2.3.4 Acidic Degradation of sNPs

To determine if the observed intracellular degradation of our sNPs could be attributed to the acidic environments of some vesicles, we tested whether acidic pH would result in similar degradation patterns in vitro (Figure 2-6). Both visual inspection (compare signal intensities for Figures 2-6A and B) and quantification of the signals from multiple treated and untreated particles (Figure 2-6C) indicate that acidic conditions promote sNP degradation with maximum degradation, roughly 40% of the transmission electron microscopy (TEM) signal, in the centers of the particles. The particles appear rough after exposure to acid, again reflecting what was observed in the cellular experiments, suggesting some surface degradation. However, the average diameter of the particles did not change significantly during the in vitro acid exposure.



2.3.5 siRNA Binding under Acidic Conditions

We hypothesized that the degradation of the sNPs would contribute to the release of siRNAs from the complexes, resulting in a more rapid activation of silencing than would be achieved by purely diffusive release. To examine whether acidic conditions promoted nucleic acid release from sNPs, we incubated complexes of sNPs with siRNAs under neutral and acidic conditions. The amount of nucleic acid retained on the particles after exposure to acid was assayed using gel electrophoresis. Acidic conditions resulted in only 4% of the original nucleic acid being retained in complexes with the sNPs (Figures 2-7A and B). The relatively minimal degradation of the naked siRNAs in acid suggested that the reduction in retained material was not due to degradation of the siRNAs, but to a reduced ability of the particles to bind them (Figures 2-7C and D).



2.4 Discussion

Designing effective, non-toxic siRNA delivery vehicles remains a critical challenge in the development of siRNA therapeutics. Here, we used sNPs as a means of identifying chemical characteristics of delivery vehicles that correlate with high activity of the delivered siRNA cargo. The sNP system is convenient as it allows for changes in the chemical functionality of the vehicle without altering its physical conformation. We plan to use the sNP system as a platform for further evaluation of other chemical functionalities (e.g., biodegradable disulfide linkages, PEGylation) that may enable high activity of the delivered siRNAs, with the goal of identifying characteristics that apply to any siRNA delivery vehicle. Moreover, by modifying the synthesis protocol, we will examine these characteristics on particles of multiple sizes. Our approach differs from purely combinatorial efforts that have been undertaken [124], where both the

chemical functionality and the molecular structure/size of the vehicle can change simultaneously, potentially confounding why some vehicles result in higher siRNA activity than others.

Our data suggest that the majority of silencing that occurs results from uptake of either LF2K lipoplexes or sNP-siRNA complexes through a clathrin/caveolin-independent, energy-dependent process mediated by scavenger receptors. While nucleic acids and gold nanoparticles have been shown to be taken up via scavenger receptor-mediated endocytosis [125,126], this uptake mechanism was limited to macrophages and was either clathrin- or caveolin-dependent. Utilization of a clathrin/caveolin-independent, scavenger receptor-mediated pathway in non-macrophage cells distinguishes this mechanism of uptake from those previously reported.

For both vehicles, there were cases where changes in siRNA uptake and silencing were not correlated. For LF2K, where uptake inhibition by chlorpromazine and filipin did not result in a reduction in silencing, this may be because the amount of reduction in siRNA levels was small despite it being statistically significant. Additionally, it has been shown that lipoplexes enter cells through multiple pathways [29,85], making the inhibition of any one or two pathways, especially if those are not primary pathways to silencing, less likely to affect silencing.

For sNPs, the results are more complex. Inhibition by chlorpromazine, either in the presence or absence of filipin, resulted in a significant reduction in uptake with no concomitant reduction in silencing. This suggests inhibition of a non-productive uptake pathway. In contrast, cytochalasin D resulted in comparable levels of inhibition of siRNA uptake and a significant reduction in silencing. This indicates that sNP-siRNA complexes associate with the actin network, either directly or while in vesicles, and that this association is essential for delivering siRNAs in a manner (e.g., to a specific subcellular location) that eventually results in silencing. It

is also worth noting that uptake, trafficking, and silencing are dynamic processes, and measurements at a single time point do not necessarily reflect a steady-state.

It is important to note that our sNPs deliver considerably more siRNA to cells than LF2K (~8-fold, Figure 2). This indicates that our sNPs deliver more siRNA than many delivery vehicles (using LF2K delivery as a reference) [127–129]. However, the degree of silencing achieved by the delivered siRNAs was only comparable to LF2K. This may indicate that a large fraction of the siRNAs delivered by sNPs is inactive due to sequestration, either by being retained on the sNPs or by being trapped in vesicles [85]. These internalized siRNAs may then be degraded prior to achieving silencing, mitigating any improvement in function that would result from delivery of higher quantities of siRNA. If this is the case, our sNPs may be valuable for delivering chemically-modified siRNAs, in particular those designed for resistance to nucleases or enhanced endosomal escape, potentially providing a facile approach for increasing or extending the persistence of maximal silencing [130].

Among the various classes of scavenger receptors, dextran sulfate is a known inhibitor of acetyl-LDL scavenger receptors, that are found among class A (SCARA1/SR-AI/II, SCARA2/MARCO) and class H (FEEL 1/stabilin-1/CLEVER-1, FEEL-2/stabilin-2/HARE) [131,132]. These receptors recognize targets with a high density of negative charges, common among bacterial polysaccharides [131]. While previously considered to be macrophage specific, scavenger receptors have been identified across multiple cell types including endothelial, smooth muscle, dendritic, fibroblast, and epithelial cells [132]. Scavenger receptors are known to induce phagocytosis and macropinocytosis, although the exact signaling mechanism remains unknown [133]. Scavenger receptors can enact a variety of functional responses due to their association with various co-receptors (SRC family kinases, toll-like receptors, β -integrins, and tetraspanins)

[133]. Our results suggest that the scavenger receptors used by our sNPs may associate with dynamin-independent GTPases of the Rho family, given their association with other scavenger receptors that had a reported role in actin polymerization and clathrin/caveolin-independent endocytosis [134].

While the trafficking of high amine-content particles such as our sNPs within acidic endosomes suggests that siRNA release into the cytoplasm is due to the proton sponge effect [135], our results do not support this mechanism for endosomal release. From our TEM images, sNPs were only observed in membrane-bound vesicles and never observed in the nucleus or cytoplasm. These observations, in concert with the inability of sNPs to deliver plasmid DNA, are inconsistent with release mechanisms that require the endosomal membrane to rupture. Rather, it seems that only the siRNAs escape the endosomes in our system and that escape occurs after the sNP-siRNA complex has dissociated. This is further substantiated by our findings that acidic conditions inhibit the binding of siRNAs to sNPs. Formation of endosomal membrane pores would enable siRNA release into the cytoplasm. However, our sNPs lack any specific functionality designed to generate pores [136], making this unlikely. It may also be that siRNAs do not need to escape the endosomes to activate RNAi. Recent evidence has shown that RNAi pathway proteins, specifically Dicer and Ago2, are associated with vesicle and ER membranes [121,137]. It is possible that siRNAs are recognized in the endosomes after release from the sNPs, with the RNAi proteins shuttling them across the endosomal membrane. Based on our current results, however, the exact mechanism by which siRNAs achieve endosomal escape and initiate silencing remains unclear.

The design of siRNA delivery vehicles remains a somewhat haphazard process, without clear rules for which chemical and physical features provide the greatest probability of high siRNA

activity. In this work, we have demonstrated that dextran associates with scavenger receptors to initiate clathrin/caveolin-independent endocytosis, and that internalization by this pathway results in active siRNA delivery. In doing so, we have identified both a vehicle design variable (presence of dextran) and a biological mechanism (clathrin/caveolin-independent, scavenger receptor-mediated endocytosis) that warrant further examination for their contributions to the high activity of delivered siRNAs. Going forward, we hope to examine the generality of these rules for siRNA delivery vehicles based on lipids, polymers, and nanoparticles.

CHAPTER 3: ENDOCYTOSIS CONTROLS SIRNA EFFICIENCY: IMPLICATIONS FOR SIRNA THERAPEUTIC DESIGN AND CELL SPECIFIC TARGETING

Note: This chapter is adapted from previously published work [138]

3.1 Abstract

While siRNAs are commonly used for laboratory studies, development of siRNA therapeutics has been slower than expected, due in part to a still limited understanding of the endocytosis and intracellular trafficking of siRNA-containing complexes. With the recent characterization of multiple clathrin/caveolin-independent endocytic pathways, i.e., those mediated by Graf1, Arf6, and flotillin, it has become clear that the endocytic mechanism influences subsequent intracellular processing of the internalized cargo. To explore siRNA delivery in light of these findings, we developed a novel assay that differentiates uptake by each of the endocytic pathways and can be used to determine whether endocytosis by a pathway leads to the initiation of RNA interference (RNAi). Using LF2K, we determined the endocytosis pathway leading to active silencing (whether by clathrin, caveolin, Arf6, Graf1, flotillin, or macropinocytosis) across multiple cell types (HeLa, H1299, HEK293, and HepG2). We showed that LF2K is internalized by Graf1-, Arf6-, or flotillin-mediated endocytosis for the initiation of RNAi, depending on cell type. Additionally, we found that a portion of siRNA-containing complexes are internalized by pathways that do not lead to initiation of silencing. Inhibition of these pathways enhanced intracellular levels of siRNAs with concomitant enhancement of silencing.

3.2 Introduction

Small molecule and protein-based drugs, while critically important therapies, cannot treat all diseases [2]. In some cases, the drugs cannot access or interact with proteins that are causing the disease phenotype. As such, alternative treatment modalities must be developed to complement existing strategies. One potential alternative is small interfering RNA (siRNA) therapeutics, that

are capable of specific inhibition of a wide range of intracellular, membrane, and extracellular proteins [3]. To function, siRNAs must be transported from the extracellular environment into the cytoplasm of the targeted eukaryotic cells. Once there, siRNAs act through RNA interference (RNAi) to degrade messenger RNAs (mRNAs) in a sequence-specific manner, thereby reducing target protein expression [11–14,99]. siRNA therapeutics are being developed as treatments for a variety of diseases, including cancers and infectious diseases, with one therapeutic approved for clinical use [4–6]. Despite the recent clinical success, development of siRNA therapeutics has been hindered by multiple technical challenges, including poor delivery efficiency [7–9]. One limitation to delivery is efficient endocytosis of delivered siRNAs to the cells of interest.

Until recently, cellular endocytic pathways were classified as macropinocytosis (MP), clathrin-mediated endocytosis (CME), caveolin-mediated endocytosis (CvME), or clathrin/caveolin-independent endocytosis (CCIE) [53]. Researchers have since characterized three distinct types of CCIE, flotillin-mediated endocytosis (FME), Arf6-dependent endocytosis (ADE), and Graf1-mediated endocytosis (GME) [54–56]. The identification of these pathways has resulted in the reclassification of the uptake mechanisms of many species [58,139,140]. For instance, adeno-associated viruses and ~50% of fluid-phase uptake, including uptake of dextrans, are now attributed to GME, though they were previously thought to occur via other pathways [55,77]. Likewise, cholera toxin B is taken up by FME but was previously thought to enter cells by MP [54].

Currently, there is no consensus regarding the optimal endocytic pathway for active siRNA delivery, as multiple endocytic pathways have been found to result in successful delivery of siRNAs and initiation of silencing. It is difficult to generalize which pathways are optimal as most studies are limited to a single cell type or did not distinguish among FME, ADE, and GME.

However, it has also recently become evident that the endocytic mechanism influences the molecular composition of the endosomes, their intracellular trafficking, and the processing of their cargo [66,83]. Thus, we hypothesized that the mechanism used by cells to endocytose siRNA-containing complexes could significantly impact the ability of the siRNAs to initiate RNAi.

In this study, we used chemical inhibitors and endocytic protein overexpression to investigate the endocytic pathways used to internalize and process siRNA-containing complexes in four cell lines. Our results show that while the complexes are internalized through multiple endocytic pathways, active delivery occurs primarily through a single pathway that varies according to cell type. The results suggest that both cell specificity and siRNA delivery efficiency can be enhanced by designing delivery vehicles to favor the preferred endocytic pathway.

3.3 Results

3.3.1 Silencing Efficiency in Different Cell Lines

To assess the role of endocytosis in siRNA accumulation and EGFP silencing, we tested the ability of LF2K to deliver siRNAs and achieve active silencing in four common human cell lines stably expressing EGFP: H1299 (lung), HeLa (cervical), HEK293 (kidney), and HepG2 (liver) (Figure 3-1). At 24 hours post-transfection, EGFP silencing and siRNA accumulation were measured in all cell lines. Silencing was greatest in H1299 cells (Figure 3-1A), yet levels of intracellular siRNAs were highest in HEK293 cells (Figure 3-1B), and the most efficient use of siRNAs (silencing/siRNA accumulation) was seen in HeLa cells (Figure 3-1C). These differences suggested that the internalization and processing of LF2K-siRNA complexes differ among cell types, possibly due to the predominance of different endocytic pathways across the different cell types.

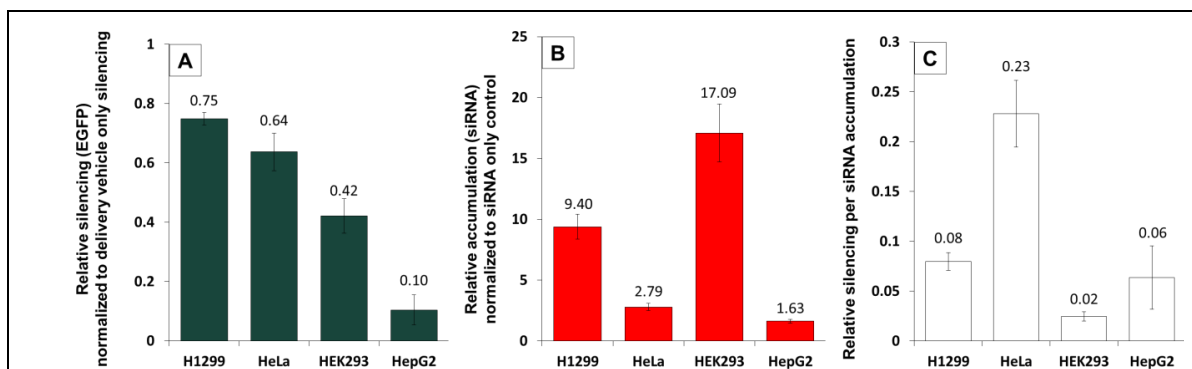


Figure 3-1 EGFP silencing and siRNA accumulation

EGFP silencing and siRNA accumulation in H1299, HeLa, HEK293, and HepG2 cells. Cells were transfected with 100 nM fluorescently-labeled siRNA and 2.3 $\mu\text{g}/\text{mL}$ LF2K and assayed 24 hours post-transfection using flow cytometry (10,000 events). A) control value = 0 and B) control value = 1. In each panel, values for each cell line were statistically different from all others, $p < .05$; error bars represent ± 1 standard deviation; $n = 4$. Statistical analysis was performed using one-way ANOVA, followed by Tukey's HSD post-hoc analysis.

3.3.2 Inhibition of siRNA Accumulation and Silencing

It is known that drug complexes are taken into cells via multiple endocytic pathways. However, in most circumstances, it is unclear whether the mechanism of uptake influences downstream function of the complexes. To differentiate among the types of endocytosis, we used a minimal set of chemical inhibitors, which, when evaluated collectively, result in unique patterns of inhibition for each endocytic mechanism (Table 3-1). Using data from the literature, a logic matrix was constructed for each inhibitor and its effect on each type of endocytosis (Table 3-2). Using this logic matrix, we identified the type of endocytosis used by LF2K for active siRNA delivery across each of the cell lines tested. By measuring the effect of inhibitors on both intracellular levels of siRNAs and EGFP silencing, we classified endocytic pathways according to their role in facilitating siRNA function. Results were normalized against siRNA accumulation and silencing in the absence of inhibitor, allowing the relative position of a data point to indicate the degree to which an inhibitor affected siRNA accumulation and silencing (Figure 3-2, also see Materials and Methods Chapter 3 information for equations).

Table 3-1 Chemical inhibitors of endocytic proteins

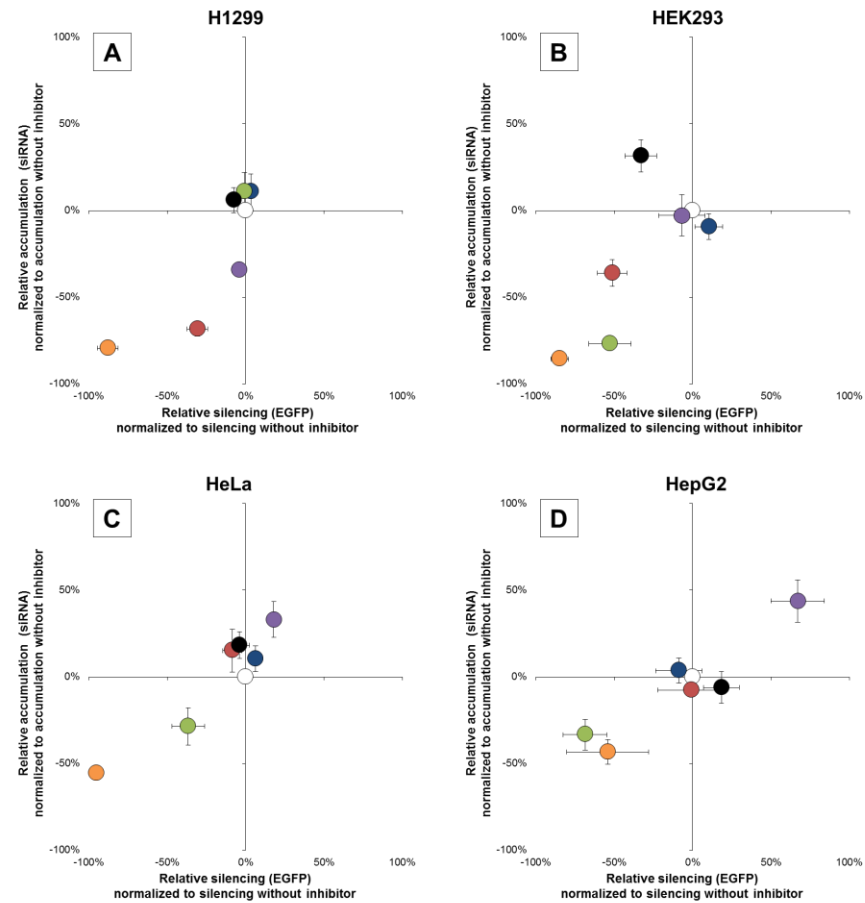
For general information about inhibitors, see Ivanov, et al [157].

Inhibitor	Mechanism of Action	Concentration	
Filipin Complex III , (Filipin)	Binds to membrane cholesterol which destabilizes caveolae	3 μ M	(2 μ g/ml)
Chlorpromazine	Sequesters clathrin and AP2 to intracellular vesicles	25 μ M	(9 μ g/ml)
5-(N,N-Dimethyl) Amiloride , (Amiloride)	Inhibits Rac1 and Cdc42 by decreasing submembranous pH	100 μ M	(29 μ g/ml)
Dynasore	Noncompetitive inhibitor of dynamin	80 μ M	(26 μ g/ml)
Cytochalasin D	Competitive inhibitor of actin polymerization	10 μ M	(5 μ g/ml)
Methyl- β -Cyclodextrin (M β CD)	Forms soluble inclusion complexes with membrane cholesterol	5 mM	(7 mg/ml)

Table 3-2 Chemical inhibitor vs endocytic pathway matrix

Logic matrix illustrating the effects of chemical inhibitors on different endocytic pathways. An X indicates decreased endocytic function as a result of the chemical inhibitor at the concentration used in our experiments, whereas empty spaces indicate that there is no known effect. It should be noted that there are conflicting reports in the literature regarding the role of dynamin in flotillin-mediated endocytosis (See Discussion 3.4 for details).

	Graf1	Clathrin	Caveolin	Arf6	Flotillin	Macro-pinocytosis
Filipin			X			
Chlorpromazine		X				
Amiloride	X					X
Dynasore	X	X	X		X	
Cytochalasin D	X	X	X	X		X
M β CD	X		X	X	X	



	No Inhibitor	Filipin	Chlorpromazine	Amiloride	Dynasore	Cytochalasin D	MβCD
Silencing							
H1299	0%	3%	-4%	-8%	-31%*	-1%	-88%*
HEK293	0%	10%	-7%	-33%*	-51%*	-53%*	-85%*
HeLa	0%	6%	18%*	-4%	-9%	-37%*	-95%*
HepG2	0%	-9%	67%*	18%	-1%	-69%*	-54%*
Accumulation							
H1299	0%	11%	-34%*	6%	-70%*	11%	-79%*
HEK293	0%	-9%	-3%	32%*	-36%*	-77%*	-86%*
HeLa	0%	10%	33%*	18%	15%	-29%*	-56%*
HepG2	0%	4%	44%*	-6%	-8%	-33%*	-43%*

Figure 3-2 Influence of endocytic inhibitors on EGFP silencing and siRNA accumulation

EGFP-expressing cells were pre-treated with endocytic inhibitors and assayed 24 hours after siRNA transfection using flow cytometry (10,000 events). x-axis: -100% (inhibited silencing) vs 100% (enhanced silencing). y-axis: -100% (inhibited siRNA accumulation) vs 100% (enhanced siRNA accumulation). Error bars represent ± 1 standard deviation; $n = 3$. Statistical analysis was performed using one-way ANOVA, followed by Tukey's HSD post-hoc analysis. *Significant difference ($p < 0.05$) as compared to delivery in the absence of an inhibitor.

In comparing the effects of the different inhibitors among the four cell lines, the strongest, most consistent inhibition of silencing (and siRNA accumulation) was from methyl- β -cyclodextrin (M β CD) (Figure 3-2 - orange). This is not unexpected, as M β CD inhibits multiple endocytic pathways (Table 3-2). M β CD, a cyclic oligomer of glucopyranoside, forms soluble inclusion complexes with cholesterol in the cell membrane, principally destabilizing lipid rafts [141]. Inhibition of EGFP silencing by M β CD demonstrates that endocytosis of LF2K-siRNA complexes by lipid-raft dependent pathways is critical for the initiation of RNAi in each of these cell types. Because EGFP silencing was inhibited by M β CD, but not filipin (Figure 3-2 - blue), the critical pathways in these cells involve one or more of the following: FME, ADE, and GME.

Cytochalasin D significantly inhibited siRNA accumulation and EGFP silencing in all but H1299 cells (Figures 3-2B-D vs. Figure 3-2A - green). Cytochalasin D, a mycotoxin that binds to F-actin and blocks its polymerization, prevents the formation of endocytic vesicles as they bud from the plasma membrane [142]. FME, however, forms endocytic vesicles through actin-independent tubular invaginations and is unaffected by cytochalasin D [143,144]. Thus, we concluded that, in H1299 cells, FME of LF2K-siRNA complexes result in the initiation of RNAi.

Dynasore also reduced EGFP silencing, but only in HEK293 and H1299 cells (Figure 3-2A&B - red). Dynasore, a noncompetitive inhibitor of dynamin, prevents endocytic vesicle fission from the cell membrane [145]. Among the lipid-raft dependent endocytic pathways, only ADE is considered dynamin-independent [146]. Because EGFP silencing in HeLa and HepG2 cells was inhibited by M β CD and cytochalasin D but not dynasore, we concluded that RNAi is initiated following ADE of LF2K-siRNA complexes in these cell lines.

Amiloride was the only other inhibitor to reduce EGFP silencing but only in HEK293 cells (Figure 3-2B - black). Amiloride, a derivative of a guanidinium-containing pyrazine, increases

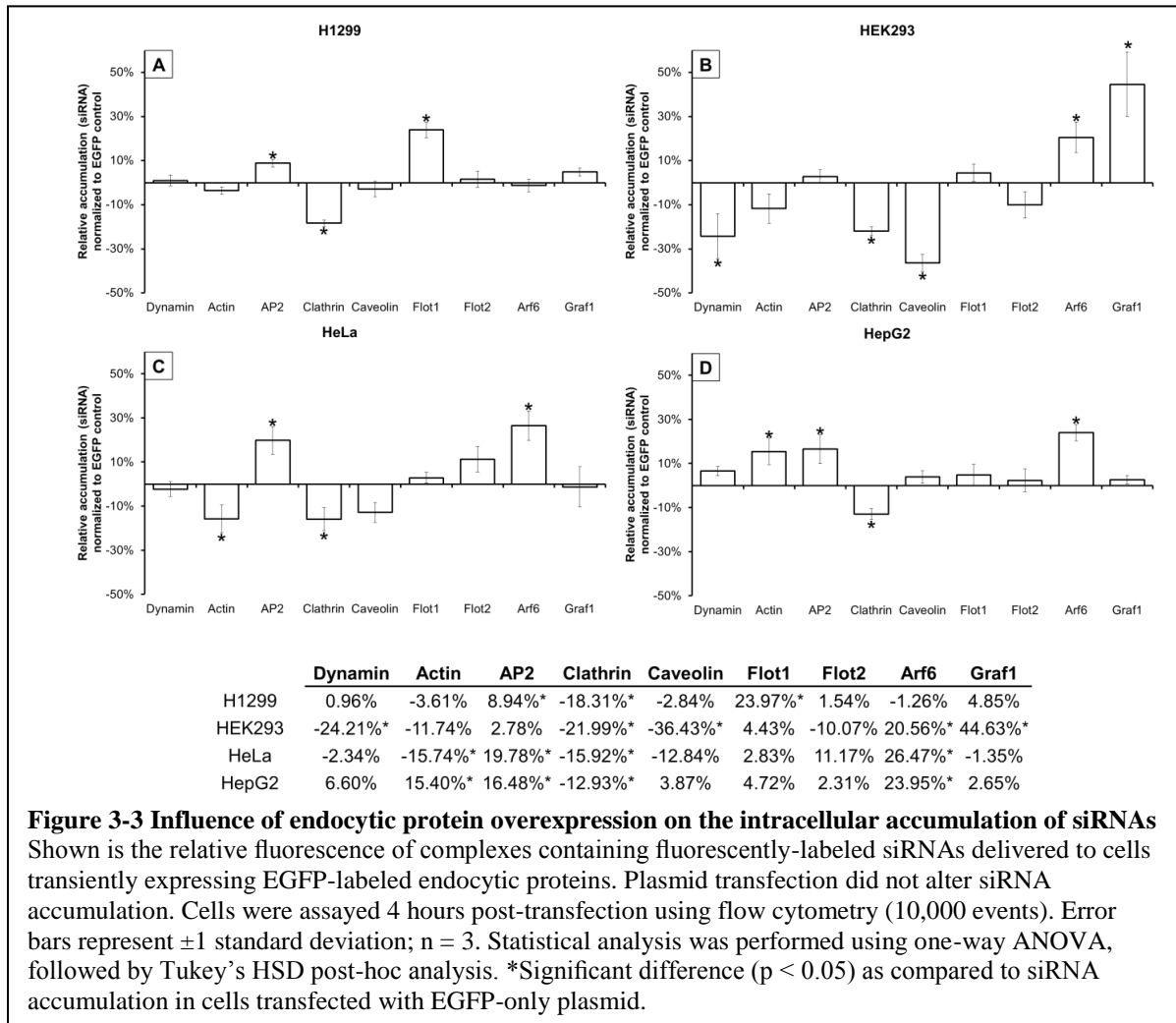
submembranous pH by inhibiting Na⁺/H⁺ exchangers [147]. Because EGFP silencing in HEK293 cells was inhibited by M β CD, dynasore, cytochalasin D, and amiloride, we concluded that GME is the principal RNAi-initiating pathway in HEK293 cells.

While inhibition of RNAi-initiating pathways is evident from reductions in EGFP silencing, inhibition of other pathways may also alter siRNA accumulation without a concomitant decrease in silencing. In H1299 cells, chlorpromazine significantly reduced siRNA accumulation without affecting EGFP silencing (Figure 3-2A - purple). Chlorpromazine, which translocates clathrin and AP2 from the plasma membrane to intracellular vesicles, inhibits the formation of clathrin-coated pits used in CME [148]. Therefore, we concluded that, in H1299 cells, CME internalizes siRNAs but does not allow them to initiate silencing. In HeLa and HepG2 cells, chlorpromazine enhanced siRNA accumulation and EGFP silencing (Figure 3-2C&D - purple), suggesting inhibition of CME in these cells results in additional siRNAs entering ADE and initiating RNAi. However, the inhibitor data does not allow us to determine whether CME is also capable of internalizing siRNAs or if the enhancement of ADE results from an intracellular connection between ADE and CME. In HEK293 cells, amiloride inhibited uptake via GME, reducing silencing. The data show that this also resulted in additional siRNAs accumulating via an uninhibited pathway. As multiple endocytic pathways are unaffected by amiloride, these data alone were insufficient to identify the pathway(s) responsible for the enhanced siRNA accumulation.

3.3.3 Overexpression of Endocytic Proteins

To validate the findings from our inhibitor experiments and make additional distinctions between pathways, we overexpressed individual endocytic proteins and measured the effects on siRNA accumulation (Figure 3-3). Green fluorescent protein (GFP)-labeled proteins were used

so that localization of the overexpressed protein could be confirmed to match that of endogenous protein (Figure A-9), and to ensure that siRNA accumulation was only measured for cells overexpressing the protein. It is critical to note that, as in the inhibitor experiments, the effects of protein overexpression are cell-specific (compare Figures 3-3A-D).



In H1299 cells, we found that siRNA accumulation was enhanced by overexpression of flotillin-1 and AP2, though reduced by clathrin overexpression (Figure 3-3A). These findings indicate that both FME and CME are capable of internalizing siRNAs, supporting the findings from our inhibitor data.

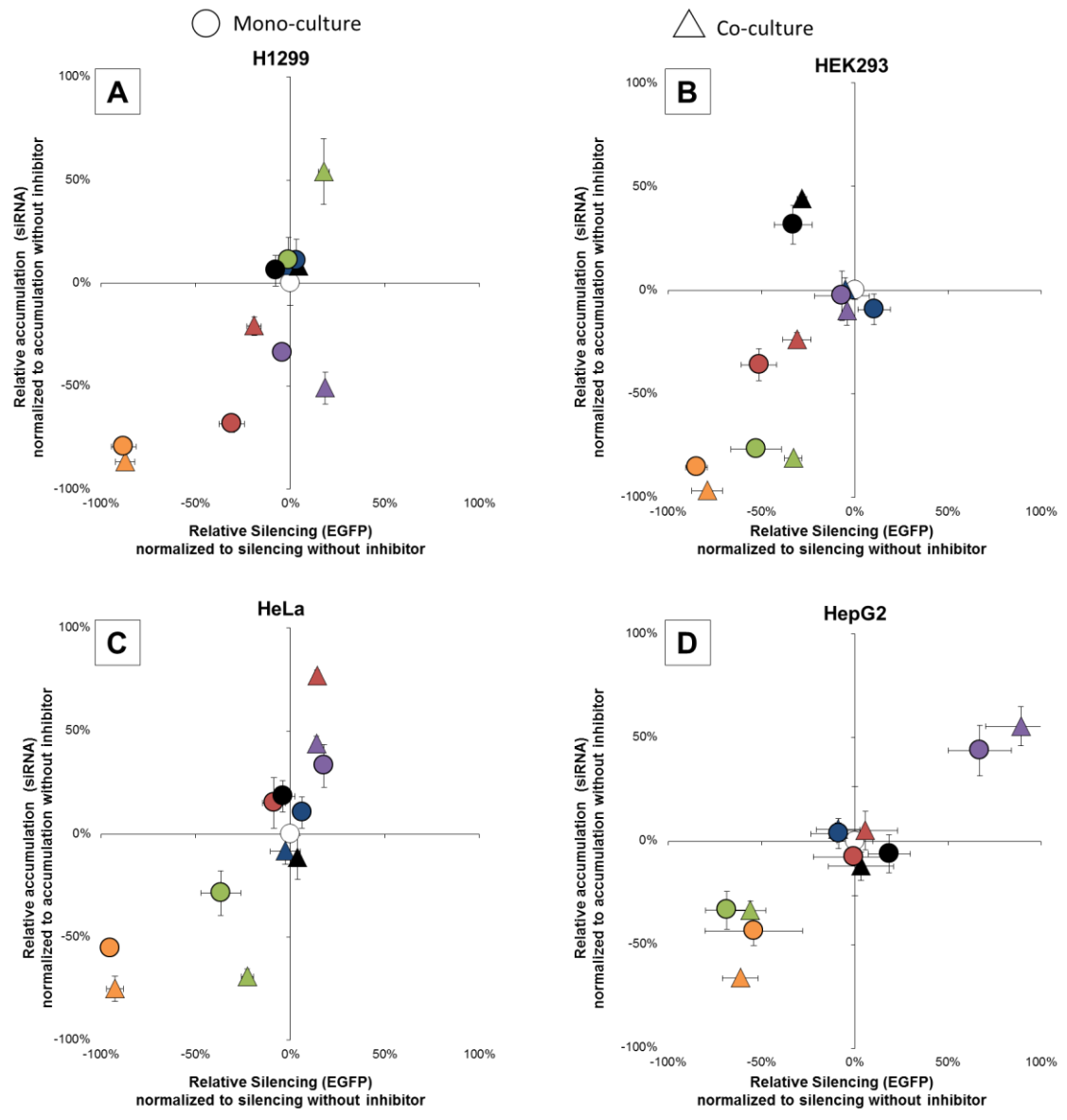
siRNA accumulation in HEK293 cells was enhanced by the overexpression of Graf1 and Arf6, though reduced by dynamin, clathrin, and caveolin overexpression (Figure 3-3B). This would suggest that both GME and ADE are capable of internalizing siRNA-LF2K complexes. This supports our inhibitor results for GME in these cells. It also demonstrates that ADE can internalize siRNAs, though without leading to RNAi, and is likely responsible for the enhanced siRNA accumulation that occurred in the presence of amiloride (Figure 3-2B). Similarly, our results suggest that CME, CvME, and GME share common regulatory elements, where overexpression of clathrin or caveolin dilutes the availability of these common elements for GME, resulting in reduced siRNA accumulation.

In HeLa and HepG2 cells, the accumulation of siRNAs was enhanced by overexpression of Arf6 and AP2 but reduced by overexpression of clathrin (Figures 3-3C and 3-3D). These findings confirm that internalization of siRNA-LF2K complexes occurs through both ADE and CME, as in our inhibitor data. It is interesting that the cell lines show different responses to the overexpression of actin (Figures 3-3C and 3-3D). This difference may partially explain why siRNA-LF2K complexes accumulate to a lesser degree and are considerably less efficient at initiating RNAi in HepG2 cells (Figure 3-1C), though a direct mechanistic link is not currently known (see 3.4 Discussion).

3.3.4 Targeted Inhibition in a Co-cultured Population

Having demonstrated that the pathways that are important for internalizing siRNAs and initiating RNAi vary by cell type, we theorized that inhibitors could be employed in a mixed cell population to enhance cell specific delivery by reducing uptake by untargeted cell types. To test this, we repeated our inhibitor assay using a co-culture consisting of H1299, HEK293, HeLa, and HepG2 cells and assessed the effect of inhibitors on siRNA accumulation and EGFP silencing

(Figure 3-4). In general, the effects of the inhibitors in co-culture were the same as the effects on mono-cultures (Figure 3-4, compare O and Δ). Three cases deviated from the mono-culture results, treatment with cytochalasin D and chlorpromazine in H1299 cells (Figure 3-4A – green, purple) and dynasore in HeLa cells (Figure 3-4C - red). For two of these cases, endocytosis of siRNA-complexes by a specific cell type was enhanced by inhibition of endocytosis by other cell types.



Silencing	No Inhibitor	Filipin	Chlorpromazine	Amiloride	Dynasore	Cytochalasin D	MβCD
H1299	0%	-1%	19%*	4%	-19%*	18%*	-87%*
HEK293	0%	-5%	-4%	-28%*	-31%*	-33%*	-79%*
HeLa	0%	-3%	14%*	4%	14%	-23%*	-93%*
HepG2	0%	-9%	89%*	3%	6%	-56%*	-61%*

Accumulation	No Inhibitor	Filipin	Chlorpromazine	Amiloride	Dynasore	Cytochalasin D	MβCD
H1299	0%	8%	-51%*	8%	-21%*	54%*	-87%*
HEK293	0%	0%	-10%	44%*	-24%*	-81%*	-97%*
HeLa	0%	-8%	44%*	-11%	77%*	-69%*	-75%*
HepG2	0%	6%	55%*	-12%	5%	-34%*	-66%*

Figure 3-4 Influence of endocytic inhibitors on EGFP silencing and siRNA accumulation in co-cultured and mono-cultured populations
 Co-cultured populations consisted of H1299, HEK293, HeLa, and HepG2 cells. EGFP-expressing cells (named in the header for each panel) were pre-treated with endocytic inhibitors and assayed 24 hours post-transfection using flow cytometry (5,000 events). x-axis: -100% (inhibited silencing) vs 100% (enhanced silencing). y-axis: -100% (inhibited siRNA accumulation) vs 100% (enhanced siRNA accumulation). Error bars represent ± 1 standard deviation; n = 3. Statistical analysis was performed using one-way ANOVA, followed by Tukey's HSD post-hoc analysis. *Significant difference ($p < 0.05$) as compared to delivery in the absence of an inhibitor.

3.4 Discussion

Using inhibition and overexpression of endocytic proteins, we showed that LF2K-siRNA complexes are internalized through multiple endocytic pathways. Moreover, the pathways used for endocytosis of LF2K-siRNA complexes were found to vary across cell types. The functional roles of these pathways were further characterized according to whether they facilitated LF2K-mediated RNAi. We also demonstrated that understanding the endocytic pathways of cells allowed targeting of specific cells in a mixed population and a resulting enhancement of siRNA accumulation and RNAi in the targeted cell populations.

We recognize that LF2K is not an option for future clinical applications and that delivery vehicle development has progressed since LF2K first became available. Nonetheless, we chose LF2K for these studies for two principal reasons. First, we have considerable prior experience using this vehicle [1,10,149]. Second, there is extensive prior literature on the use of this vehicle [150,151], allowing our results to be compared to the extant literature. We are not suggesting that the pathways used by LF2K are those that will be preferred by other vehicles. Rather, as our results show, the same vehicle works differently depending on the cell type, and uptake alone is not sufficient to achieve activity. These lessons can be applied to the development of any vehicle.

Previous studies regarding the cellular uptake of lipoplexes have reported that internalization occurs by CME or through direct fusion with the plasma membrane [152–155]. The differences in our conclusions relative to these prior studies may be a result of differences in the concentrations of inhibitors used, the presence of serum in the treatment media, wash procedures, or inhibitor exposure time. It may also be that the inhibitors chosen for this study, and an improved understanding of their impacts on cell function, allowed us to identify endocytic pathways with more clarity than was possible previously. We and others have shown that

transfection at low temperature (4°C) reduces silencing [1,152], supporting our current conclusions that the best pathways for endocytosis of siRNA-containing complexes in the cell types tested are energy-dependent.

Chemical inhibitors, siRNAs, and protein overexpression are commonly used to characterize the function of endocytic pathways [140]. Our inhibitor logic matrix was derived from the current understanding of the proteins targeted by the inhibitors and their associations with each endocytic pathway, including any known side effects at the concentrations used in our experiments (Table 3-2). We chose to use inhibitors, as they work more quickly than siRNAs and overexpression, and result in a shorter-term reversible disruption of native cell function. However, among the many chemical inhibitors used to evaluate endocytosis, none possesses absolute specificity for a single endocytic pathway [156]. In many cases, the molecular target of an inhibitor is utilized by multiple endocytic pathways. In addition, experimental conditions (high concentrations, prolonged incubation, and serum protein interactions) can cause unintended side effects [157]. For example, M β CD, which inhibits lipid-raft dependent endocytosis, can also inhibit CME when used at concentrations > 10mM [158]. Fluorescent endocytic markers are generally used to determine the effective concentration of an inhibitor. To date, however, none has been established that is specific for GME, ADE, or FME, and those traditionally associated with CvME (albumin) [70,71] and MP (dextran) [56] have been shown to be endocytosed via multiple pathways.

It is still unclear what factors impact whether pathways are used for endocytosis of siRNA-containing complexes or which pathways lead to initiation of RNAi. Intracellular trafficking of endocytic vesicles varies across cell type and disease state [159]. Many of these variations are observed in relation to processing through the early endosome (EE), a common node among

intracellular trafficking pathways. In HeLa cells, the time for cargo to reach the EE was 5-10 minutes via CME and 30-60 minutes for ADE [55]. FME is capable of retrograde transport directly to the Golgi, bypassing the EE [160]. ADE and GME have been shown to form intermediate endosomal compartments capable of sorting cargo before joining the EE [55,72,161]. These differences alone could explain the differences in siRNA accumulation and silencing across cell types. In addition, the pH and composition of the endosomal vesicles differ among endocytic pathways [87,116], which could alter endosomal escape, depending on the mechanism (e.g., formation of membrane pores, pH buffering, or membrane fusion) [87]. Thus, differences in the endosomal release kinetics for each endocytic pathway, in addition to uptake, may result in the differences in siRNA activity we observed among the different endocytic pathways and cell types. Differences in release kinetics may also explain why the active endocytic pathway for uptake of drugs and other molecules differs depending on the cell type [152,162–165].

By measuring both the intracellular accumulation of siRNA and its functional activity in silencing EGFP, we identified multiple endocytic pathways used to internalize siRNA-LF2K complexes. In three cases, we observed a significant increase in siRNA accumulation (see Figure 3-2B-black and Figures 3-2C&D - purple). In each case we identified a regulatory protein common to both the inhibited and enhanced pathway (Cdc42 for amiloride and AP2 for chlorpromazine), that was also directly affected by the inhibitor. Given the duration of incubation with inhibitor, it is unlikely that the increase in endocytic activity is caused by increased protein levels. It is more likely a reallocation of cellular resources. AP2, which regulates CME, is in turn regulated by Arf6. Sequestration of AP2 to intracellular compartments by chlorpromazine would, in theory, increase the availability of Arf6 for ADE. In this way, the

relative activities of endocytic pathways are affected by competition for common resources. Indeed, if this is the case, the relative expression of endocytic and regulatory proteins in a cell may control the relative activities of the respective endocytosis pathways.

We concluded that FME facilitates LF2K-mediated RNAi in H1299 cells. In FME, flotillin-1 and flotillin-2 co-assemble into plasma membrane microdomains in lipid rafts and are internalized after phosphorylation by FYN [81]. Previously, FME has been implicated in the uptake of CD59 [54], cholera toxin B [54], silica nanoparticles [80], and cationic polyplexes [79]. The role of dynamin in this process, however, is still undefined and possibly dependent on cell type or cargo [82]. Based on our inhibitor data with dynasore, we concluded that FME is dynamin-dependent in H1299 cells. Interestingly, the progression of malignancy in non-small cell lung cancers (NSCLC), like H1299s, is characterized by increased expression of flotillin-2, and decreased expression of flotillin-1 and caveolin-1 [166]. This aligns with our findings where siRNA accumulation was unaffected by overexpression of flotillin-2 but enhanced by the overexpression of flotillin-1. Expression profiles of the mRNAs for the flotillins and caveolin-1 correlate across tissue samples, with the highest expression levels in heart, lung, and skeletal muscle tissue [167]. Using gene expression data, we found that ETS1, a transcription factor for both flotillins and caveolin-1, was 9.6x higher in H1299 cells than HeLa, HEK293, and HepG2 cells (Table A-6). This suggests that elevated expression of the flotillins, caveolin-1, or ETS-1 may facilitate uptake by FME and initiation of RNAi.

In HEK293 cells, we concluded that the cells use GME to initiate RNAi. Since its discovery, GME has been implicated in the uptake of GPI-linked proteins [56], adeno-associated virus [77], and dextran [78]. It was also identified as a major source of uptake of extracellular fluid [56]. In GME, Graf1 and dynamin form a stable complex that regulates the scission and stability of the

tubulovesicular structures [56]. Interestingly, Graf1 in this complex has a higher affinity for dynamin-1 (DNM1), thought to be exclusive to neurons, than dynamin-2 (DNM2), which has ubiquitous expression [56,76]. Comparing gene expression data for Graf1, DNM1, and DNM2 among the four cell lines, we found that similar expression levels of DNM1, DNM2, and Graf1 only occurred in HEK293 cells (Table A-6). It is possible then that the relative expression levels of DNM1, DNM2, and GRAF1 determine the prominence of GME in a given cell type. Additionally, mRNA expression levels of proteins associated with GME (Graf1, Cdc42, and Arf1) were significantly higher in HEK293 cells relative to the other cell lines tested (Table A-6).

ADE is regulated by the GTP cycle of Arf6 [55]. Internalization through ADE leads to the formation of Arf6-containing endosomes that are either recycled to the plasma membrane or trafficked to the EE, a process dependent upon the hydrolysis of Arf6-GTP [168]. ADE has currently been suggested as the route of internalization of Tac [72], major histocompatibility complex class I proteins (MHCI) [73], β -integrin [74], and the herpes simplex virus [75]. We found that both HeLa and HepG2 use ADE to initiate RNAi, albeit with different efficiency. In ADE, localization and phosphorylation of Arf6 is dependent upon actin polymerization [55]. Overexpression of actin in HeLa cells reduced siRNA accumulation, whereas in HepG2 cells, actin overexpression enhanced siRNA accumulation. Basal HeLa cell expression of actin mRNA is 2.3-fold higher than in HepG2 cells (Table A-6). Given the different responses of the cell types to actin overexpression, it may be that there is an optimal amount of actin to support ADE, with too much or too little being inhibitory.

We also showed that endocytic inhibitors could be used in a co-cultured population of cells to enhance silencing in multiple cell types or achieve preferential uptake in a given cell type

(Figure 3-4). This was principally observed through treatment with chlorpromazine in H1299, HeLa, and HepG2 cells (Figure 3-4 – purple), cytochalasin D in H1299 cells (Figure 3-4A vs Figure 3-4B-D – green), and dynasore in HeLa cells (Figure 3-4C vs Figure 3-4A, B, & D - red). Given our results, we believe that controlling the design of siRNA delivery vehicles and accounting for the variability in endocytic pathways when delivering siRNAs could allow improved cell specificity in vivo, thereby enhancing the overall delivery efficiency and efficacy of siRNA-based therapeutics.

Although the specific pathways utilized by LF2K are, almost certainly, not ubiquitous among delivery systems, our findings demonstrate that 1) uptake alone is not sufficient to achieve silencing and 2) the role of CCIE endocytosis in siRNA therapeutics warrant additional study. Overall, these findings also support a growing body of evidence that the endocytic pathway used for internalization is dependent on cell type in addition to the characteristics of the cargo. In the field of siRNA therapeutics, these findings suggest that delivery vehicles should be designed to utilize specific endocytic pathways when targeting a particular cell type. By simultaneously enhancing uptake through pathways that initiate RNAi and avoiding uptake through pathways that do not, the efficacy and specificity of siRNA-based therapeutics could be markedly enhanced.

CHAPTER 4: KINETIC ANALYSIS OF THE INTRACELLULAR PROCESSING OF siRNAs BY CONFOCAL MICROSCOPY

4.1 Abstract

Here, we describe a method for tracking intracellular processing of siRNA-containing complexes using automated microscopy controls and image acquisition to minimize user effort and time. This technique uses fluorescence colocalization to monitor dual-labeled fluorescent siRNAs delivered by silica nanoparticles (sNPs) in different intracellular locations, including the early/late endosomes, fast/slow recycling endosomes, lysosomes, and the endoplasmic reticulum. Combining the temporal association of siRNAs with each intracellular location, we reconstructed the intracellular pathways used in siRNA processing, and demonstrate how these pathways vary based on the chemical composition of the delivery vehicle.

4.2 Introduction

Understanding the intracellular processing of siRNA-containing complexes is critical to the design of siRNA delivery vehicles. While siRNAs trafficked to the cytoplasm can be actively incorporated into the RNA interference (RNAi) pathway, endosomal recycling and endolysosomal retention can result in siRNAs being exocytosed or degraded [84,85]. It is estimated that <1% of internalized siRNAs reach the cytoplasm [85]. Thus, to maximize siRNA activity, it is useful to design delivery vehicles to enhance the trafficking of siRNAs to the cytoplasm. However, it is unclear how to optimize delivery vehicle characteristics for optimal intracellular processing [90].

Confocal microscopy is the preferred method to study intracellular trafficking, as fluorescent colocalization analysis can quantify spatiotemporal biological interactions. However, it is currently considered labor intensive, requiring constant operator supervision to maintain well position, focal plane, and cell viability over the duration of the experiment [169,170]. Here, we

describe a method that uses automated multi-well fluorescence imaging of stable cell lines to increase the throughput of live-cell imaging and decrease the labor associated with image collection, while not sacrificing data quantity or quality. We applied our method to characterize the intracellular processing of siRNA-containing complexes and measure kinetic variations that arise from delivery by silica nanoparticles (sNPs) with different chemical compositions.

During the development of our assay, several points of automation were included to reduce operator intervention and improve the throughput of live-cell imaging. Long-term cell viability and function were maintained with a stage-top incubator equipped with temperature, humidity, and CO₂ control. Automated stage controls were used to record and recall the exact X/Y coordinate of an image position, allowing multiple wells to be imaged in a single live-cell experiment. Nikon's Perfect Focus System (PFS) was used to prevent axial drift in the focal plane during long term and multi-well imaging [171]. Finally, a dry objective was used to collect images across multiple wells/positions without continual application of liquid immersion media.

Fluorophores used in live-cell imaging are susceptible to photobleaching, depending on the sensitivity of the fluorophore and the frequency of image acquisition [172]. For our assay, intracellular organelles were labeled through the constitutive expression of fluorescent chimeric proteins, thereby minimizing photobleaching through the continual supply of new fluorophores. Photobleaching of both the siRNA strands and organelles was further minimized by collecting images at multiple positions in each well. This allowed wells to be imaged at short intervals (~30 minutes) while the specific positions in each well were imaged at longer intervals (~1.5 hours) (Figure 4-1).

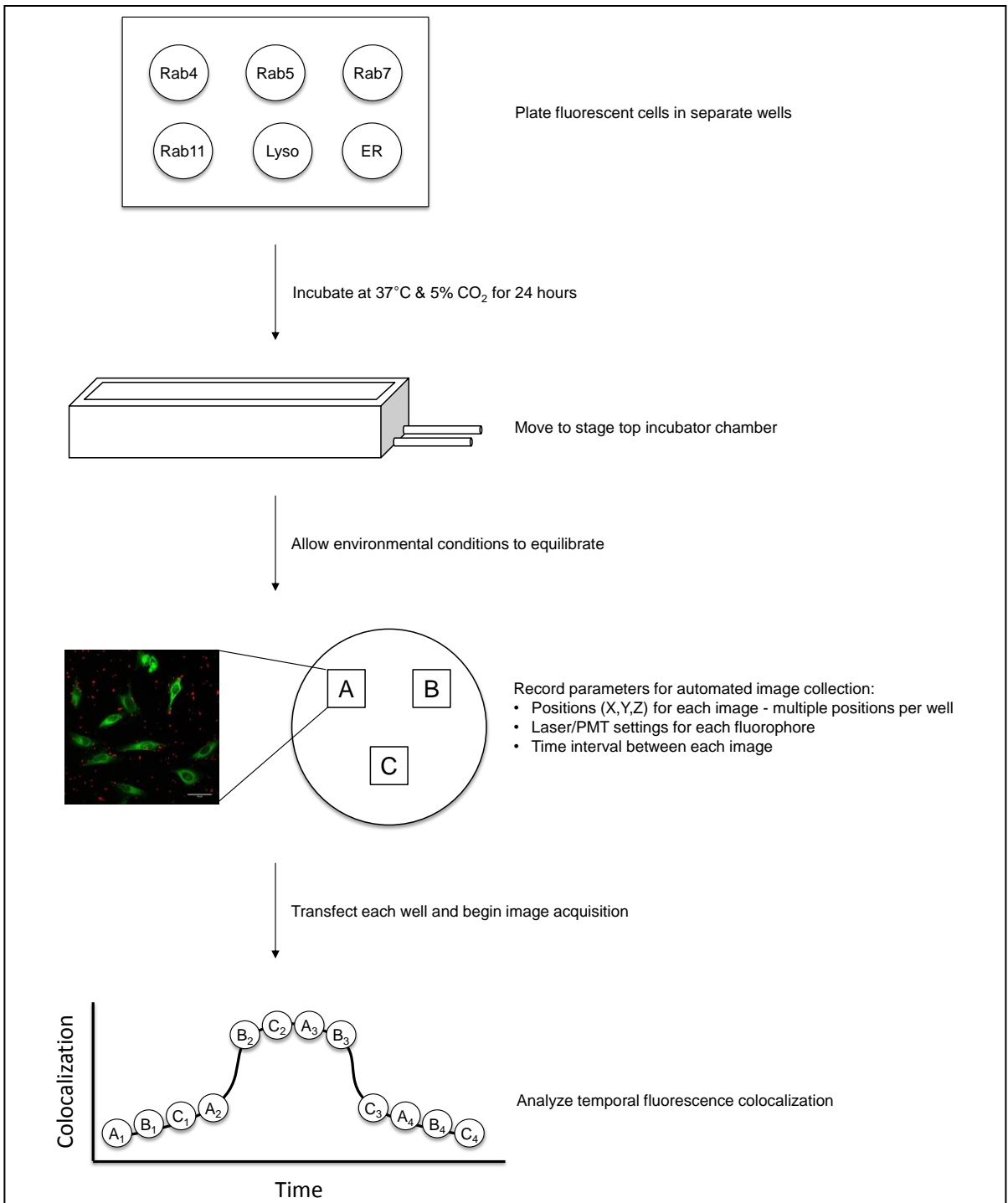


Figure 4-1 Intracellular trafficking flowchart

A flow chart for tracking the intracellular localization of endocytosed molecules. Shown is the protocol for generating live-cell, kinetic colocalization profiles between the molecules and multiple intracellular locations.

To characterize the kinetic association of siRNAs with intracellular locations common to endocytosis and intracellular trafficking, we engineered HeLa cells to express chimeric EGFP-labeled proteins associated with intracellular trafficking: Rab4, Rab5, Rab7, Rab11, Lysosomal Associated Membrane Protein 1 (LAMP1), and Calreticulin (Endoplasmic Reticulum –ER) (Figure 4-2). Ras-like GTPases (Rab) proteins, of which over 60+ members have been identified in humans, are associated with membrane trafficking [173]. Each Rab protein has distinct intracellular localization and trafficking through their association with motor, membrane, and SNARE proteins [173]. Endosomal membranes often contain multiple Rab proteins that promote sorting of contents to distinct regions of the membrane and trafficking to different intracellular destinations [174]. Rab5 is associated with the recycling endosome and endosomal maturation, but the majority of activated Rab5 is localized to the early endosome (EE) [175]. Rab4, also localized in the EE, regulates fast endosomal recycling from the EE to the plasma membrane (PM) [176]. Rab11 mediates slow endosomal recycling from the EE to an intermediate recycling endosome (RE) before trafficking to the PM [177]. Rab7 directs trafficking and fusion of the LE to the lysosome [178]. Endosomal maturation from EE to LE is characterized by a simultaneous increase in Rab7 and decrease in Rab5 [179]. Lamp1 is a transmembrane protein primarily residing in the lysosome [180]. Calreticulin is a calcium binder that resides in storage compartments of the ER [181].

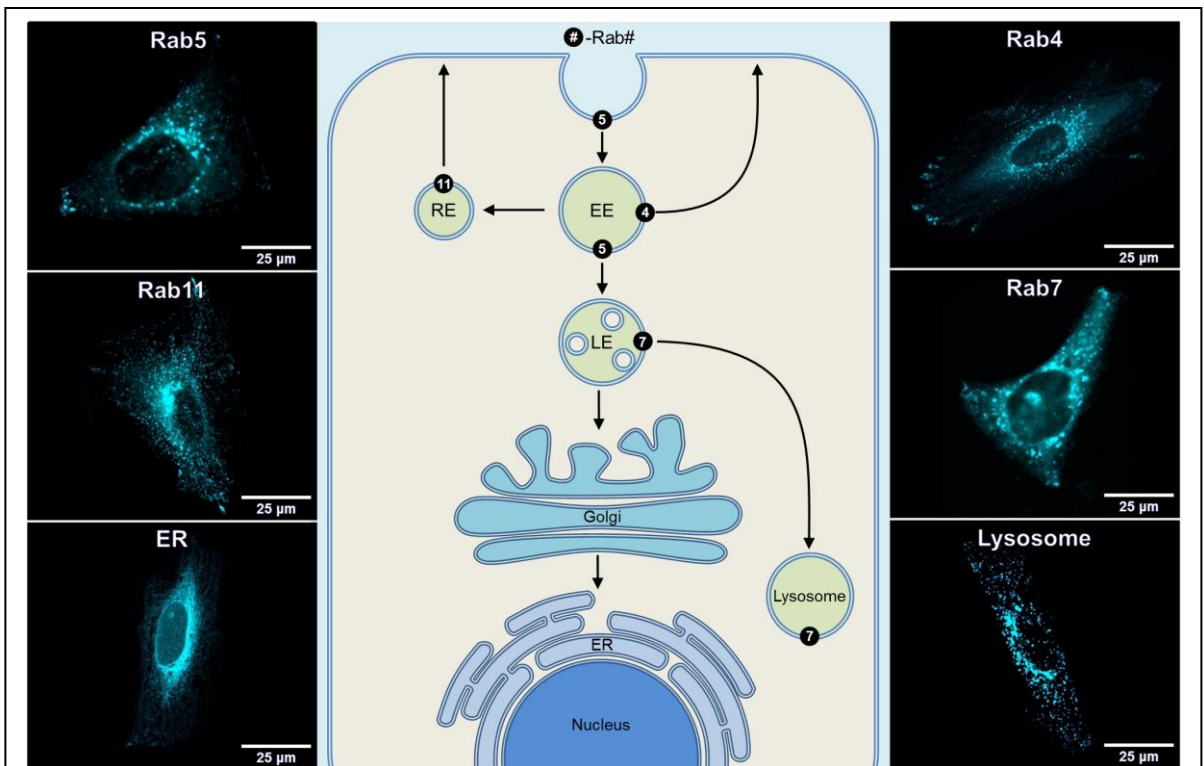
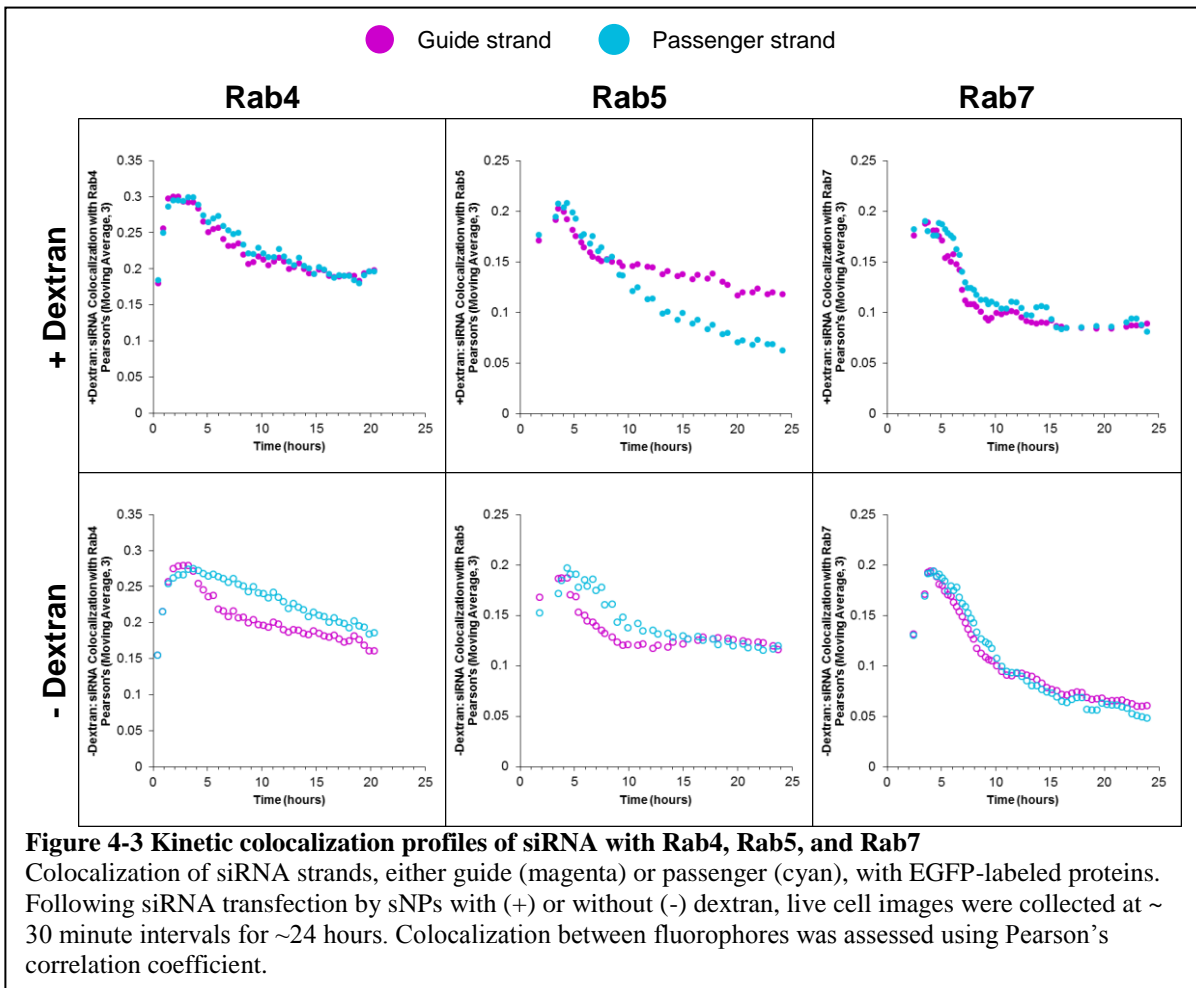


Figure 4-2 Intracellular trafficking pathways in eukaryotic cells

To track the intracellular location of fluorescent molecules, HeLa cells were engineered to express EGFP-labeled proteins. Rab5 (5) facilitates receptor mediated endocytosis and vesicle fusion with the early endosome (EE). Rab4 (4) regulates fast endosomal recycling from the EE to the plasma membrane (PM), and Rab11 (11) mediates slow endosomal recycling through the recycling endosome (RE). Rab7 (7) directs trafficking and fusion of the late endosome (LE) with the lysosome. Lysosomal Associated Membrane Protein 1 (LAMP1) is used as a marker for the Lysosome, and Calreticulin as a marker for the endoplasmic reticulum (ER).

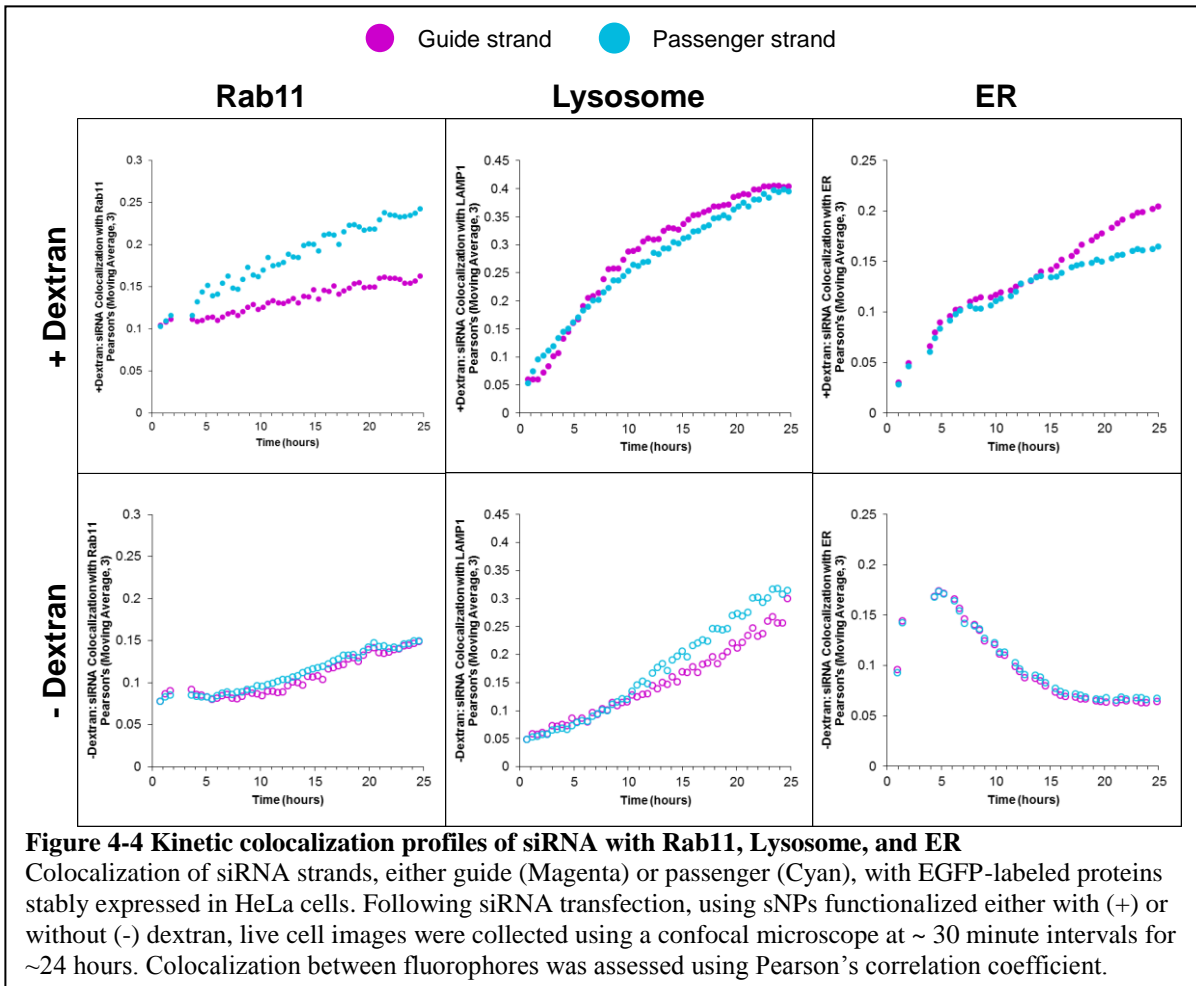
In our previous work, we demonstrated that the activity of siRNAs was altered by the presence of dextran in the sNP delivery vehicles [1]. As both formulations of sNPs (with and without dextran) were capable of delivering siRNAs to cells (as quantified through flow cytometry), we hypothesized that the addition of dextran significantly altered the intracellular processing of the siRNAs. Here, we have investigated the kinetics of siRNA intracellular trafficking associated with delivery by sNPs +/-dextran over a ~24 hour period, with data collected at ~ 30 minute intervals (Figures 4-3 & 4-4). The kinetic association of each siRNA strand (guide and passenger) with Rab4-, Rab5-, and Rab7-containing vesicles was similar, with

rapid accumulation, retention, and decay for siRNAs delivered by either sNP (Figure 4-3). While siRNAs trafficked to Rab7 were unaffected by dextran functionalization, siRNAs delivered by the -dextran sNP had greater retention of the passenger strands in Rab4- and Rab5-containing vesicles than the guide strands. This would suggest that functionalizing sNPs with dextran alters the way siRNA strands are initially processed in fast/early endosomes (Rab4/5) but does not affect their subsequent trafficking to late endosomes (Rab7).



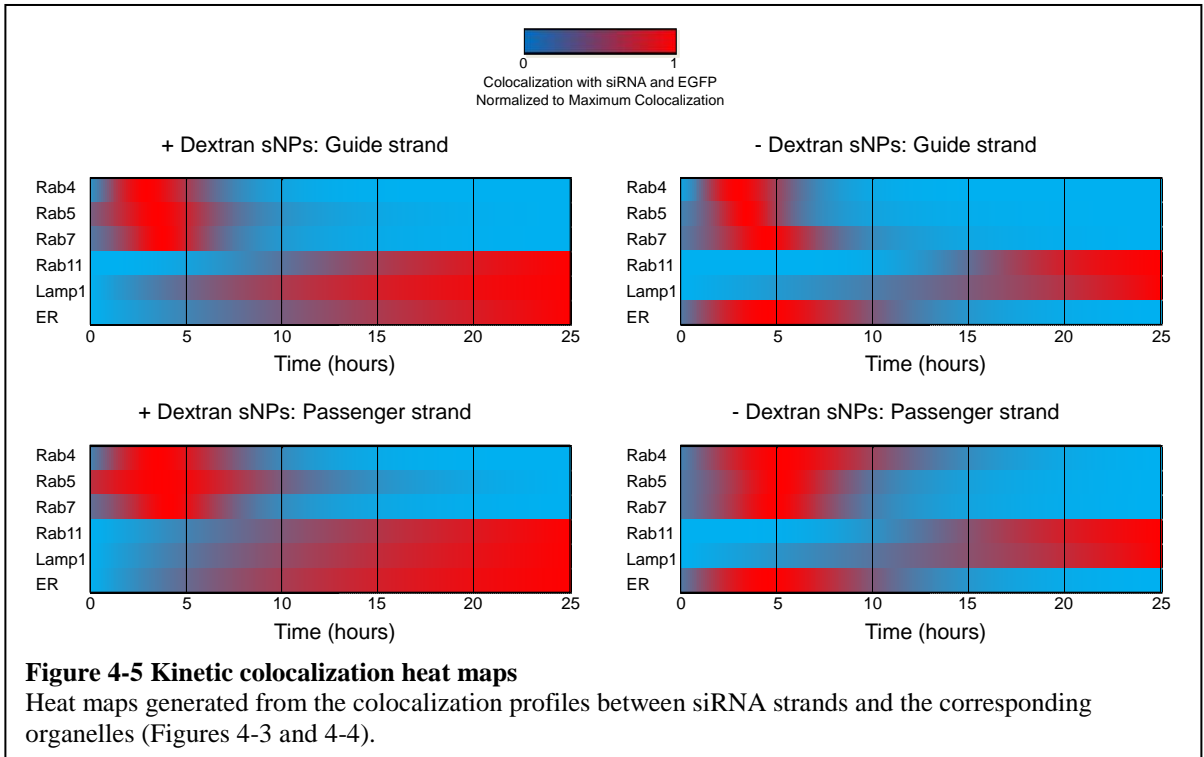
In Rab11-containing vesicles, the accumulation of passenger/guide strands was similar when delivered by sNPs -dextran, whereas siRNAs delivered by sNPs +dextran had greater accumulation of passenger strands than guide strands. In the lysosome, there was little difference between the trafficking of siRNA strands when delivered by either sNP, however the rate of

siRNA accumulation in the lysosome decreased over the duration of the experiment for sNPs +dextran, but increased for sNPs -dextran. The greatest difference in siRNA trafficking between sNPs was observed in the ER where siRNA strands delivered by sNPs -dextran were only briefly localized, whereas siRNA strands delivered by sNPs +dextran steadily accumulate over time.



Using the combined data sets of intracellular localization, we determined the intracellular pathway used by each siRNA strand and compared the differences between delivery by the different sNPs (Figure 4-5). Initially, siRNAs rapidly accumulate in the EE and colocalize to regions associated with fast endosomal recycling (Rab4) and endosomal maturation (Rab5/7). Variations in siRNA strand trafficking are observed, with greater retention of the passenger strand than the guide strand in Rab5 vesicles. After the EE, siRNAs began to accumulate in

lysosomes, recycling endosomes (Rab11), and the ER. The primary distinction in siRNA trafficking between sNPs +/-dextran occurred in the ER, where siRNA colocalization diminishes over time for sNPs -dextran but increases for sNPs +dextran. Further, the accumulation and retention of the passenger strand was biased towards fast endosomal recycling when delivered using sNPs -dextran but slow endosomal recycling when using sNPs +dextran.



4.3 Discussion

Here, we have described an automated method that increases the throughput of confocal microscopy for analyzing the trafficking of endocytosed material. Comparing the kinetic colocalization profiles of guide and passenger siRNAs, this assay was capable of detecting changes in colocalization across multiple intracellular locations and methods of delivery. This assay is beneficial to studying of the impact of the characteristics of delivery vehicles on siRNA trafficking and activity. However, there is considerable potential for further optimization, by expanding the scope of the assay to include additional intracellular pathways and organelles.

Further, we believe that the findings presented demonstrate the potential applications of this assay to a variety of cellular processes involving the intracellular transport of therapeutic cargo, such as DNA, mRNA, small molecules, and peptides.

CHAPTER 5: CONCLUSIONS AND FUTURE WORK

5.1 Conclusions

The purpose of these studies was to better understand how the characteristics of delivery vehicles impact the active delivery of siRNAs. The use of sNPs allowed changes to be made in the chemical functionality of the particles while maintaining relatively constant physical characteristics. By varying amine content, it was shown that optimizing siRNA binding affinity enhances silencing. Additionally, the utility of sNPs was enhanced through dextran functionalization, which facilitated uptake by a clathrin/caveolin-independent endocytic pathway. The combination of these findings resulted in a sNP with no observable cytotoxicity and silencing comparable to LF2K. These findings could be applied to additional delivery systems, such as lipids or polymers, to further enhance the efficiency of siRNA delivery vehicles.

In light of recently discovered CCIE pathways, we developed a novel assay that differentiates uptake by each of the endocytic pathways and can be used to determine the functional role of a pathway in initiating RNAi. Our results are the first to demonstrate that LF2K utilizes GME, ADE, or FME for the initiation of RNAi, depending on the cell type. We also showed that, in each cell type, a portion of the siRNA-containing complexes is internalized by endocytic mechanisms that do not lead to silencing. Moreover, we demonstrated that understanding the endocytic pathways that are important for uptake of siRNA-containing complexes allow enhancement of cell-specific uptake in a mixed cell population. These findings suggest delivery vehicles should be designed to utilize specific endocytic pathways.

While siRNA therapeutics have been approved for clinical use, their continued development is hindered by a lack of information regarding the intracellular pathways used by endocytosed siRNAs. To address these shortcomings, we developed a confocal based assay that uses live-cell

automated image acquisition to assess the intracellular trafficking of siRNAs. Here we identified the intracellular pathways used by siRNAs and correlated differences in siRNA trafficking to specific delivery vehicle characteristics, i.e., dextran functionalization enhanced siRNA accumulation and retention in the ER. These findings suggest that delivery vehicle characteristics can be used to optimize the intracellular trafficking of siRNAs.

5.2 Future Work

The results of these studies, while beneficial to the design of delivery vehicles, also present new questions for the field of siRNA therapeutics. Outlined below are possible future directions resulting from the studies presented in this dissertation.

5.2.1 Silica Nanoparticle Optimization

Given the success of the dextran sNPs and the well-established synthesis methods using the modified Stöber process [182], additional experiments could be performed on a variety of delivery vehicle characteristics and functional groups. While some initial experiments were conducted on sNPs of different sizes and types of dextran, optimizing the reproducibility of nanoparticle synthesis would aid in the discovery of characteristics essential for siRNA delivery. In addition to the current methods used to characterize the sNPs (dynamic light scattering (DLS), zeta-potential, and TEM), it would be beneficial to further characterize the sNPs for their respective molecular weight [183], concentration of accessible amines/dextran [184,185], and their stability in solution [186], to ensure consistency between syntheses.

Once fully characterized, the silencing capacity of different delivery vehicle characteristics could be assessed across multiple cell types to generate cell specific design criteria. Delivery vehicle characteristics could also be assessed for their specific role in endocytosis and intracellular trafficking using the assays outlined in chapters 3 and 4 of this dissertation.

5.2.2 Predicting Optimal Endocytic Pathways

The work presented in chapter 3 suggested that endocytic pathways compete for shared resources. The relative expression of these regulatory proteins in a cell may predict which endocytic pathway is optimal for a siRNA delivery vehicle. The first step would be determining the best endocytic pathway for siRNAs in multiple cell types and, then identifying trends in proteins expression that correlate with uptake by a particular endocytic pathways. As discussed in chapter 3, the oncogenesis of NSCLC is characterized by changes in the expression of flotillin and caveolin proteins. Comparing the optimal endocytic pathway for siRNA delivery in both healthy lung cells and in H1299s would make possible the study of the effect of disease states on endocytosis. Further, if a disease state altered the expression of regulatory proteins to the extent that the optimal endocytic pathway for siRNA delivery is changed, then inhibition of the original endocytic pathway would limit siRNA delivery to diseased cells.

5.2.3 Additional Intracellular Pathways

As stated in previous chapters, there is a lack of information regarding the intracellular events associated with siRNA delivery [90]. While the assay detailed in chapter 4 incorporates the basic intracellular locations associated with cargo transport, the overall scope of the assay would be enhanced by additional cell lines. In addition to the those presented in chapter 4, stable EGFP constructs were also generated in HeLa cells for the following endocytosis-related proteins, clathrin, caveolin, Arf6, Graf1, flotillin-1, flotillin-2, actin, and dynamin; RNAi-related proteins, TRBP, Dicer, and Ago2; and trafficking-related proteins, TPST2 (Golgi) and Rab9. Generating stable constructs for the following Rab proteins would allow the intracellular trafficking assay to encompass retrograde transport and exocytosis of siRNAs [173]: Rab22 (EE → Golgi), Rab24

(Golgi/ER → Lysosome), Rab13 (Golgi → RE), Rab31 (Golgi → EE/LE), Rab2 (Golgi → ER),
Rab1 (ER → Golgi).

APPENDICES

APPENDIX A: Materials and Methods for Chapter 2

Materials

- 4-Well Confocal Plate (LabTek, #155383)
- 96-Well Plate (Costar, #3610)
- Acetic Acid (J.T. Baker, #15500760)
- Ammonium Hydroxide (Sigma, #320145-500ML)
- APTES: (3-Aminopropyl) triethoxysilane (Sigma, #A3648-100ML)
- Chlorpromazine hydrochloride (Sigma, #C8138-5G)
- Copper Grids, 200 Mesh (Electron Microscopy Sciences, #G200-Cu)
- Cytochalasin D (Sigma, #C2618-200uL)
- DAPI: (4',6-Diamidino-2-phenylindole dihydrochloride) (Sigma, #10236276001)
- Dextran Sulfate, Mw 500k (Sigma, #D6001)
- Dextran, Mw 10k (Sigma, #D9260-10G)
- DMEM (Life Technologies, #11965092)
- DPBS: Dulbecco's NaCl/Pi (Life Technologies, #14040133)
- Ethanol (VWR, #89125-164)
- Fetal Bovine Serum (Life Technologies, #16000044)
- Filipin Complex III (Sigma, #F4767-1MG)
- Formaldehyde/Glutaraldehyde, 2.5% each in 0.1M Sodium Cacodylate Buffer, pH 7.4 (Electron Microscopy Sciences, #15949)
- Formvar Solution in Ethylene Dichloride (Electron Microscopy Sciences, #RT 15820)
- Geneticin (Life Technologies, #10131-035)
- Heparin (Sigma, #H3393-25KU)
- Lead Citrate (Electron Microscopy Sciences, #512-26-5)
- Lipofectamine 2000 (Life Technologies, #11668019)
- Milli-Q Water, 18 M Ω (Millipore, #QTUM000IX)
- Opti-MEM (Life Technologies, #11058021)
- Osmium Tetroxide, 1% (Electron Microscopy Sciences, #19152)
- pDNA (pd2EGFP-N1, clontech #6009-1)
- Penicillin/Streptomycin (Life Technologies, #15140122)
- Round-Bottom Tubes, 5 ml (BD Falcon, #352063)
- siRNA: Sense 5'-GCUGACCCUGAAGUUCAUC-3'; Antisense 5'-GAUGAACUUCAGGGUCAGC-3' (Dharmacon)
- Fluorescent siRNA: Sense DY547-5'-GCUGACCCUGAAGUUCAUC-3'; Antisense 5'-GAUGAACUUCAGGGUCAGC-3' (Dharmacon)
- Sodium Cacodylate Buffer (Electron Microscopy Sciences, #11653)
- Sphero Rainbow Calibration Particles (Spherotech)
- Spurr Resin (Electron Microscopy Sciences, #14300)
- SYBR gold staining (Life Technologies, #S-11494)
- TEOS: Tetraethyl Orthosilicate (Sigma, #86578-250ML)
- Trypsin (Life Technologies, #25200056)
- Ultracel Regenerated Cellulose Membrane, 30 kDa NMWL, 47 mm (Millipore, #PLTK04710)
- Uranyl Acetate (Electron Microscopy Sciences, #22400)

Cell Culture

H1299 cells constitutively expressing a 2 h half-life EGFP were generously provided by Dr. J. Kjems (University of Aarhus, Denmark). H1299 and HeLa cells were maintained in DMEM High Glucose, 10% fetal bovine serum, and 1% penicillin/streptomycin. 1% Geneticin was included in the H1299 culture medium to maintain EGFP expression. Cells were incubated at 37°C in 5% CO₂, at 100% relative humidity, and subcultured every 4–5 days by trypsinization.

Synthesis of Silicon Nanoparticles

A 500 mL round bottom Schlenk flask was charged with 150 mL of absolute ethanol and 50 mL of Milli-Q water with constant stirring. Dextran (9-11 kDa, 2.4×10^{-6} mol, 24 mg) was dissolved in 10 mL of Milli-Q water and added, followed by 10 mL of NH₄OH (~30% as NH₃). Tetraethyl orthosilicate (TEOS) (2.4 mmol, 0.53 mL) was added dropwise via syringe. The mixture was stirred for 10 minutes at room temperature (RT) under nitrogen followed by addition of (3-Aminopropyl) triethoxysilane (APTES) (concentration varied as mole percentage of TEOS; e.g., 40% APTES used 0.96 mmol, 0.224 mL). The reaction mixture was stirred for 24 h at RT under nitrogen atmosphere and purified by pressure filtration using an Ultracel regenerated cellulose membrane (Millipore) at 40 psi and rinsed three times with Milli-Q water (18 MΩ). The filtered solids were suspended in Milli-Q water and sonicated until well dispersed.

Zeta Potential

A Malvern Zetasizer Nano ZS was used to determine the zeta potential (mV) of sNPs. Measurements were collected using 1 mg/mL of sNP in HEPES buffer.

EGFP Silencing Analysis

H1299-EGFP cells were seeded in 96-well plates at a density of 200,000 cells/ml in 100 μ l of growth media without antibiotics. Cells were treated 24 h post-seeding with a 50 μ L transfection solution containing Opti-MEM, siRNA, and delivery vehicle that was mixed for 30 min prior to addition to the cells. Final concentrations were maintained at 100 nM siRNA in either 2.3 μ g/ml Lipofectamine 2000 (LF2K) or 200 μ g/mL sNP. Cells were incubated in the transfection solutions at 37°C, 5% CO₂, and 100% humidity. At 24 h after transfection, cells were washed twice with Dulbecco's NaCl/Pi (DPBS), and EGFP fluorescence was quantified with a Gemini EM fluorescent plate reader (Molecular Devices) at 480 nm excitation and 525 nm emission. Fluorescence intensity was normalized to control wells treated with a delivery vehicle but no siRNA. Cell morphology and EGFP expression as a measure of cytotoxicity was assessed by microscopy and was not observed in any of the treatments (Figure 2-6).

HeLa cells were seeded in 96-well plates at a density of 100,000 cells/ml in 100 μ l of antibiotic-free growth media. Cells were treated 24 h post-seeding with a 50 μ L transfection solution containing Opti-MEM, 20 ng pd2EGFP-N1, and 2.3 μ g/ml LF2K. Cells were then treated with a 50 μ L transfection solution containing Opti-MEM, siRNA, and delivery vehicle that was mixed for 30 min prior to addition to the cells. Final concentrations were maintained at 100 nM siRNA in either 2.3 μ g/ml LF2K or 200 μ g/mL sNP. Cells were incubated in the transfection solutions at 37°C, 5% CO₂, and 100% humidity. Cells were washed 4 h post-transfection with antibiotic free growth media. At 24 h after transfection, cells were washed twice with DPBS, and EGFP fluorescence was quantified with a Gemini EM fluorescent plate at 480 nm excitation and 525 nm emission. Fluorescence intensity was normalized to control wells treated with a delivery vehicle but no siRNA (Figure 2-5). Cell morphology and EGFP

expression as a measure of cytotoxicity was assessed by microscopy and was not observed in any of the treatments.

Inhibition experiments

EGFP-expressing H1299 cells were seeded in 12-well plates at a density of 150,000 cells/well and cultured in antibiotic free growth media. Immediately prior to transfection, cells were washed with media and replaced with inhibitor containing media for the appropriate pre-treatment time: chlorpromazine (10 µg/ml, 30 min), filipin complex III (2µg/ml, 60 min), cytochalasin D (5µg/ml, 15 min), temperature (4°C, 60 min), and 500 kDa Dextran Sulfate (200 µg/ml, 30 min). Following pre-treatment, cells were treated with 100 µL of various transfection solutions in Opti-MEM (200 nM siRNA and either 2.3 µg/mL LF2K or 200 µg/mL sNP) and incubated at 37°C, 5% CO₂, and 100% relative humidity. Cells were washed 4 h post-transfection with media containing 20 µg/mL heparin for 15 minutes at 37°C to remove extracellularly bound complexes. Antibiotic-free media was then added to the cells.

For FACS analysis, cells were trypsinized 24 h post-transfection, pelleted by centrifugation (200 g) at 4°C, and re-suspended in DPBS. The cells were then transferred into 5 mL round bottom tubes. Immediately prior to analysis, cells were treated with DAPI at a final concentration of 1 µg/mL for live/dead analysis. Cells were analyzed using a Becton Dickinson Influx Flow Cytometer to detect DAPI (355/460), EGFP (488/530), and Dy547 tagged siRNA (561/585), gated to include 10,000 events/sample. For comparison across experiments, the instrument was calibrated using Sphero Rainbow Calibration particles. Geometric mean was used to calculate fluorescence intensity values among samples. EGFP fluorescence was normalized to particle

only controls treated with the corresponding inhibitor. Dy547 fluorescence was normalized to the uptake of siRNA only (no vehicle) controls.

HeLa cells were seeded in 96-well plate in antibiotic-free growth media. Cells were transiently transfected 24 h post-seeding with pd2EGFP-N1 and LF2K. Immediately prior to transfection, cells were washed with media and replaced with inhibitor containing media for the appropriate pre-treatment time and incubated at 37 °C, 5% CO₂, and 100% humidity. Cells were washed 4 h post-transfection with antibiotic free growth media. Cells were washed twice with DPBS 24 h post-transfection and EGFP fluorescence was quantified using a Gemini EM fluorescent plate reader at 480 nm excitation and 525 nm emission. Fluorescence intensity was normalized to control wells treated with a delivery vehicle but no siRNA (Figure 2-5). Cell morphology and EGFP expression as a measure of cytotoxicity was assessed by microscopy and was not observed in any of the treatments.

Transmission Electron Microscopy/Energy Dispersive X-ray Spectroscopy (EDS)

Intracellular TEM: EGFP-expressing H1299 cells were seeded in 6-well plates at a density of 400,000 cells/well and cultured in antibiotic-free media. Cells were treated 24 h post-seeding with 200 µL transfection solutions (Opti-MEM, 200 nM siRNA, and 200 µg/mL sNP) and incubated at 37°C, 5% CO₂, and 100% relative humidity. Cells were trypsinized 24 h post-transfection and pelleted by centrifugation (200 RCF) at 4°C. Samples were fixed using 2.5% formaldehyde/glutaraldehyde in DPBS, stained with 1% osmium tetroxide in DPBS, dehydrated through a graded series of ethanol concentrations, and embedded in Spurr resin. Samples were sectioned to a thickness of ~90 nm using an RMC MYX ultramicrotome and placed onto a 200 mesh formvar coated copper grid. Samples were additionally stained with uranyl acetate and lead

citrate. Images were acquired using a JEOL 100CXII transmission electron microscope operating at an accelerating voltage of 100 keV and equipped with an Olympus MegaView III digital camera. EDS analysis was performed on JEOL 2200FS transmission electron microscope operating at an accelerating voltage of 200 keV.

Confocal Microscopy

EGFP-expressing H1299 cells were seeded in 4-well plates at a density of 75,000 cells/well and cultured in antibiotic free growth media. Immediately prior to transfection, cells were washed with media and replaced with inhibitor-containing media for the appropriate pre-treatment time: chlorpromazine (10 $\mu\text{g/ml}$, 30 min), filipin complex III (2 $\mu\text{g/ml}$, 60 min), cytochalasin D (5 $\mu\text{g/ml}$, 15 min), and 500 kDa Dextran Sulfate (200 $\mu\text{g/ml}$, 30 min). Following pre-treatment, cells were treated with 100 μL of various transfection solutions in Opti-MEM (200 nM siRNA and either 2.3 $\mu\text{g/mL}$ LF2K or 200 $\mu\text{g/mL}$ sNP) and incubated at 37°C, 5% CO₂, and 100% relative humidity. Cells were washed 4 h post-transfection with Opti-MEM to remove extracellularly bound complexes and imaged 4 h and 24 h post-transfection (Figures 2-7 and 2-8).

Confocal images were taken using an Olympus FluoView 1000 Spectral-based Laser Scanning Confocal Microscope. An Olympus PLAPON 60x/1.42 oil objective was used to acquire all images. EGFP (488/530) fluorescence was measured using an excitation of 488 nm with a multi-line Argon laser, and displayed as green (LUT). Dy547 (559/568) fluorescence (siRNA) was excited at 559 nm by a HeNe laser, and displayed as red (LUT). The focal plane for each image was chosen based on the highest intensity EGFP fluorescence. All images were collected sequentially as single XY images and used 2 count Line Kalman averaging.

Acidic Degradation

sNPs were dispersed in acetic acid (pH 4.75) at a concentration of 0.5 mg/ml and incubated at RT. After 16 h, the samples were centrifuged and washed three times with DPBS (Invitrogen). Samples were prepared for imaging by placing 5 μ l of sample onto a 200 mesh formvar coated copper grid and air dried overnight. Images were acquired using a JEOL 100CXII transmission electron microscope operating at an accelerating voltage of 100 keV and equipped with an Olympus MegaView III digital camera.

Polyacrylamide Binding Gels

Solutions were prepared in DPBS, using 200 nM siRNA, and 200 μ g/ml sNP, and allowed to incubate for 30 min. Milli-Q water (pH 7, control) or acetic acid (pH 4.75) was added to the sample and incubated at RT. After 16 h, the samples were centrifuged to pellet the sNPs, washed with Milli-Q water, and suspended in DPBS. Each sample was mixed with 300 μ g/ml heparin (Sigma) for 3 min to elute the siRNAs from the sNPs and then resolved on a 12% polyacrylamide gel. In lieu of centrifugation and washing, siRNA samples without sNP were diluted with Milli-Q water. Nucleic acid detection was performed with SYBR gold staining, imaging was performed with the Molecular Imager ChemiDoc XRS System, and analysis was performed using ImageJ [187].

Statistical analyses

Multiple comparisons were performed with two-way ANOVA followed by Tukey's HSD post hoc analysis (Tables 2-3, 2-3, & 2-4). Analyses were performed using OriginPro 8 and Microsoft Excel.

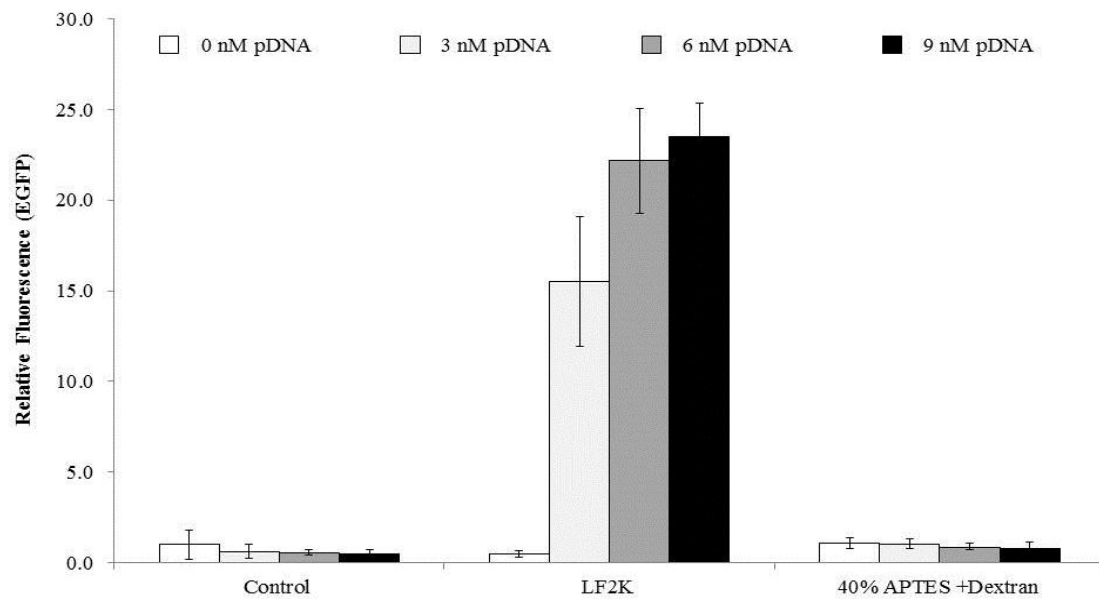


Figure A-1 Plasmid transfection efficiency of sNPs

The relative fluorescence of EGFP in HeLa cells 24 h post-transfection with pd2EGFP-N1 vehicle complexes. Results are normalized to the EGFP fluorescence of vehicle-only control cells at 0 nM pDNA. The complexes contain either 2.3 $\mu\text{g/ml}$ of LF2K or 200 $\mu\text{g/ml}$ of 40% APTES +dextran sNP, and either 0, 3, 6, or 9 nM of pDNA. Error bars represent + 1 standard deviation; n = 3.

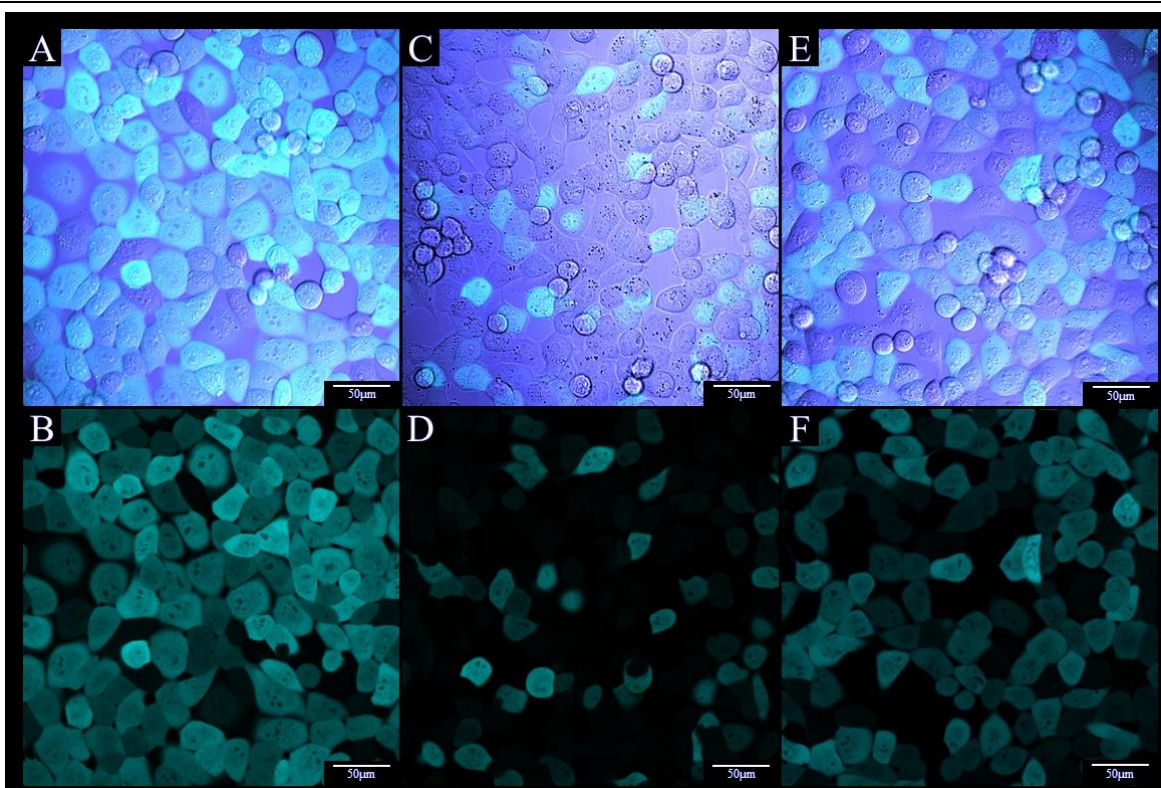


Figure A-2 Confocal microscopy of non-inhibited silencing – 24 h post-transfection

Confocal images of various siRNA-vehicle complexes 24 h post transfection into EGFP-expressing H1299 cells. Cyan fluorescence represents the EGFP-expressing cells. Gray scale images were obtained from a phase contrast objective. A,B) Control cells with no delivery vehicle. C,D) 2.3 µg/ml of LF2K and 100 nM siRNA. E,F) 200 µg/ml of 40% APTES +dextran and 100 nM siRNA. Scale bars are 50 µm.

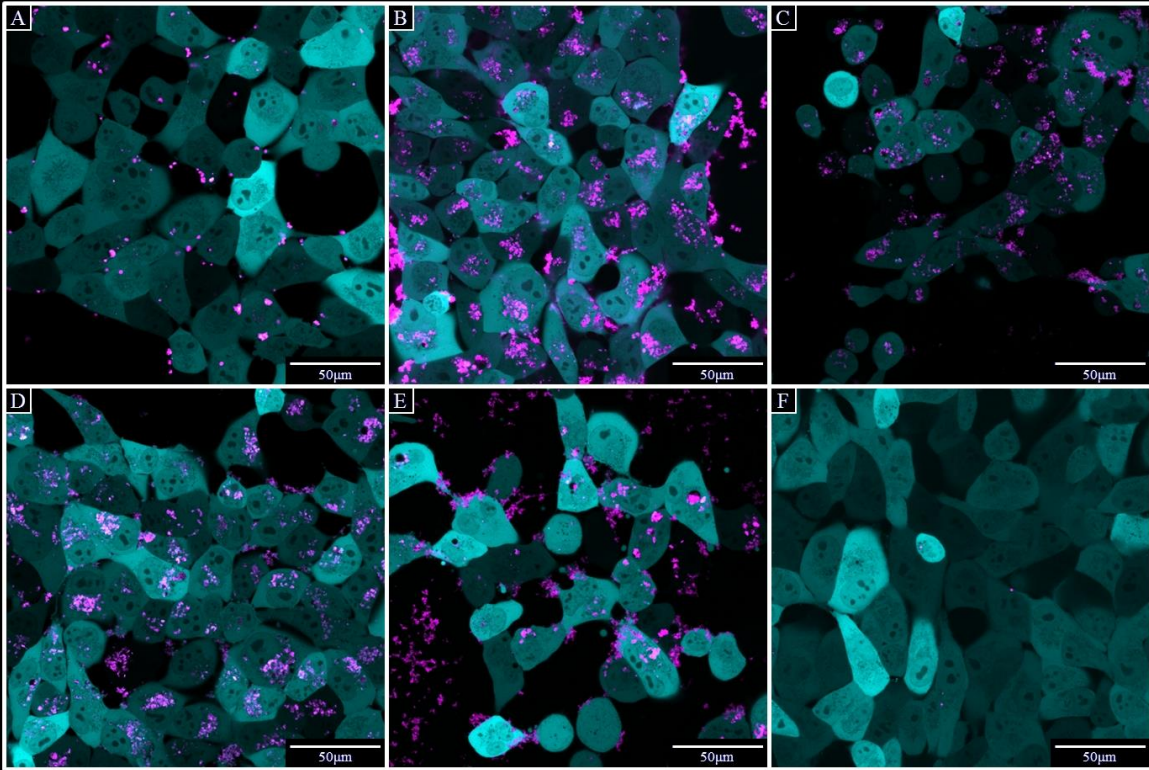


Figure A-3 Confocal microscopy of inhibited silencing - 4 h post-transfection

Confocal images of EGFP-expressing H1299 cells (Cyan) using 100 nM fluorescently labeled siRNA (Magenta) and either (A) 2.3 µg/ml LF2K or (B-F) 200 µg/ml of 40% APTES +dextran sNP. Images (C-F) were pre-treated with endocytosis inhibitors and imaged 4 h post-transfection. Inhibited pathway (inhibitor): C) Clathrin (Chlorpromazine), D) Caveolae (Filipin), E) Actin (Cytochalasin D), and F) Scavenger Receptors (Dextran Sulfate).

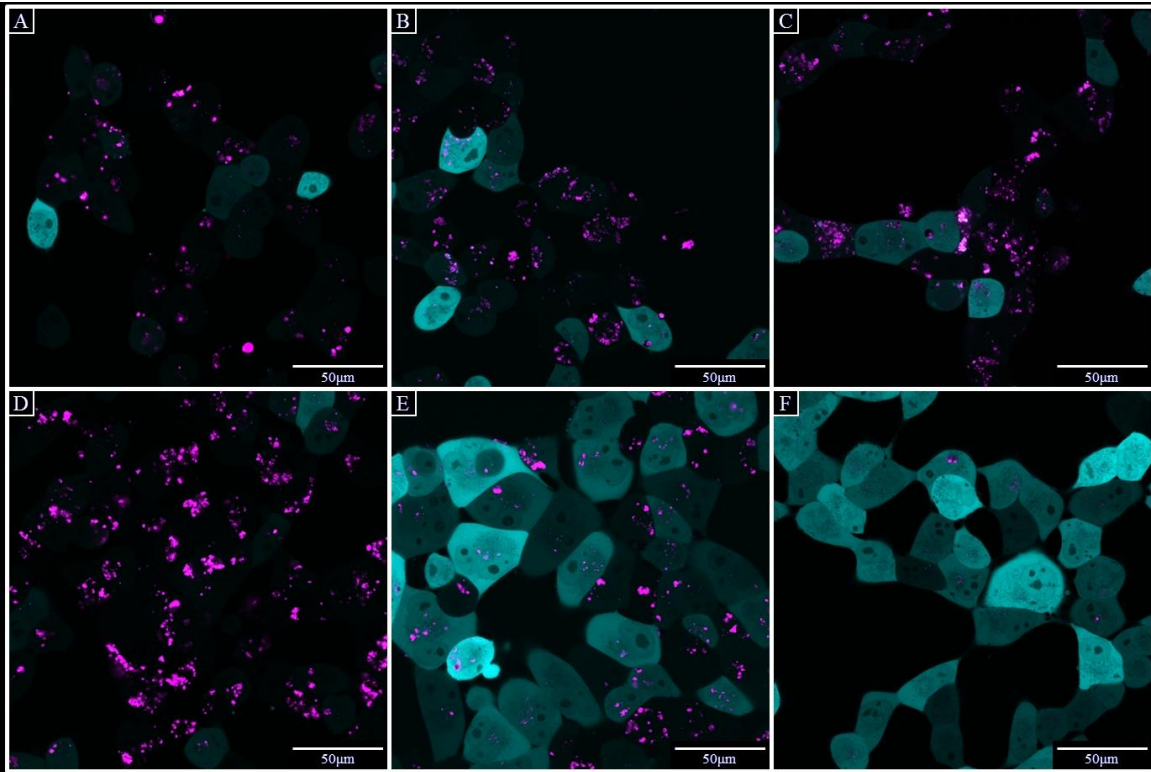


Figure A-4 Confocal microscopy of inhibited silencing – 24 h post-transfection
 Confocal images of EGFP-expressing H1299 cells (Cyan) using 100 nM fluorescently labeled siRNA (Magenta) and either (A) 2.3 µg/ml LF2K or (B-F) 200 µg/ml of 40% APTES +dextran sNP. Images (C-F) were pre-treated with endocytosis inhibitors and imaged 24 h post-transfection. Inhibited pathway (inhibitor): C) Clathrin (Chlorpromazine), D) Caveolae (Filipin), E) Actin (Cytochalasin D), and F) Scavenger Receptors (Dextran Sulfate).

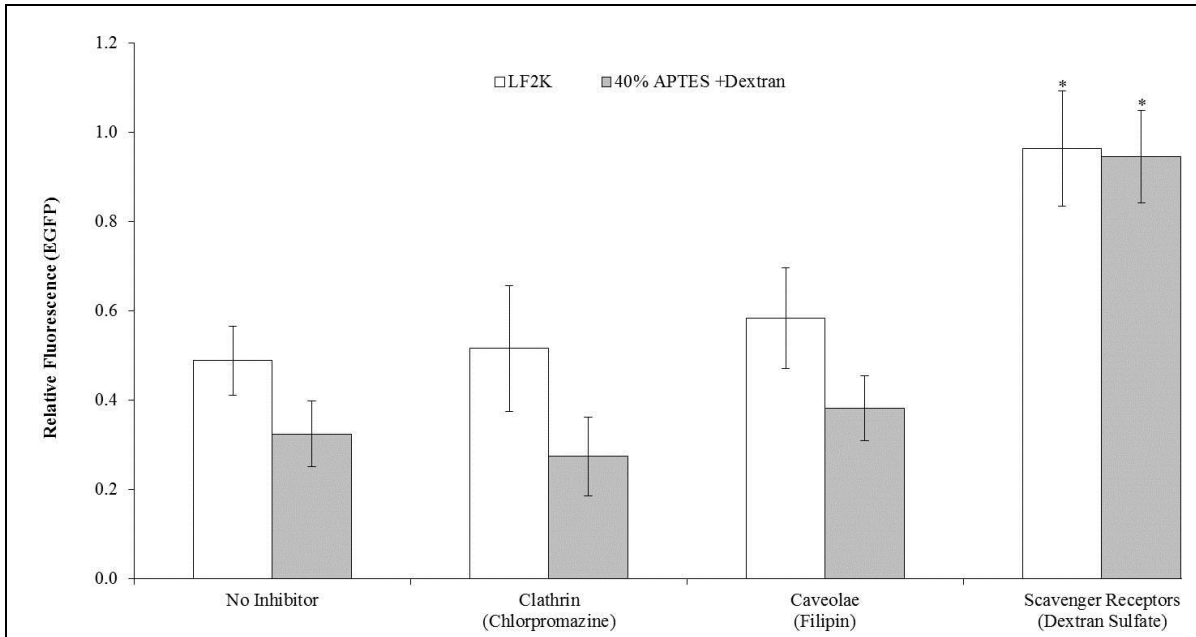


Figure A-5 EGFP silencing in the presence of endocytotic inhibitors (HeLa)

Relative fluorescence of EGFP-expressing HeLa cells transfected with siRNA complexes. Cells were pre-treated with endocytosis inhibitors and assayed 24 h post-transfection by flow cytometry. Results were normalized to particle-only controls within corresponding inhibitors. Error bars represent + 1 standard deviation; n = 3. Statistical analysis was performed using two-way ANOVA, followed by Tukey's HSD post-hoc analysis. *Significant difference ($p < 0.05$) as compared to conditions without inhibitors.

Table A-1 Statistical analysis for Figures 2-2 and 2-3

Analyses were performed using two-way ANOVA, followed by Tukey's HSD post-hoc analysis in Origin 8. DF - Degrees of Freedom, Sig Flag - Significance flag, where 0 indicates no significance ($p > 0.05$) level and 1 indicates significance ($p < 0.05$).

		Control (EGFP Fluorescence)					LF2K (EGFP Fluorescence)					40% APTES + Dextran (EGFP Fluorescence)				
		DF	t value	P-Value	Alpha	Sig Flag	DF	t value	P-Value	Alpha	Sig Flag	DF	t value	P-Value	Alpha	Sig Flag
		No Inhibitor	Clathrin (Chlorpromazine)	12	1.466	0.940	0.05	0	12	0.022	1.000	0.05	0	12	0.800	0.997
Caveolae (Filipin)	12		0.436	1.000	0.05	0	12	0.485	1.000	0.05	0	12	1.060	0.988	0.05	0
Clathrin and Caveolae	12		0.344	1.000	0.05	0	12	1.000	0.990	0.05	0	12	1.778	0.864	0.05	0
Actin (Cytochalasin D)	12		0.495	1.000	0.05	0	12	4.427	0.091	0.05	0	12	8.033	1.36E-04	0.05	1
Active Delivery (4oC)	12		0.503	1.000	0.05	0	12	12.688	1.77E-05	0.05	1	12	10.040	4.56E-06	0.05	1
Scavenger Receptors (Dextran Sulfate)	12		0.238	1.000	0.05	0	12	16.762	8.09E-07	0.05	1	12	14.404	0.00E+0	0.05	1

		Control (siRNA Uptake)					LF2K (siRNA Uptake)					40% APTES + Dextran (siRNA Uptake)				
		DF	t value	P-Value	Alpha	Sig Flag	DF	t value	P-Value	Alpha	Sig Flag	DF	t value	P-Value	Alpha	Sig Flag
		No Inhibitor	Clathrin (Chlorpromazine)	12	21.701	2.80E-07	0.05	1	12	1.096	0.985	0.05	0	12	10.264	0.000
Caveolae (Filipin)	12		0.053	1.000	0.05	0	12	1.446	0.944	0.05	0	12	1.665	0.896	0.05	0
Clathrin and Caveolae	12		19.995	1.55E-07	0.05	1	12	2.309	0.664	0.05	1	12	11.449	0.000	0.05	1
Actin (Cytochalasin D)	12		3.870	0.170	0.05	0	12	1.258	0.971	0.05	0	12	13.141	0.000	0.05	1
Active Delivery (4oC)	12		25.724	1.15E-07	0.05	1	12	3.403	0.239	0.05	1	12	37.931	0.000	0.05	1
Scavenger Receptors (Dextran Sulfate)	12		6.048	0.014	0.05	1	12	2.836	0.437	0.05	1	12	36.914	0.000	0.05	1

Table A-2 Statistical analysis for Figure A-6

Analyses were performed using two-way ANOVA, followed by Tukey's HSD post-hoc analysis in Origin 8. DF - Degrees of Freedom, Sig Flag - Significance flag, where 0 indicates no significance ($p > 0.05$) level and 1 indicates significance ($p < 0.05$).

		Control (EGFP Fluorescence)					LF2K (EGFP Fluorescence)					40% APTES + Dext (EGFP Fluorescenc				
		DF	t value	P-Value	Alpha	Sig Flag	DF	t value	P-Value	Alpha	Sig Flag	DF	t value	P-Value	Alpha	
No Inhibitor	Clathrin (Chlorpromazine)	6	0.779	0.943	0.05	0	6	0.132	1.000	0.05	0	6	1.803	0.608	0.05	
	Caveolae (Filipin)	6	0.255	0.998	0.05	0	6	1.849	0.591	0.05	0	6	0.514	0.982	0.05	
	Scavenger Receptors (Dextran Sulfate)	6	0.092	1.000	0.05	0	6	7.586	0.007	0.05	1	6	10.049	0.002	0.05	

		No Inhibitor (EGFP Fluorescence)					Clathrin-Chlorpromazine (EGFP Fluorescence)				
		DF	t value	P-Value	Alpha	Sig Flag	DF	t value	P-Value	Alpha	Sig Flag
Control	LF2K	6	8.141	0.003	0.05	1	6	7.230	0.005	0.05	1
	40% APTES + Dextran	6	10.997	0.001	0.05	1	6	12.021	3.56E-04	0.05	1
LF2K		6	2.856	0.188	0.05	0	6	4.791	0.034	0.05	1

		Caveolae - Filipin (EGFP Fluorescence)					Scavenger Receptors- Dextran Sulfate (EGFP Fluorescence)				
		DF	t value	P-Value	Alpha	Sig Flag	DF	t value	P-Value	Alpha	Sig Flag
Control	LF2K	6	6.548	0.009	0.05	1	6	0.647	0.893	0.05	0
	40% APTES + Dextran	6	10.738	0.001	0.05	1	6	1.039	0.753	0.05	0
LF2K		6	4.191	0.057	0.05	0	6	0.393	0.959	0.05	0

Table 6-3 Statistical analysis for Figure 2-7

Analyses were performed using one-way ANOVA, followed by Tukey's HSD post-hoc analysis in Origin 8. Sig Flag - Significance flag, where 0 indicates no significance ($p > 0.05$) level and 1 indicates significance ($p < 0.05$).

		siRNA Binding (Relative Intensity)					siRNA Degradation (Relative Intensity)				
		q Value	Alpha	Sig Flag	F Value	P-Value	q Value	Alpha	Sig Flag	F Value	P-Value
Acidic Conditions (4.75 pH)	Neutral Conditions (7.00 pH)	102.532	0.05	1	5256.463	.00216	2.778	0.05	0	3.859	0.121

APPENDIX B: Materials and Methods for Chapter 3

Materials

Cell Culture

- 96-Well Plate (Costar, #3610)
- 24-Well Plate (Costar, #3513)
- 24-Well Confocal Plate (Ibidi, #82406)
- DMEM (Life Technologies, #11965092)
- Fetal Bovine Serum (Atlanta Biological, #S11550)
- Paraformaldehyde (Sigma, #P6148-500g)
- DPBS: Dulbecco's (+Mg/Ca) (Life Technologies, #14040133)
- PBS: Dulbecco's (-Mg/Ca) (Sigma, #D8537)
- Trypsin (Life Technologies, #25200056)
- Opti-MEM (Life Technologies, #11058021)
- Heparin Sulfate (Sigma, #H3393-25KU)
- Lipofectamine 2000 (Life Technologies, #11668019)
- Fluorescent siRNA: Sense DY547-5'-GGCUACGUCCAGGAGCGCA-3';
- Antisense 5'-UGCGCUCCUGGACGUAGCC-3' (Dharmacon)

Inhibitors

- Chlorpromazine hydrochloride (Sigma, #C8138-5G)
- Cytochalasin D (Sigma, #C2618-200uL)
- Filipin Complex III (Sigma, #F4767-1MG)
- Dynasore hydrate (Sigma, #D7693-25MG)
- 5-(N,N-Dimethyl)amiloride (Sigma, #A4562-25MG)
- Methyl- β -Cyclodextrin (Sigma, #C4555-5G)

Plasmids

- pd2EGFP-N1, (Clontech #6009-1)
- wt-dynamin-2-pEGFP, (Addgene #34686)
- EGFP-Actin-7 (Addgene #56421)
- GFP-alpha-adaptin[1]
- GFP-clathrin[2]
- Cav1-GFP (Addgene #14433)
- pFlot-1-GFP-N1[3]
- pFlot-2-GFP-N1[3]
- pDEST47-ARF6-GFP (Addgene #67394)
- pEGFP-C3-GRAF1[4]

Solutions

- Paraformaldehyde Solutions: 2% Paraformaldehyde (w/v) in PBS
- Heparin Solution: 20 μ g/mL heparin sulfate in DPBS

- Media: 10% FBS (v/v) in DMEM

Equations

The following equations were used in the normalization of fluorescent data. Signals used in the equations below are labeled as Signal (raw fluorescence) experimental conditions:

$$\begin{aligned}
 \text{Toxicity} &= 1 - \left[\frac{\text{GFP}_{+Inhibitor,-siRNA,+LF2K}}{\text{GFP}_{-Inhibitor,-siRNA,+LF2K}} \right] \text{ (Table A-1)} \\
 \text{Relative silencing (EGFP)} &= \left[\frac{1 - \left[\frac{\text{GFP}_{+Inhibitor,+siRNA,+LF2K}}{\text{GFP}_{+Inhibitor,-siRNA,+LF2K}} \right]}{1 - \left[\frac{\text{GFP}_{-Inhibitor,+siRNA,+LF2K}}{\text{GFP}_{-Inhibitor,-siRNA,+LF2K}} \right]} \right] - 1 \text{ (Figures 3-1, 3-2, and A-1)} \\
 \text{Relative accumulation (siRNA)} &= \left[\frac{\left[\frac{\text{siRNA}_{+Inhibitor,+siRNA,+LF2K}}{\text{siRNA}_{+Inhibitor,+siRNA,-LF2K}} \right]}{\left[\frac{\text{siRNA}_{-Inhibitor,+siRNA,+LF2K}}{\text{siRNA}_{-Inhibitor,+siRNA,-LF2K}} \right]} \right] - 1 \text{ (Figures 3-1 and 3-2)} \\
 \text{Relative accumulation (siRNA)} &= \left[\frac{\text{siRNA}_{+p(endocytic\ protein),+siRNA}}{\text{siRNA}_{+pdzEGFP-N1,+siRNA,+siRNA}} \right] - 1 \text{ (Figure 3-3)}
 \end{aligned}$$

Cell Lines

EGFP-expressing H1299 and HeLa cells were generously provided by Dr. Jørgen Kjems and Dr. Manfred Gossen, respectively [188,189]. HepG2 and HEK293 cells constitutively expressing EGFP (HepG2-EGFP and HEK293-EGFP) were generated using the methods outlined in Gossen *et al* [189]. Briefly, cells were seeded in 6-well plates and transfected 24 hours post-seeding with 4 µg pEGFP and 10 µL Lipofectamine 2000 (LF2K). Three days post-transfection, cells were sorted and re-plated according to their EGFP expression using a flow cytometer. This process was repeated at seven and fourteen days post-transfection. The average EGFP expression of the final population was analyzed over several cell cycles and found to be stable. All cell lines were maintained in antibiotic-free DMEM supplemented with 10% fetal bovine serum (FBS). Cells

were incubated at 37°C in 5% CO₂, at 100% relative humidity, and subcultured every 4–5 days by trypsinization.

EGFP Silencing

EGFP-expressing cells were seeded in 24-well plates at 200,000 cells/well (400,000 cells/well for HepG2 cells) in 500 µL of antibiotic-free DMEM/FBS. Cells were treated 24 hours post-seeding with 100 µL of transfection solution containing Opti-MEM, siRNA, and LF2K, yielding final concentrations of 100 nM siRNA and 2.3 µg/mL LF2K. Cells were washed 4 hours post-transfection with DMEM/FBS and incubated in DPBS (+Mg/Ca) containing 20 µg/mL heparin sulfate for 5 minutes to remove any extracellular siRNAs. The heparin sulfate solution was subsequently removed and replaced with DMEM/FBS. At 24 hours post-transfection, cells were trypsinized, fixed in 2% paraformaldehyde (v/v in DPBS (-Mg/Ca)), and stored in DPBS (-Mg/Ca) at 4°C until analysis (typically less than 3 days; results were stable 24 days post-fixation). Cells were analyzed by using a Becton Dickinson Influx Flow Cytometer to detect both EGFP (488/530), and Dy547 tagged siRNA (557/574) signal in each event. Samples were, gated to include 10,000 events/sample. EGFP fluorescence was measured using an excitation of 488 nm with a multi-line Argon laser. Dy547-tagged siRNA fluorescence was excited at 552 nm by a HeNe laser. Geometric mean was used to calculate fluorescence intensity values among samples. Incubations were conducted at 37°C, 5% CO₂, and 100% humidity. Cell morphology and EGFP expression as a measure of cytotoxicity were assessed by microscopy and were not significant in any of the treatments.

Endocytic Inhibitors

Endocytic inhibitors were used for 5 hours at concentrations based on the literature and our own toxicity and dose response experiments (Table 3-1, Table A-1, and Figure A-1). The specificity (or lack thereof) of the inhibitors was assessed from the literature yielding a logic matrix that allows for differentiation of the function of different endocytic pathways through comparison of the effects of multiple inhibitors (Table 3-2).

Inhibition Experiments

EGFP-expressing cells were seeded in 24-well plates at 200,000 cells/well (400,000 cells/well for HepG2 cells) in 500 μ L of antibiotic-free DMEM/FBS. After 23 hours, cells were washed with DMEM and incubated for 1 hour in DMEM containing inhibitors (Table 3-1). Cells were then transfected with siRNAs as above. Cells were washed 4 hours post-transfection with antibiotic-free DMEM/FBS and incubated in heparin sulfate solution for 5 minutes to remove extracellular siRNAs. The heparin sulfate solution was subsequently removed and replaced with antibiotic-free DMEM/FBS. At 24 hours post-transfection, cells were trypsinized, fixed using a 2% paraformaldehyde solution, and stored in DPBS (-Mg/Ca) at 4°C until analysis. All incubations were conducted at 37°C, 5% CO₂, and 100% humidity. Cells were then analyzed by flow cytometry and microscopy (Figure A-2 and A-3) as above.

Co-culture Inhibitor Experiments

HeLa, H1299, HEK293, and HepG2 cell lines, only one expressing EGFP, were mixed and seeded into 24-well plates at a density of 50,000 cells/well for HeLa, H1299, and HEK293 and

100,000 cells/well for HepG2 (total cell concentration of 250,000 cells/well) in 500 μ L of DMEM/FBS. Cells were treated with siRNAs, fixed, and analyzed by flow cytometry as above.

Endocytic Protein Overexpression Experiments

Cells were seeded in 24-well plates at a density of 150,000 cells/well (300,000 cells/well for HepG2 cells) in 500 μ L of antibiotic-free DMEM/FBS. After 24 hours, cells were transfected with a 100 μ L transfection solution containing Opti-MEM, Lipofectamine 3000 (LF3K), and one of the following plasmids: pd2EGFP-N1 (EGFP; control), wt dynamin 2 pEGFP (Dynamin), EGFP-Actin-7 (Actin), GFP-alpha-adaptin (AP2) (kindly provided by J. Rappoport [190]), GFP-clathrin (Clathrin) (kindly provided by J. Keen [191]), Cav1-GFP (Caveolin), pFlot-1-GFP-N1 (Flot 1) (kindly provided by R. Tikkanen [192]), pFlot-2-GFP-N1 (Flot 2) (kindly provided by R. Tikkanen [192]), pDEST47-ARF6-GFP (Arf6), and pEGFP-C3-GRAF1 (Graf1) (kindly provided by R. Lundmark [56]). Concentrations (after addition to the growth media) were optimized for both toxicity and expression level: HeLa and H1299 (150 ng plasmid, 0.55 μ g LF3K), HEK293 (600 ng plasmid, 2.2 μ g LF3K), and HepG2 (800 ng plasmid, 4.4 μ g LF3K). Cells were washed 6 hours after plasmid transfection with antibiotic-free DMEM/FBS. 24 hours after plasmid transfection, cells were transfected with siRNAs, as above. Cells were then fixed and analyzed by flow cytometry and microscopy (Figure A-4) as above.

Statistics

Statistical analyses were performed using one-way ANOVA, followed by Tukey's HSD post-hoc analysis (Table A-2).

Endocytic Inhibitor Toxicity and Dose Response

Each endocytic inhibitor was evaluated over a range of concentrations for each cell line to assess both toxicity and dose response. EGFP-expressing cells were seeded in 96-well plates at 20,000 cells/well (40,000 cells/well for HepG2 cells) in 100 μ L of antibiotic-free DMEM/FBS. After 23 hours, cells were washed with DMEM and incubated for 1 hour in DMEM containing inhibitors. For toxicity assessment, cells were then treated with 50 μ L Opti-MEM (Table A-1). For dose response, cells were transfected with 50 μ L of solution containing Opti-MEM, siRNA, and LF2K, yielding final concentrations of 100 nM siRNA and 2.3 μ g/mL LF2K (Figure A-1). Cells were washed 4 hours post-transfection with antibiotic-free DMEM/FBS and incubated in heparin sulfate solution for 5 minutes to remove extracellular siRNAs. The heparin sulfate solution was subsequently removed and replaced with antibiotic-free DMEM/FBS. At 24 hours post-transfection, cells were washed with DPBS (+Mg/Ca) and analyzed using a BioTek Synergy H1 plate reader. All incubations were conducted at 37°C, 5% CO₂, and 100% humidity.

Confocal Microscopy

For the cellular images of the inhibitor experiments, cells were fixed 24 hours post-transfection, using a 2% paraformaldehyde solution, and stored in DPBS (+Mg/Ca) at 4°C. Confocal images were taken using a Nikon A1 laser scanning confocal microscope. Nikon Plan Apo 20x/.75NA and Apo 60x/1.4NA objectives were used to acquire all images. EGFP (488/530) fluorescence was measured using an excitation of 488 nm with a multi-line Argon laser and displayed as green (LUT). Dy547-tagged siRNA (557/574) fluorescence was excited at 560 nm by a HeNe laser and displayed as red (LUT). The focal plane for each image was chosen to include the highest intensity EGFP fluorescence and maintained using the Nikon Perfect

Focus System. All images were collected sequentially as single XY images and used 2 count Line Kalman averaging. For overexpression images (Figure A-2), cells were fixed 1 hour after siRNA transfection using a 2% paraformaldehyde solution and stored in DPBS (+Mg/Ca) at 4°C. Confocal images were taken as above.

Table A-4 Inhibitor toxicity
 Inhibitor toxicity was assessed in each cell line by measuring EGFP fluorescence over a range of inhibitor concentrations. Reported below is the concentration at which 5% toxicity was observed (μM) (Figure 3-5).

Cell Lines	Filipin	Chlorpromazine	Amiloride	Dynasore	Cytochalasin D	MBCD
H1299	6.14	40.1	179	101	43.0	11,500
HEK293	7.09	37.2	118	94.5	12.6	5,050
HeLa	7.22	37.3	172	80.6	12.6	5,730
HepG2	8.38	28.4	120	88.2	10.3	7,390

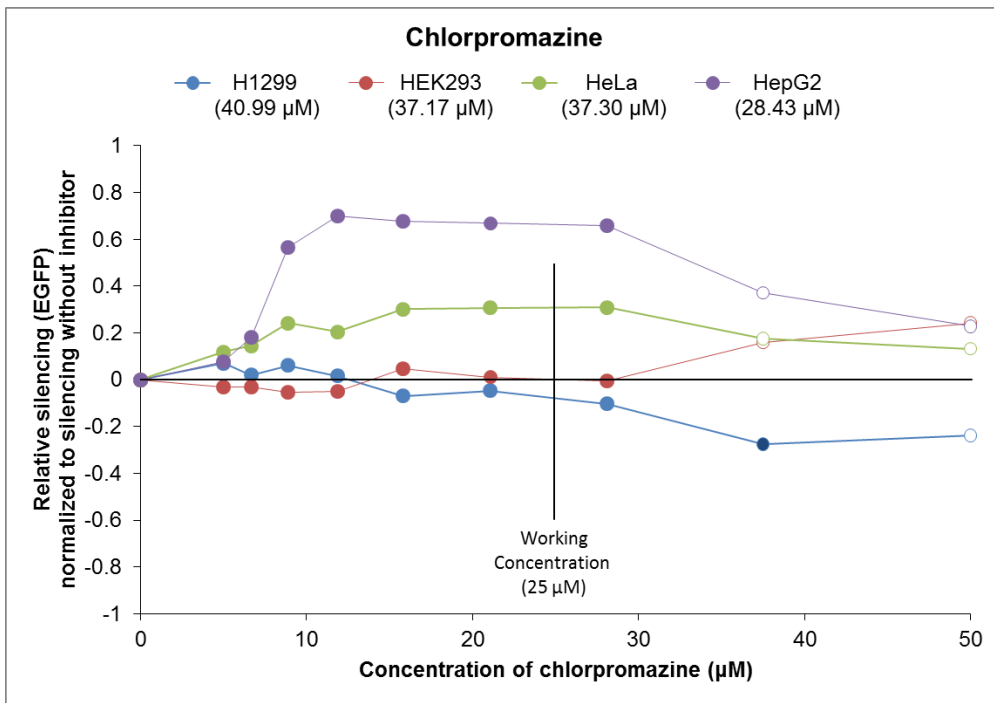
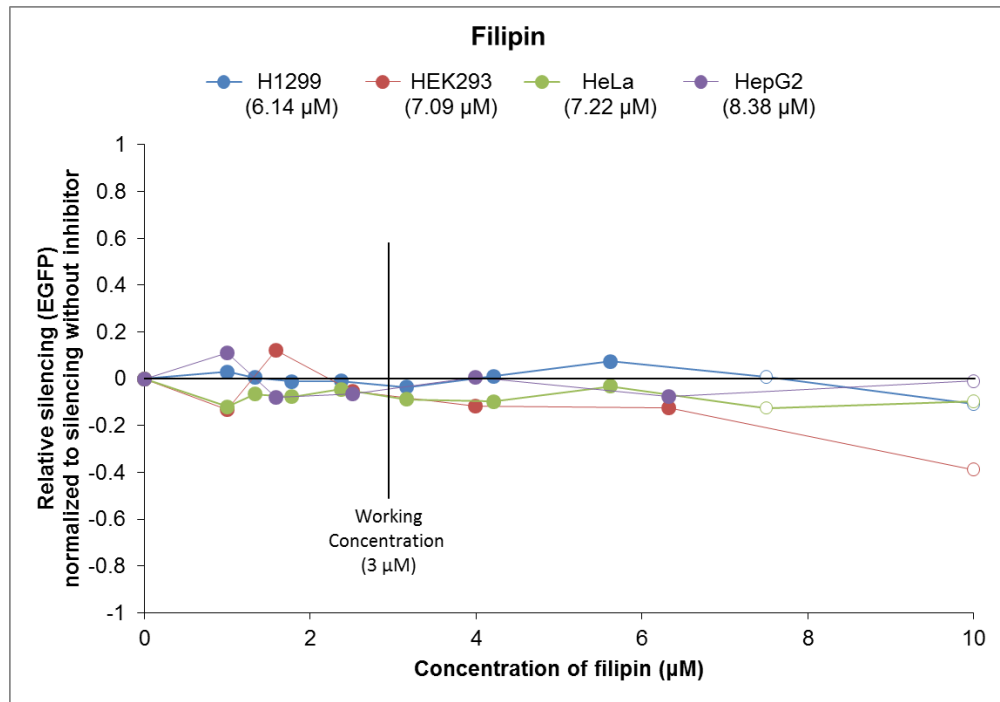


Figure A-6 Inhibitor dose response

The effect of each inhibitor on EGFP silencing was assessed over a range of inhibitor concentrations. The value listed below each cell line represents the inhibitor concentration at which 5% toxicity was observed (Table A-1). Data points that exceed the 5% toxicity dose are indicated with open symbols. The working concentration chosen for each inhibitor is indicated with a vertical black line.

Figure A-6 (cont'd)

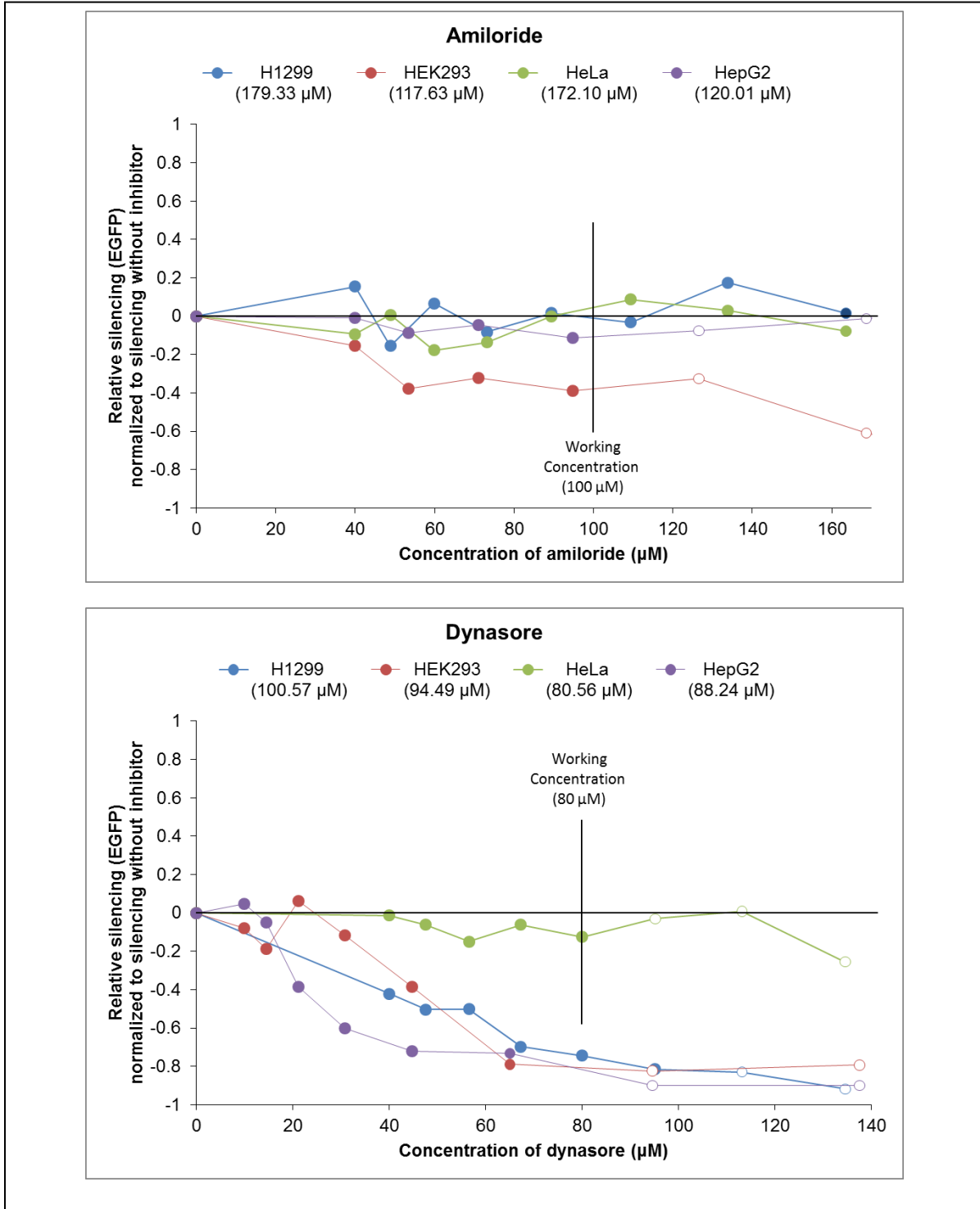
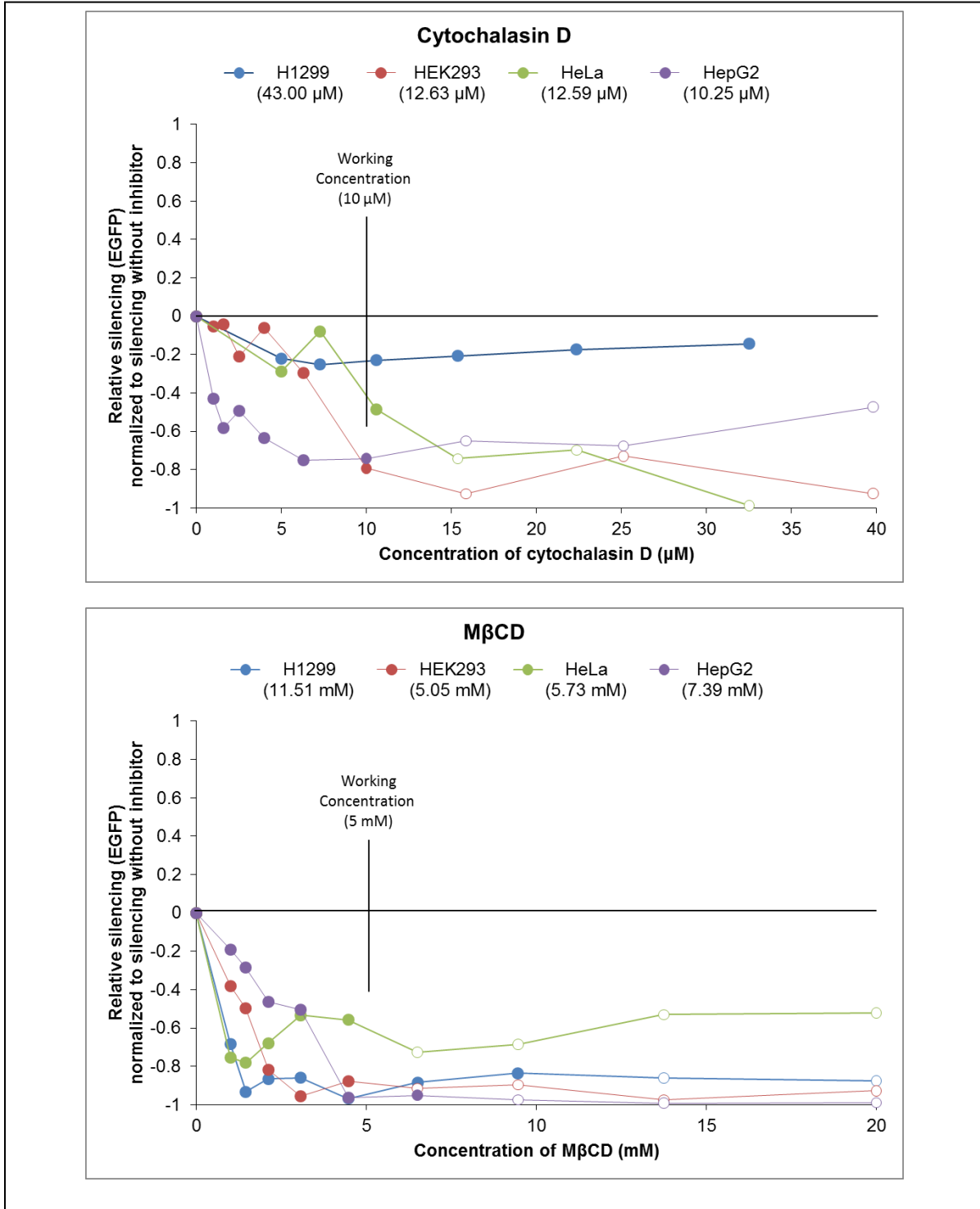


Figure A-6 (cont'd)



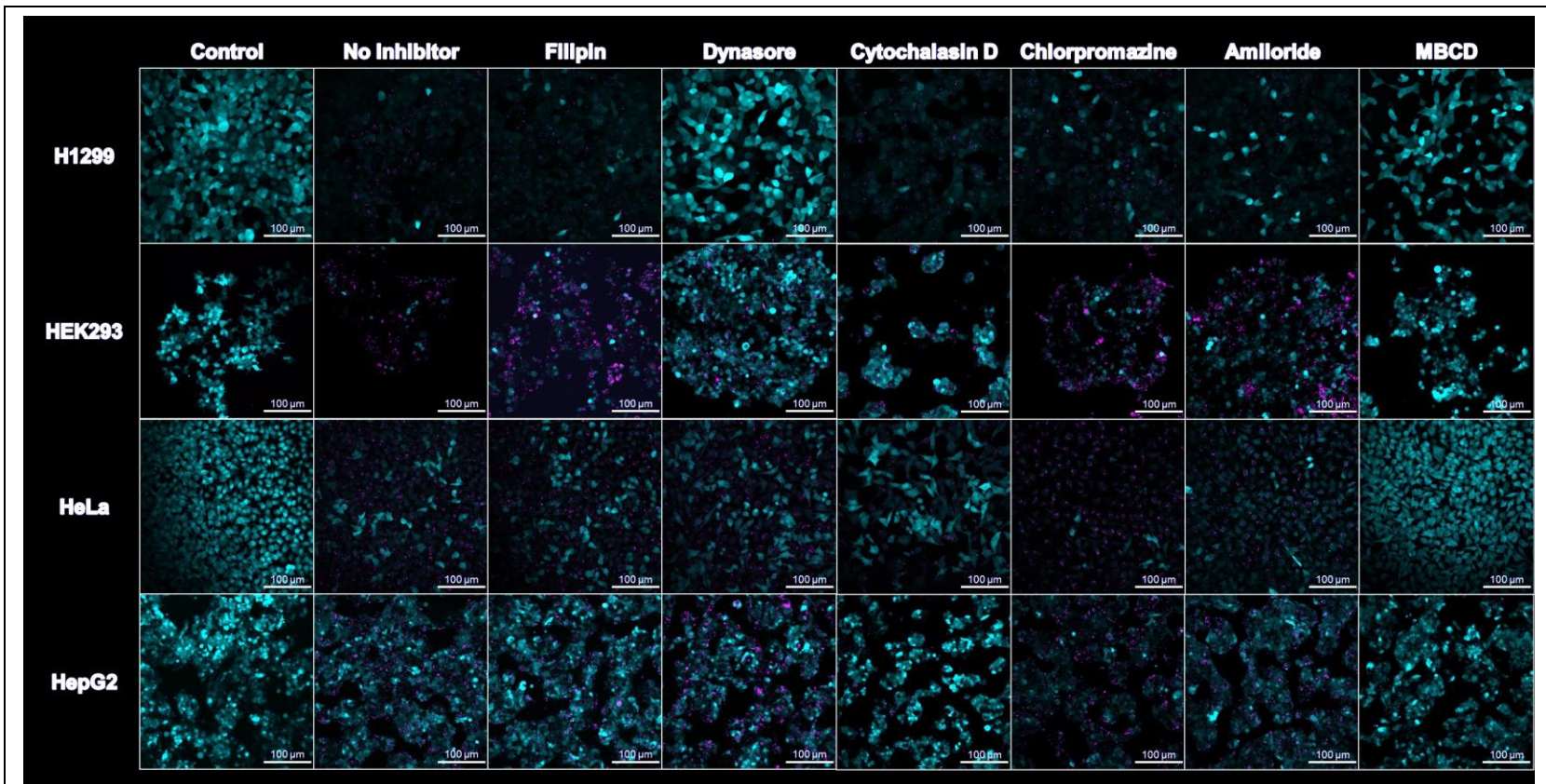


Figure A-7 Inhibitor microscopy experiments

Confocal microscopy images of EGFP-expressing cells (Cyan) transfected with 100 nM fluorescently labeled siRNA (Magenta) and 2.3 $\mu\text{g/ml}$ LF2K. Cells were pre-treated with endocytosis inhibitors and imaged 24 hours post-transfection. Scale bars are 100 μm .

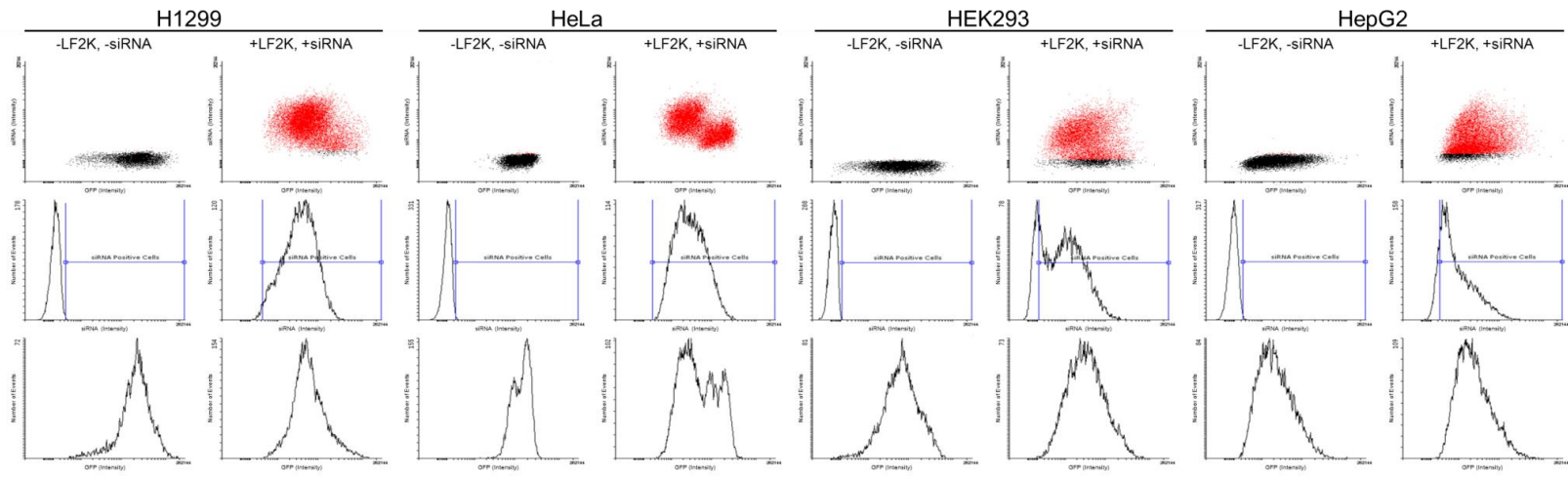


Figure A-8 Flow cytometry fluorescence distribution

Fluorescence distribution of siRNA and EGFP in un-inhibited cell lines. The fluorescent signal in the siRNA channel of un-transfected cell (-LF2K, -siRNA) was to establish a population gate for siRNA positive cells.

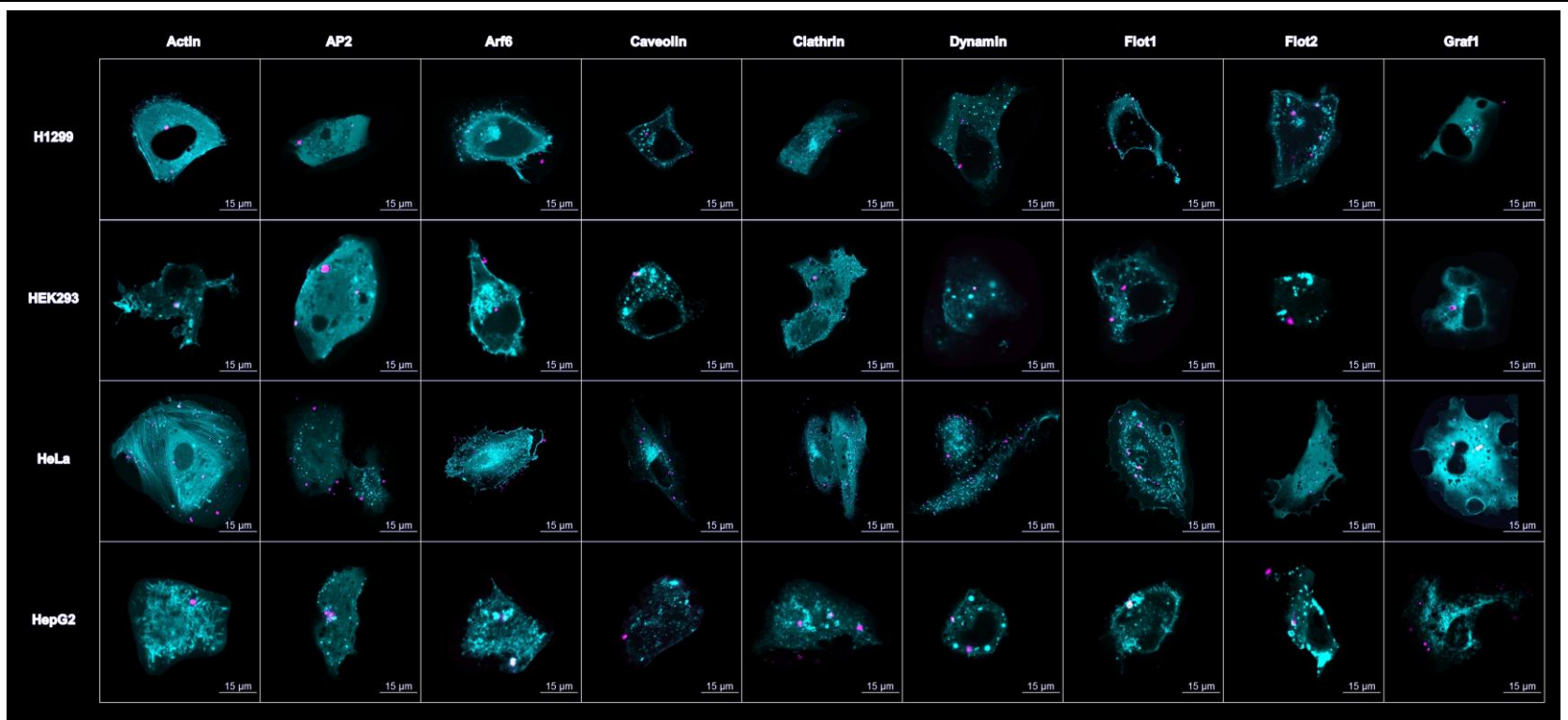


Figure A-10 Overexpression microscopy experiment

Confocal microscopy images of cells overexpressing EGFP-labeled endocytic proteins (Cyan) and transfected with 100 nM fluorescently labeled siRNA (Magenta) and 2.3 μg/ml LF2K. Cells were fixed and imaged 1 hour after transfection of siRNA-LF2K complexes. Scale bars are 15 μm.

Table A-5 Statistical analysis for Figures 3-2, 3-3, and 3-4

p-values for Figures 3-2, 3-3, and 3-4. Analyses were performed using two-way ANOVA, followed by Tukey's HSD post-hoc analysis in Origin 8. $p < 0.05$ was used to determine significance.

Silencing	Filipin	Chlorpromazine	Amiloride	Dynasore	Cytochalasin D	MBCD
H1299	0.951	0.852	0.282	1.92E-07	1.000	0.000
HEK293	0.674	0.867	4.46E-04	6.82E-07	3.98E-07	6.24E-08
HeLa	0.624	0.001	0.918	0.275	8.71E-08	0.000
HepG2	0.980	1.551E-04	0.698	1.000	8.92E-05	0.002

Accumulation	Filipin	Chlorpromazine	Amiloride	Dynasore	Cytochalasin D	MBCD
H1299	0.505	0.000	0.950	7.60E-08	0.516	6.44E-08
HEK293	0.471	0.996	4.31E-05	5.34E-06	8.98E-08	3.68E-07
HeLa	0.553	2.26E-04	0.067	0.192	0.001	1.31E-07
HepG2	0.979	5.97E-08	0.669	0.452	4.16E-07	5.78E-08

Overexpression	Dynamin	Actin	AP2	Clathrin	Caveolin	Flot1	Flot2	Arf6	Graf1
H1299	1.000	0.755	0.011	1.88E-06	0.919	1.08E-07	0.999	1.000	0.403
HEK293	0.012	0.558	1.000	0.027	1.48E-04	0.998	0.734	0.044	9.96E-06
HeLa	1.000	0.042	0.006	0.039	0.149	0.999	0.282	2.63E-04	1.000
HepG2	0.559	0.004	0.002	0.019	0.959	0.456	0.999	1.92E-05	0.997

Silencing: Co-culture	Filipin	Chlorpromazine	Amiloride	Dynasore	Cytochalasin D	MBCD
H1299	0.889	0.001	0.350	2.03E-04	0.001	0.000
HEK293	0.584	1.000	8.03E-05	2.81E-05	6.69E-05	4.16E-08
HeLa	0.935	0.003	0.915	0.007	7.30E-05	0.000
HepG2	0.966	2.81E-06	0.998	1.000	0.007	0.001

Accumulation: Co-culture	Filipin	Chlorpromazine	Amiloride	Dynasore	Cytochalasin D	MBCD
H1299	1.000	4.01E-04	1.000	0.043	1.43E-06	1.31E-07
HEK293	0.829	0.107	1.26E-07	1.82E-05	0.000	0.000
HeLa	0.907	1.41E-05	0.246	1.74E-06	1.23E-07	3.40E-07
HepG2	0.996	0.001	0.849	0.998	0.040	1.01E-04

Table A-6 Gene expression

Gene expression data for endocytic proteins. Expression is listed in transcripts per million (TPM) from Affymetrix data and normalized in GENEVESTIGATOR®. The following experimental IDs were used: HS-00859, HS-01099, HS-00217, HS-01921, HS-00048, and HS-00856.

Cell Line	ETS1	Graf1	DNM1	DNM2	Cdc42	Arf1	Actb
H1299	<u>44474</u>	706	1422	6142	22471	73898	381161
HEK293	4594	<u>3136</u>	<u>2456</u>	<u>3396</u>	<u>31679</u>	<u>133453</u>	370573
HeLa	3379	1001	10590	5497	22698	96894	<u>579685</u>
HepG2	1513	2854	802	3673	8178	48984	<u>251226</u>

APPENDIX C: Materials and Methods for Chapter 4

Materials

Cell Culture

- 6-Well Plate (Costar, #3516)
- 15-Well Confocal Plate (Ibidi, #81506)
- DMEM (Life Technologies, #11965092)
- FluoroBrite™ DMEM (Life Technologies, #A1896701)
- Fetal Bovine Serum (Atlanta Biological, #S11550)
- Trypsin (Life Technologies, #25200056)
- Opti-MEM (Life Technologies, #11058021)
- Lipofectamine 2000 (Life Technologies, #11668019)
- Antisense siRNA: 5'-UGCGCUCCUGGACGUAGCCUU-3'-Q570- (Sigma)
- Sense siRNA: 5'-GGCUACGUCCAGGAGCGCAUU-3-Q670' (Sigma)

Plasmids

- pEGFP-C1 RAB11A, (Addgene #12674)
- pEGFP-C1-RAB4b, (Addgene #49468)
- pEGFP-ER-14, (Addgene #56432)
- pEGFP-N3-LAMP1, (Addgene #16290)

Cell Lines

HeLa cells constitutively expressing EGFP labeled proteins Rab5 and Rab7 were generously provided by Matthew Seaman (University of Cambridge). HeLa cells constitutively expressing EGFP labeled proteins (Rab4, Rab11, Lamp1, and Calreticulin) were generated using published methods [18]. Briefly, cells were seeded in 6-well plates and transfected 24 hours post-seeding with 10 μ L Lipofectamine 2000 (LF2K) and 4 μ g of one of the following plasmids: pEGFP-C1 RAB11A (Rab11), pEGFP-C1-RAB4b (Rab4), pEGFP-ER-14 (Endoplasmic Reticulum), or pEGFP-N3-LAMP1 (Lysosome). Three days post-transfection, cells were sorted and re-plated according to their EGFP expression using a flow cytometer. This process was repeated at seven and fourteen days post-transfection. The average EGFP expression of the final population was analyzed over several cell cycles and found to be stable. All cell lines were maintained in

antibiotic-free DMEM supplemented with 10% fetal bovine serum (FBS). Cells were incubated at 37°C in 5% CO₂, at 100% relative humidity, and subcultured every 4–5 days by trypsinization.

Intracellular Trafficking

HeLa cells constitutively expressing an EGFP-labeled protein (Rab4, Rab5, Rab7, Rab11, Calreticulin, and Lamp1) were seeded in 15-well confocal plates at a density of 1000 cells/well and cultured in antibiotic-free growth media (DMEM+FBS). 24 hours after seeding, cells were transferred to a stage-top incubator chamber and incubated at 37°C, 5% CO₂ and 100% relative humidity. The X, Y, and Z positions were recorded for 3 locations in each well. Cells were then treated with 10 µL of transfection solution containing Opti-MEM, siRNA, and sNPs, yielding final concentrations of 100 nM siRNA and 200 µg/mL sNP. After verifying the X, Y, and Z positions in each well, images were collected at ~30 minute intervals over ~24 hours. Cell morphology was monitored for signs of cytotoxicity, which was not observed at any time.

Image Acquisition and Analysis

Images were acquired on a Nikon A1 confocal laser scanning microscope using a Nikon Plan Fluor 40×/.75 dry objective. EGFP (488/530) fluorescence was measured using an excitation of 488 nm with a multi-line Argon laser. Q570 (560/595) fluorescence (siRNA guide strand) was excited at 560 nm by a HeNe laser. Q670 (647/700) fluorescence (siRNA passenger strand) was excited at 647 nm by a HeNe laser. The focal plane for each image was chosen to maximize EGFP fluorescence intensity, which should be the focal plane through the middle of the cells, and maintained using the Nikon Perfect Focus System.

Images were acquired sequentially as single XY images using two-count Line Kalman averaging. Each well was imaged at its first position prior to returning to the first well and then imaging the second position in each well. After acquiring images at three positions in each well, the sequence began again at the first position in the first well. Using this imaging approach minimized photobleaching while also minimizing the time between images for a given well. To determine the Pearson's correlation coefficient for each fluorophore pairing, images were analyzed in batch through Fiji [193] using the Bio-Formats and JACoP plugins [194].

BIBLIOGRAPHY

BIBLIOGRAPHY

- 1 Vocelle, D., Chesniak, O.M., Malefyt, A.P., Comiskey, G., Adu-Berchie, K., Smith, M.R., Chan, C. and Walton, S.P. (2016) Dextran Functionalization Enhances Nanoparticle-Mediated SiRNA Delivery and Silencing. *TECHNOLOGY*, **04**, 42–54. <https://doi.org/10.1142/S2339547816400100>.
- 2 Burnett, J.C. and Rossi, J.J. (2012) RNA-Based Therapeutics: Current Progress and Future Prospects. *Chemistry & Biology*, Elsevier Ltd, **19**, 60–71. <https://doi.org/10.1016/j.chembiol.2011.12.008>.
- 3 Angart, P., Vocelle, D., Chan, C. and Walton, S.P. (2013) Design of SiRNA Therapeutics from the Molecular Scale. *Pharmaceuticals*, **6**, 440–468. <https://doi.org/10.3390/ph6040440>.
- 4 Yin, H., Kanasty, R.L., Eltoukhy, A.A., Vegas, A.J., Dorkin, J.R. and Anderson, D.G. (2014) Non-Viral Vectors for Gene-Based Therapy. *Nature Reviews Genetics*, Nature Publishing Group, **15**, 541–555. <https://doi.org/10.1038/nrg3763>.
- 5 Garber, K. (2018) Alnylam Launches Era of RNAi Drugs. *Nature Biotechnology*, **36**, 777–778. <https://doi.org/10.1038/nbt0918-777>.
- 6 Springer, A.D. and Dowdy, S.F. (2018) GalNAc-SiRNA Conjugates: Leading the Way for Delivery of RNAi Therapeutics. *Nucleic Acid Therapeutics*, **28**, 109–118. <https://doi.org/10.1089/nat.2018.0736>.
- 7 Knudsen, K.B., Northeved, H., Kumar EK, P., Permin, A., Gjetting, T., Andresen, T.L., Larsen, S., Wegener, K.M., Lykkesfeldt, J., Jantzen, K., Loft, S., Møller, P. and Roursgaard, M. (2015) In Vivo Toxicity of Cationic Micelles and Liposomes. *Nanomedicine: Nanotechnology, Biology and Medicine*, The Authors., **11**, 467–477. <https://doi.org/10.1016/j.nano.2014.08.004>.
- 8 Mutlu, G.M., Budinger, G.R.S., Green, A.A., Urich, D., Soberanes, S., Chiarella, S.E., Alheid, G.F., McCrimmon, D.R., Szleifer, I. and Hersam, M.C. (2010) Biocompatible Nanoscale Dispersion of Single-Walled Carbon Nanotubes Minimizes in Vivo Pulmonary Toxicity. *Nano Letters*, **10**, 1664–1670. <https://doi.org/10.1021/nl9042483>.
- 9 Moghimi, S.M., Hunter, A.C. and Andresen, T.L. (2012) Factors Controlling Nanoparticle Pharmacokinetics: An Integrated Analysis and Perspective. *Annual Review of Pharmacology and Toxicology*, **52**, 481–503. <https://doi.org/10.1146/annurev-pharmtox-010611-134623>.
- 10 Malefyt, A.P., Wu, M., Vocelle, D.B., Kappes, S.J., Lindeman, S.D., Chan, C. and Walton, S.P. (2014) Improved Asymmetry Prediction for Short Interfering RNAs. *FEBS Journal*, **281**, 320–330. <https://doi.org/10.1111/febs.12599>.

- 11 Sakurai, K., Amarzguioui, M., Kim, D.-H., Alluin, J., Heale, B., Song, M., Gatignol, A., Behlke, M. and Rossi, J.J. (2011) A Role for Human Dicer in Pre-RISC Loading of SiRNAs. *Nucleic Acids Research*, **39**, 1510–1525. <https://doi.org/10.1093/nar/gkq846>.
- 12 Tomari, Y., Matranga, C., Haley, B., Martinez, N. and Zamore, P.D. (2004) A Protein Sensor for SiRNA Asymmetry. *Science (New York, N.Y.)*, **306**, 1377–80. <https://doi.org/10.1126/science.1102755>.
- 13 MacRae, I.J., Ma, E., Zhou, M., Robinson, C. V and Doudna, J.A. (2008) In Vitro Reconstitution of the Human RISC-Loading Complex. *Proceedings of the National Academy of Sciences*, **105**, 512–517. <https://doi.org/10.1073/pnas.0710869105>.
- 14 Gredell, J.A., Dittmer, M.J., Wu, M., Chan, C. and Walton, S.P. (2010) Recognition of SiRNA Asymmetry by TAR RNA Binding Protein. *Biochemistry*, **49**, 3148–3155. <https://doi.org/10.1021/bi902189s>.
- 15 Liu, Q. (2003) R2D2, a Bridge Between the Initiation and Effector Steps of the Drosophila RNAi Pathway. *Science*, **301**, 1921–1925. <https://doi.org/10.1126/science.1088710>.
- 16 Matranga, C., Tomari, Y., Shin, C., Bartel, D.P. and Zamore, P.D. (2005) Passenger-Strand Cleavage Facilitates Assembly of SiRNA into Ago2-Containing RNAi Enzyme Complexes. *Cell*, **123**, 607–620. <https://doi.org/10.1016/j.cell.2005.08.044>.
- 17 Khvorova, A., Reynolds, A. and Jayasena, S.D. (2003) Functional SiRNAs and MiRNAs Exhibit Strand Bias. *Cell*, **115**, 209–216. [https://doi.org/10.1016/S0092-8674\(03\)00801-8](https://doi.org/10.1016/S0092-8674(03)00801-8).
- 18 Burnett, J.C., Rossi, J.J. and Tiemann, K. (2011) Current Progress of SiRNA/ShRNA Therapeutics in Clinical Trials. *Biotechnology Journal*, **6**, 1130–1146. <https://doi.org/10.1002/biot.201100054>.
- 19 Williford, J.-M., Wu, J., Ren, Y., Archang, M.M., Leong, K.W. and Mao, H.-Q. (2014) Recent Advances in Nanoparticle-Mediated SiRNA Delivery. *Annual Review of Biomedical Engineering*, **16**, 347–370. <https://doi.org/10.1146/annurev-bioeng-071813-105119>.
- 20 Haussecker, D. (2008) The Business of RNAi Therapeutics. *Human gene therapy*, **19**, 451–462. <https://doi.org/10.1089/hum.2008.007>.
- 21 Samuel-Abraham, S. and Leonard, J.N. (2010) Staying on Message: Design Principles for Controlling Nonspecific Responses to SiRNA. *FEBS Journal*, **277**, 4828–4836. <https://doi.org/10.1111/j.1742-4658.2010.07905.x>.
- 22 Seow, Y. and Wood, M.J. (2009) Biological Gene Delivery Vehicles: Beyond Viral Vectors. *Molecular Therapy*, **17**, 767–777. <https://doi.org/10.1038/mt.2009.41>.
- 23 Mellott, A.J., Forrest, M.L. and Detamore, M.S. (2013) Physical Non-Viral Gene Delivery Methods for Tissue Engineering. *Annals of Biomedical Engineering*, **41**, 446–468.

<https://doi.org/10.1007/s10439-012-0678-1>.

- 24 Wang, H., Jiang, Y., Peng, H., Chen, Y., Zhu, P. and Huang, Y. (2015) Recent Progress in MicroRNA Delivery for Cancer Therapy by Non-Viral Synthetic Vectors. *Advanced Drug Delivery Reviews*, Elsevier B.V., **81**, 142–160. <https://doi.org/10.1016/j.addr.2014.10.031>.
- 25 Spagnou, S., Miller, A.D. and Keller, M. (2004) Lipidic Carriers of SiRNA: Differences in the Formulation, Cellular Uptake, and Delivery with Plasmid DNA †. *Biochemistry*, **43**, 13348–13356. <https://doi.org/10.1021/bi048950a>.
- 26 Whitehead, K.A., Sahay, G., Li, G.Z., Love, K.T., Alabi, C.A., Ma, M., Zurenko, C., Querbes, W., Langer, R.S. and Anderson, D.G. (2011) Synergistic Silencing: Combinations of Lipid-like Materials for Efficacious SiRNA Delivery. *Molecular Therapy*, Nature Publishing Group, **19**, 1688–1694. <https://doi.org/10.1038/mt.2011.141>.
- 27 Malam, Y., Loizidou, M. and Seifalian, A.M. (2009) Liposomes and Nanoparticles: Nanosized Vehicles for Drug Delivery in Cancer. *Trends in Pharmacological Sciences*, **30**, 592–599. <https://doi.org/10.1016/j.tips.2009.08.004>.
- 28 Lonez, C., Vandenbranden, M. and Ruyschaert, J.-M. (2008) Cationic Liposomal Lipids: From Gene Carriers to Cell Signaling. *Progress in Lipid Research*, **47**, 340–347. <https://doi.org/10.1016/j.plipres.2008.03.002>.
- 29 Schroeder, A., Levins, C.G., Cortez, C., Langer, R. and Anderson, D.G. (2010) Lipid-Based Nanotherapeutics for SiRNA Delivery. *Journal of Internal Medicine*, **267**, 9–21. <https://doi.org/10.1111/j.1365-2796.2009.02189.x>.
- 30 Whitehead, K.A., Matthews, J., Chang, P.H., Niroui, F., Dorkin, J.R., Severgnini, M. and Anderson, D.G. (2012) In Vitro – In Vivo Translation of Lipid Nanoparticles for Hepatocellular SiRNA Delivery. *ACS Nano*, **6**, 6922–6929. <https://doi.org/10.1021/nn301922x>.
- 31 Elsabahy, M. and Wooley, K.L. (2012) Design of Polymeric Nanoparticles for Biomedical Delivery Applications. *Chemical Society Reviews*, **41**, 2545. <https://doi.org/10.1039/c2cs15327k>.
- 32 Kamaly, N., Xiao, Z., Valencia, P.M., Radovic-Moreno, A.F. and Farokhzad, O.C. (2012) Targeted Polymeric Therapeutic Nanoparticles: Design, Development and Clinical Translation. *Chemical Society Reviews*, **41**, 2971. <https://doi.org/10.1039/c2cs15344k>.
- 33 Siegwart, D.J., Whitehead, K. a, Nuhn, L., Sahay, G., Cheng, H., Jiang, S., Ma, M., Lytton-Jean, A., Vegas, A., Fenton, P., Levins, C.G., Love, K.T., Lee, H., Cortez, C., Collins, S.P., Li, Y.F., Jang, J., Querbes, W., Zurenko, C., Novobrantseva, T., Langer, R. and Anderson, D.G. (2011) Combinatorial Synthesis of Chemically Diverse Core-Shell Nanoparticles for Intracellular Delivery. *Proceedings of the National Academy of Sciences of the United States of America*, **108**, 12996–13001. <https://doi.org/10.1073/pnas.1106379108>.

- 34 Storm, G., Belliot, S.O., Daemen, T. and Lasic, D.D. (1995) Surface Modification of Nanoparticles to Oppose Uptake by the Mononuclear Phagocyte System. *Advanced Drug Delivery Reviews*, **17**, 31–48. [https://doi.org/10.1016/0169-409X\(95\)00039-A](https://doi.org/10.1016/0169-409X(95)00039-A).
- 35 Rejman, J., Bragonzi, A. and Conese, M. (2005) Role of Clathrin- and Caveolae-Mediated Endocytosis in Gene Transfer Mediated by Lipo- and Polyplexes. *Molecular Therapy*, **12**, 468–474. <https://doi.org/10.1016/j.ymthe.2005.03.038>.
- 36 Lemarchand, C., Gref, R. and Couvreur, P. (2004) Polysaccharide-Decorated Nanoparticles. *European Journal of Pharmaceutics and Biopharmaceutics*, **58**, 327–341. <https://doi.org/10.1016/j.ejpb.2004.02.016>.
- 37 Davis, M.E. (2009) The First Targeted Delivery of SiRNA in Humans via a Nanoparticle : From Concept to Clinic. *Molecular Pharmaceutics*, **6**, 659–668. <https://doi.org/10.1021/mp900015y>.
- 38 Nair, L.S. and Laurencin, C.T. (2007) Biodegradable Polymers as Biomaterials. *Progress in Polymer Science*, **32**, 762–798. <https://doi.org/10.1016/j.progpolymsci.2007.05.017>.
- 39 Ulery, B.D., Nair, L.S. and Laurencin, C.T. (2011) Biomedical Applications of Biodegradable Polymers. *Journal of Polymer Science, Part B: Polymer Physics*, **49**, 832–864. <https://doi.org/10.1002/polb.22259>.
- 40 Yang, X., Sierant, M., Janicka, M., Peczek, L., Martinez, C., Hassell, T., Li, N., Li, X., Wang, T. and Nawrot, B. (2012) Gene Silencing Activity of SiRNA Molecules Containing Phosphorodithioate Substitutions. *ACS Chemical Biology*, **7**, 1214–1220. <https://doi.org/10.1021/cb300078e>.
- 41 Cheung, W., Pontoriero, F., Taratula, O., Chen, A.M. and He, H. (2010) DNA and Carbon Nanotubes as Medicine. *Advanced Drug Delivery Reviews*, Elsevier B.V., **62**, 633–649. <https://doi.org/10.1016/j.addr.2010.03.007>.
- 42 Santosh, M., Panigrahi, S., Bhattacharyya, D., Sood, a. K. and Maiti, P.K. (2012) Unzipping and Binding of Small Interfering RNA with Single Walled Carbon Nanotube: A Platform for Small Interfering RNA Delivery. *The Journal of Chemical Physics*, **136**, 065106. <https://doi.org/10.1063/1.3682780>.
- 43 Kesharwani, P., Gajbhiye, V. and Jain, N.K. (2012) A Review of Nanocarriers for the Delivery of Small Interfering RNA. *Biomaterials*, Elsevier Ltd, **33**, 7138–7150. <https://doi.org/10.1016/j.biomaterials.2012.06.068>.
- 44 Dobrovolskaia, M.A., Aggarwal, P., Hall, J.B. and Mcneil, S.E. (2008) Interaction with the Immune System and Its Potential Effects on Nanoparticle Biodistribution. *Molecular pharmaceutics*, **5**, 487–495. <https://doi.org/10.1021/mp800032f>.
- 45 Li, Y.Y., Sun, L., Jin, M., Du, Z., Liu, X., Guo, C., Li, Y.Y., Huang, P. and Sun, Z. (2011) Size-Dependent Cytotoxicity of Amorphous Silica Nanoparticles in Human Hepatoma HepG2 Cells. *Toxicology in Vitro*, Elsevier Ltd, **25**, 1343–1352.

<https://doi.org/10.1016/j.tiv.2011.05.003>.

- 46 Slowing, I.I., Trewyn, B.G., Giri, S. and Lin, V.S.-Y. (2007) Mesoporous Silica Nanoparticles for Drug Delivery and Biosensing Applications. *Advanced Functional Materials*, **17**, 1225–1236. <https://doi.org/10.1002/adfm.200601191>.
- 47 Shen, J., Kim, H.-C., Su, H., Wang, F., Wolfram, J., Kirui, D., Mai, J., Mu, C., Ji, L.-N., Mao, Z.-W. and Shen, H. (2014) Cyclodextrin and Polyethylenimine Functionalized Mesoporous Silica Nanoparticles for Delivery of SiRNA Cancer Therapeutics. *Theranostics*, **4**, 487–497. <https://doi.org/10.7150/thno.8263>.
- 48 Asefa, T. and Tao, Z. (2012) Biocompatibility of Mesoporous Silica Nanoparticles. *Chemical Research in Toxicology*, **25**, 2265–2284. <https://doi.org/10.1021/tx300166u>.
- 49 Fadeel, B. and Garcia-Bennett, A.E. (2010) Better Safe than Sorry: Understanding the Toxicological Properties of Inorganic Nanoparticles Manufactured for Biomedical Applications. *Advanced Drug Delivery Reviews*, Elsevier B.V., **62**, 362–374. <https://doi.org/10.1016/j.addr.2009.11.008>.
- 50 Khlebtsov, N. and Dykman, L. (2011) Biodistribution and Toxicity of Engineered Gold Nanoparticles: A Review of in Vitro and in Vivo Studies. *Chem. Soc. Rev.*, **40**, 1647–1671. <https://doi.org/10.1039/C0CS00018C>.
- 51 Cho, E.C., Zhang, Q. and Xia, Y. (2011) The Effect of Sedimentation and Diffusion on Cellular Uptake of Gold Nanoparticles. *Nature nanotechnology*, Nature Publishing Group, **6**, 385–391. <https://doi.org/10.1038/nnano.2011.58>.
- 52 Kong, W.H., Bae, K.H., Jo, S.D., Kim, J.S. and Park, T.G. (2012) Cationic Lipid-Coated Gold Nanoparticles as Efficient and Non-Cytotoxic Intracellular SiRNA Delivery Vehicles. *Pharmaceutical Research*, **29**, 362–374. <https://doi.org/10.1007/s11095-011-0554-y>.
- 53 Malefyt, A.P., Walton, S.P. and Chan, C. (2012) Endocytosis Pathways for Nucleic Acid Therapeutics. *Nano LIFE*, **2**, 1241005. <https://doi.org/10.1142/S179398441241005X>.
- 54 Glebov, O.O., Bright, N.A. and Nichols, B.J. (2006) Flotillin-1 Defines a Clathrin-Independent Endocytic Pathway in Mammalian Cells. *Nature Cell Biology*, **8**, 46–54. <https://doi.org/10.1038/ncb1342>.
- 55 Radhakrishna, H. and Donaldson, J.G. (1997) ADP-Ribosylation Factor 6 Regulates a Novel Plasma Membrane Recycling Pathway. *The Journal of Cell Biology*, **139**, 49–61. <https://doi.org/10.1083/jcb.139.1.49>.
- 56 Lundmark, R., Doherty, G.J., Howes, M.T., Cortese, K., Vallis, Y., Parton, R.G. and McMahon, H.T. (2008) The GTPase-Activating Protein GRAF1 Regulates the CLIC/GEEC Endocytic Pathway. *Current Biology*, Elsevier Ltd, **18**, 1802–1808. <https://doi.org/10.1016/j.cub.2008.10.044>.

- 57 Degors, I.M.S., Wang, C., Rehman, Z.U. and Zuhorn, I.S. (2019) Carriers Break Barriers in Drug Delivery: Endocytosis and Endosomal Escape of Gene Delivery Vectors. *Accounts of Chemical Research*, research-article, American Chemical Society, **52**, acs.accounts.9b00177. <https://doi.org/10.1021/acs.accounts.9b00177>.
- 58 Doherty, G.J. and McMahon, H.T. (2009) Mechanisms of Endocytosis. *Annual Review of Biochemistry*, **78**, 857–902. <https://doi.org/10.1146/annurev.biochem.78.081307.110540>.
- 59 Kerr, M.C. and Teasdale, R.D. (2009) Defining Macropinocytosis. *Traffic*, **10**, 364–371. <https://doi.org/10.1111/j.1600-0854.2009.00878.x>.
- 60 Koivusalo, M., Welch, C., Hayashi, H., Scott, C.C., Kim, M., Alexander, T., Touret, N., Hahn, K.M. and Grinstein, S. (2010) Amiloride Inhibits Macropinocytosis by Lowering Submembranous PH and Preventing Rac1 and Cdc42 Signaling. *The Journal of Cell Biology*, **188**, 547–563. <https://doi.org/10.1083/jcb.200908086>.
- 61 Xiang, S., Tong, H., Shi, Q., Fernandes, J.C., Jin, T., Dai, K. and Zhang, X. (2012) Uptake Mechanisms of Non-Viral Gene Delivery. *Journal of Controlled Release*, Elsevier B.V., **158**, 371–378. <https://doi.org/10.1016/j.jconrel.2011.09.093>.
- 62 Dergai, M., Iershov, A., Novokhatska, O., Pankivskyi, S. and Rynditch, A. (2016) Evolutionary Changes on the Way to Clathrin-Mediated Endocytosis in Animals. *Genome Biology and Evolution*. <https://doi.org/10.1093/gbe/evw028>.
- 63 Sousa, R., Liao, H.S., Cuéllar, J., Jin, S., Valpuesta, J.M., Jin, A.J. and Lafer, E.M. (2016) Clathrin-Coat Disassembly Illuminates the Mechanisms of Hsp70 Force Generation. *Nature Structural and Molecular Biology*, **23**, 821–829. <https://doi.org/10.1038/nsmb.3272>.
- 64 Almeida, J.P.M., Figueroa, E.R. and Drezek, R.A. (2014) Gold Nanoparticle Mediated Cancer Immunotherapy. *Nanomedicine: Nanotechnology, Biology, and Medicine*. <https://doi.org/10.1016/j.nano.2013.09.011>.
- 65 Gabrielson, N.P. and Pack, D.W. (2009) Efficient Polyethylenimine-Mediated Gene Delivery Proceeds via a Caveolar Pathway in HeLa Cells. *Journal of Controlled Release*, Elsevier B.V., **136**, 54–61. <https://doi.org/10.1016/j.jconrel.2009.02.003>.
- 66 Juliano, R.L. (2018) Intracellular Trafficking and Endosomal Release of Oligonucleotides: What We Know and What We Don't. *Nucleic Acid Therapeutics*, **28**, 166–177. <https://doi.org/10.1089/nat.2018.0727>.
- 67 Pelkmans, L. and Helenius, A. (2002) Endocytosis Via Caveolae. *Traffic*, **3**, 311–320. <https://doi.org/10.1034/j.1600-0854.2002.30501.x>.
- 68 Nabi, I.R. and Le, P.U. (2003) Caveolae/Raft-Dependent Endocytosis. *The Journal of Cell Biology*, **161**, 673–677. <https://doi.org/10.1083/jcb.200302028>.
- 69 Kirkham, M. and Parton, R.G. (2005) Clathrin-Independent Endocytosis: New Insights

- into Caveolae and Non-Caveolar Lipid Raft Carriers. *Biochimica et Biophysica Acta - Molecular Cell Research*. <https://doi.org/10.1016/j.bbamcr.2005.06.002>.
- 70 Milhaud, J. (1992) Permeabilizing Action of Filipin III on Model Membranes through a Filipin-Phospholipid Binding. *Biochimica et Biophysica Acta (BBA) - Biomembranes*, **1105**, 307–318. [https://doi.org/10.1016/0005-2736\(92\)90209-5](https://doi.org/10.1016/0005-2736(92)90209-5).
- 71 Li, H.H., Li, J., Wasserloos, K.J., Wallace, C., Sullivan, M.G., Bauer, P.M., Stolz, D.B., Lee, J.S., Watkins, S.C., St Croix, C.M., Pitt, B.R. and Zhang, L.M. (2013) Caveolae-Dependent and -Independent Uptake of Albumin in Cultured Rodent Pulmonary Endothelial Cells. *PLoS ONE*, **8**, 1–12. <https://doi.org/10.1371/journal.pone.0081903>.
- 72 Naslavsky, N., Weigert, R. and Donaldson, J.G. (2003) Convergence of Non-Clathrin- and Clathrin-Derived Endosomes Involves Arf6 Inactivation and Changes in Phosphoinositides. Mostov, K., Ed., *Molecular Biology of the Cell*, **14**, 417–431. <https://doi.org/10.1091/mbc.02-04-0053>.
- 73 Naslavsky, N., Weigert, R. and Donaldson, J.G. (2004) Characterization of a Nonclathrin Endocytic Pathway: Membrane Cargo and Lipid Requirements. *Molecular Biology of the Cell*, **15**, 3542–3552. <https://doi.org/10.1091/mbc.e04-02-0151>.
- 74 Brown, F.D., Rozelle, A.L., Yin, H.L., Balla, T. and Donaldson, J.G. (2001) Phosphatidylinositol 4,5-Bisphosphate and Arf6-Regulated Membrane Traffic. *The Journal of Cell Biology*, **154**, 1007–1018. <https://doi.org/10.1083/jcb.200103107>.
- 75 Nishi, K. and Saigo, K. (2007) Cellular Internalization of Green Fluorescent Protein Fused with Herpes Simplex Virus Protein VP22 via a Lipid Raft-Mediated Endocytic Pathway Independent of Caveolae and Rho Family GTPases but Dependent on Dynamin and Arf6. *Journal of Biological Chemistry*, **282**, 27503–27517. <https://doi.org/10.1074/jbc.M703810200>.
- 76 Urrutia, R., Henley, J.R., Cook, T. and McNiven, M.A. (1997) The Dynamins: Redundant or Distinct Functions for an Expanding Family of Related GTPases? *Proceedings of the National Academy of Sciences*, **94**, 377–384. <https://doi.org/10.1073/pnas.94.2.377>.
- 77 Nonnenmacher, M. and Weber, T. (2011) Adeno-Associated Virus 2 Infection Requires Endocytosis through the CLIC/GEEC Pathway. *Cell Host & Microbe*, Elsevier Inc., **10**, 563–576. <https://doi.org/10.1016/j.chom.2011.10.014>.
- 78 Francis, M.K., Holst, M.R., Vidal-Quadras, M., Henriksson, S., Santarella-Mellwig, R., Sandblad, L. and Lundmark, R. (2015) Endocytic Membrane Turnover at the Leading Edge Is Driven by a Transient Interaction between Cdc42 and GRAF1. *Journal of Cell Science*, **128**, 4183–4195. <https://doi.org/10.1242/jcs.174417>.
- 79 Vercauteren, D., Piest, M., van der Aa, L.J., Al Soraj, M., Jones, A.T., Engbersen, J.F.J., De Smedt, S.C. and Braeckmans, K. (2011) Flotillin-Dependent Endocytosis and a Phagocytosis-like Mechanism for Cellular Internalization of Disulfide-Based Poly(Amido Amine)/DNA Polyplexes. *Biomaterials*, Elsevier Ltd, **32**, 3072–3084.

<https://doi.org/10.1016/j.biomaterials.2010.12.045>.

- 80 Kasper, J., Hermanns, M.I., Bantz, C., Koshkina, O., Lang, T., Maskos, M., Pohl, C., Unger, R.E. and Kirkpatrick, C.J. (2013) Interactions of Silica Nanoparticles with Lung Epithelial Cells and the Association to Flotillins. *Archives of Toxicology*, **87**, 1053–1065. <https://doi.org/10.1007/s00204-012-0876-5>.
- 81 Riento, K., Frick, M., Schafer, I. and Nichols, B.J. (2009) Endocytosis of Flotillin-1 and Flotillin-2 Is Regulated by Fyn Kinase. *Journal of Cell Science*, **122**, 912–918. <https://doi.org/10.1242/jcs.039024>.
- 82 Otto, G.P. and Nichols, B.J. (2011) The Roles of Flotillin Microdomains - Endocytosis and Beyond. *Journal of Cell Science*, **124**, 3933–3940. <https://doi.org/10.1242/jcs.092015>.
- 83 Elkin, S.R., Lakoduk, A.M. and Schmid, S.L. (2016) Endocytic Pathways and Endosomal Trafficking: A Primer. *Wiener Medizinische Wochenschrift*, **166**, 196–204. <https://doi.org/10.1007/s10354-016-0432-7>.
- 84 Shu, Y., Pi, F., Sharma, A., Rajabi, M., Haque, F., Shu, D., Leggas, M., Evers, B.M. and Guo, P. (2014) Stable RNA Nanoparticles as Potential New Generation Drugs for Cancer Therapy. *Advanced Drug Delivery Reviews*, Elsevier B.V., **66**, 74–89. <https://doi.org/10.1016/j.addr.2013.11.006>.
- 85 Sahay, G., Querbes, W., Alabi, C., Eltoukhy, A., Sarkar, S., Zurenko, C., Karagiannis, E., Love, K., Chen, D., Zoncu, R., Buganim, Y., Schroeder, A., Langer, R. and Anderson, D.G. (2013) Efficiency of SiRNA Delivery by Lipid Nanoparticles Is Limited by Endocytic Recycling. *Nature Biotechnology*, Nature Publishing Group, **31**, 653–658. <https://doi.org/10.1038/nbt.2614>.
- 86 Akinc, A., Thomas, M., Klivanov, A.M. and Langer, R. (2005) Exploring Polyethylenimine-Mediated DNA Transfection and the Proton Sponge Hypothesis. *Journal of Gene Medicine*, **7**, 657–663. <https://doi.org/10.1002/jgm.696>.
- 87 Varkouhi, A.K., Scholte, M., Storm, G. and Haisma, H.J. (2011) Endosomal Escape Pathways for Delivery of Biologicals. *Journal of Controlled Release*, Elsevier B.V., **151**, 220–228. <https://doi.org/10.1016/j.jconrel.2010.11.004>.
- 88 Wang, F., Wang, Y., Zhang, X., Zhang, W., Guo, S. and Jin, F. (2014) Recent Progress of Cell-Penetrating Peptides as New Carriers for Intracellular Cargo Delivery. *Journal of Controlled Release*, Elsevier B.V., **174**, 126–136. <https://doi.org/10.1016/j.jconrel.2013.11.020>.
- 89 Cho, Y.W., Kim, J.-D. and Park, K. (2003) Polycation Gene Delivery Systems: Escape from Endosomes to Cytosol. *Journal of Pharmacy and Pharmacology*. <https://doi.org/10.1211/002235703765951311>.
- 90 Setten, R.L., Rossi, J.J. and Han, S. (2019) The Current State and Future Directions of RNAi-Based Therapeutics. *Nature Reviews Drug Discovery*, Springer US, **18**, 421–446.

<https://doi.org/10.1038/s41573-019-0017-4>.

- 91 Vigneswara, V. and Ahmed, Z. (2016) Long-Term Neuroprotection of Retinal Ganglion Cells by Inhibiting Caspase-2. *Cell Death Discovery*, **2**, 16044. <https://doi.org/10.1038/cddiscovery.2016.44>.
- 92 Demirjian, S., Ailawadi, G., Polinsky, M., Bitran, D., Silberman, S., Shernan, S.K., Burnier, M., Hamilton, M., Squiers, E., Erlich, S., Rothenstein, D., Khan, S. and Chawla, L.S. (2017) Safety and Tolerability Study of an Intravenously Administered Small Interfering Ribonucleic Acid (SiRNA) Post On-Pump Cardiothoracic Surgery in Patients at Risk of Acute Kidney Injury. *Kidney International Reports*, Elsevier Inc, **2**, 836–843. <https://doi.org/10.1016/j.ekir.2017.03.016>.
- 93 Lee, T.J., Yoo, J.Y., Shu, D., Li, H., Zhang, J., Yu, J.G., Jaime-Ramirez, A.C., Acunzo, M., Romano, G., Cui, R., Sun, H.L., Luo, Z., Old, M., Kaur, B., Guo, P. and Croce, C.M. (2017) RNA Nanoparticle-Based Targeted Therapy for Glioblastoma through Inhibition of Oncogenic MiR-21. *Molecular Therapy*, Elsevier Ltd., **25**, 1544–1555. <https://doi.org/10.1016/j.ymthe.2016.11.016>.
- 94 Nair, J.K., Attarwala, H., Sehgal, A., Wang, Q., Aluri, K., Zhang, X., Gao, M., Liu, J., Indrakanti, R., Schofield, S., Kretschmer, P., Brown, C.R., Gupta, S., Willoughby, J.L.S., Boshar, J.A., Jadhav, V., Charisse, K., Zimmermann, T., Fitzgerald, K., Manoharan, M., Rajeev, K.G., Akinc, A., Hutabarat, R. and Maier, M.A. (2017) Impact of Enhanced Metabolic Stability on Pharmacokinetics and Pharmacodynamics of GalNAc-SiRNA Conjugates. *Nucleic Acids Research*, Oxford University Press, **45**, 10969–10977. <https://doi.org/10.1093/nar/gkx818>.
- 95 McLennan, D.N., Porter, C.J.H. and Charman, S.A. (2005) Subcutaneous Drug Delivery and the Role of the Lymphatics. *Drug Discovery Today: Technologies*, **2**, 89–96. <https://doi.org/10.1016/j.ddtec.2005.05.006>.
- 96 Wittrup, A., Ai, A., Liu, X., Hamar, P., Trifonova, R., Charisse, K., Manoharan, M., Kirchhausen, T. and Lieberman, J. (2015) Visualizing Lipid-Formulated SiRNA Release from Endosomes and Target Gene Knockdown. *Nature Biotechnology*, Nature Publishing Group, **33**, 870–876. <https://doi.org/10.1038/nbt.3298>.
- 97 Rozema, D.B., Lewis, D.L., Wakefield, D.H., Wong, S.C., Klein, J.J., Roesch, P.L., Bertin, S.L., Reppen, T.W., Chu, Q., Blokhin, A. V, Hagstrom, J.E. and Wolff, J. a. (2007) Dynamic PolyConjugates for Targeted in Vivo Delivery of SiRNA to Hepatocytes. *Proceedings of the National Academy of Sciences*, **104**, 12982–12987. <https://doi.org/10.1073/pnas.0703778104>.
- 98 Michael Lord, J. and Roberts, L.M. (2002) Toxin Entry: Retrograde Transport through the Secretory Pathway. *The Journal of Cell Biology*, **140**, 733–736. <https://doi.org/10.1083/jcb.140.4.733>.
- 99 Noland, C.L., Ma, E. and Doudna, J.A. (2011) SiRNA Repositioning for Guide Strand Selection by Human Dicer Complexes. *Molecular Cell*, Elsevier Inc., **43**, 110–121.

<https://doi.org/10.1016/j.molcel.2011.05.028>.

- 100 Whitehead, K.A., Dahlman, J.E., Langer, R.S. and Anderson, D.G. (2011) Silencing or Stimulation? SiRNA Delivery and the Immune System. *Annual Review of Chemical and Biomolecular Engineering*, **2**, 77–96. <https://doi.org/10.1146/annurev-chembioeng-061010-114133>.
- 101 Layzer, J.M., McCaffrey, A.P., Tanner, A.K., Huang, Z., Kay, M.A. and Sullenger, B.A. (2004) In Vivo Activity of Nuclease-Resistant SiRNAs. *RNA (New York, N.Y.)*, **10**, 766–771. <https://doi.org/10.1261/rna.5239604>.
- 102 Huang, Y., Hong, J., Zheng, S., Ding, Y., Guo, S., Zhang, H., Zhang, X., Du, Q. and Liang, Z. (2011) Elimination Pathways of Systemically Delivered SiRNA. *Molecular therapy : the journal of the American Society of Gene Therapy*, Nature Publishing Group, **19**, 381–385. <https://doi.org/10.1038/mt.2010.266>.
- 103 Kanasty, R., Dorkin, J.R., Vegas, A. and Anderson, D. (2013) Delivery Materials for SiRNA Therapeutics. *Nature Materials*, Nature Publishing Group, **12**, 967–977. <https://doi.org/10.1038/nmat3765>.
- 104 Moros, M., Hernáez, B., Garet, E., Dias, J.T., Sáez, B., Grazú, V., González-Fernández, Á., Alonso, C. and de la Fuente, J.M. (2012) Monosaccharides versus PEG-Functionalized NPs: Influence in the Cellular Uptake. *ACS Nano*, **6**, 1565–1577. <https://doi.org/10.1021/nn204543c>.
- 105 Gosnell, H., Kasman, L.M., Potta, T., Vu, L., Garrett-Mayer, E., Rege, K. and Voelkel-Johnson, C. (2014) Polymer-Enhanced Delivery Increases Adenoviral Gene Expression in an Orthotopic Model of Bladder Cancer. *Journal of Controlled Release*, Elsevier B.V., **176**, 35–43. <https://doi.org/10.1016/j.jconrel.2013.12.012>.
- 106 Barros, S.A. and Gollob, J.A. (2012) Safety Profile of RNAi Nanomedicines. *Advanced Drug Delivery Reviews*, **64**, 1730–1737. <https://doi.org/10.1016/j.addr.2012.06.007>.
- 107 Zhang, H., Ma, Y. and Sun, X.-L. (2009) Recent Developments in Carbohydrate-Decorated Targeted Drug/Gene Delivery. *Medicinal Research Reviews*, **30**. <https://doi.org/10.1002/med.20171>.
- 108 Prijic, S. and Sersa, G. (2011) Magnetic Nanoparticles as Targeted Delivery Systems in Oncology. *Radiology and Oncology*, **45**, 1–16. <https://doi.org/10.2478/v10019-011-0001-z>.
- 109 Kim, J.S., Oh, M.H., Park, J.Y., Park, T.G. and Nam, Y.S. (2013) Protein-Resistant, Reductively Dissociable Polyplexes for in Vivo Systemic Delivery and Tumor-Targeting of SiRNA. *Biomaterials*, Elsevier Ltd, **34**, 2370–2379. <https://doi.org/10.1016/j.biomaterials.2012.12.004>.
- 110 Passirani, C., Barratt, G., Devissaguet, J.P. and Labarre, D. (1998) Interactions of Nanoparticles Bearing Heparin or Dextran Covalently Bound to Poly(Methyl

- Methacrylate) with the Complement System. *Life Sciences*, **62**, 775–785.
[https://doi.org/10.1016/S0024-3205\(97\)01175-2](https://doi.org/10.1016/S0024-3205(97)01175-2).
- 111 Rouzes, C., Gref, R., Leonard, M., De Sousa Delgado, a. and Dellacherie, E. (2000) Surface Modification of Poly(Lactic Acid) Nanospheres Using Hydrophobically Modified Dextrans as Stabilizers in an o/w Emulsion/Evaporation Technique. *Journal of Biomedical Materials Research*, **50**, 557–565. [https://doi.org/10.1002/\(SICI\)1097-4636\(20000615\)50:4<557::AID-JBM11>3.0.CO;2-R](https://doi.org/10.1002/(SICI)1097-4636(20000615)50:4<557::AID-JBM11>3.0.CO;2-R).
- 112 Coombes, A.G.A., Tasker, S., Lindblad, M., Holmgren, J., Hoste, K., Toncheva, V., Schacht, E., Davies, M.C., Illum, L. and Davis, S.S. (1997) Biodegradable Polymeric Microparticles for Drug Delivery and Vaccine Formulation: The Surface Attachment of Hydrophilic Species Using the Concept of Poly(Ethylene Glycol) Anchoring Segments. *Biomaterials*, **18**, 1153–1161. [https://doi.org/10.1016/S0142-9612\(97\)00051-3](https://doi.org/10.1016/S0142-9612(97)00051-3).
- 113 Letourneur, D., Parisel, C., Prigent-Richard, S. and Cansell, M. (2000) Interactions of Functionalized Dextran-Coated Liposomes with Vascular Smooth Muscle Cells. *Journal of Controlled Release*, **65**, 83–91. [https://doi.org/10.1016/S0168-3659\(99\)00240-0](https://doi.org/10.1016/S0168-3659(99)00240-0).
- 114 Cansell, M., Parisel, C., Jozefonvicz, J. and Letourneur, D. (1999) Liposomes Coated with Chemically Modified Dextran Interact with Human Endothelial Cells. *Journal of Biomedical Materials Research*, **44**, 140–148. [https://doi.org/10.1002/\(SICI\)1097-4636\(199902\)44:2<140::AID-JBM3>3.0.CO;2-5](https://doi.org/10.1002/(SICI)1097-4636(199902)44:2<140::AID-JBM3>3.0.CO;2-5).
- 115 Enochs, W.S., Harsh, G., Hochberg, F. and Weissleder, R. (1999) Improved Delineation of Human Brain Tumors on MR Images Using a Long-Circulating, Superparamagnetic Iron Oxide Agent. *Journal of Magnetic Resonance Imaging*, **9**, 228–232. [https://doi.org/10.1002/\(SICI\)1522-2586\(199902\)9:2<228::AID-JMRI12>3.0.CO;2-K](https://doi.org/10.1002/(SICI)1522-2586(199902)9:2<228::AID-JMRI12>3.0.CO;2-K).
- 116 Ma, D. (2014) Enhancing Endosomal Escape for Nanoparticle Mediated SiRNA Delivery. *Nanoscale*, **6**, 6415. <https://doi.org/10.1039/c4nr00018h>.
- 117 Lu, J.J., Langer, R. and Chen, J. (2009) A Novel Mechanism Is Involved in Cationic Lipid-Mediated Functional SiRNA Delivery. *Molecular Pharmaceutics*, **6**, 763–771. <https://doi.org/10.1021/mp900023v>.
- 118 Vieira, O., Botelho, R. and Grinstein, S. (2002) Phagosome Maturation: Aging Gracefully. *Biochemical Journal*, **366**, 689–704. <https://doi.org/10.1042/BJ20020691>.
- 119 Rettig, G.R. and Behlke, M.A. (2012) Progress Toward In Vivo Use of SiRNAs-II. *Molecular Therapy*, Nature Publishing Group, **20**, 483–512. <https://doi.org/10.1038/mt.2011.263>.
- 120 Nguyen, J. and Szoka, F.C. (2012) Nucleic Acid Delivery: The Missing Pieces of the Puzzle? *Accounts of Chemical Research*, **45**, 1153–1162. <https://doi.org/10.1021/ar3000162>.
- 121 Nechaev, S., Gao, C., Moreira, D., Swiderski, P., Jozwiak, A., Kowolik, C.M., Zhou, J.,

- Armstrong, B., Raubitschek, A., Rossi, J.J. and Kortylewski, M. (2013) Intracellular Processing of Immunostimulatory CpG–SiRNA: Toll-like Receptor 9 Facilitates SiRNA Dicing and Endosomal Escape. *Journal of Controlled Release*, Elsevier B.V., **170**, 307–315. <https://doi.org/10.1016/j.jconrel.2013.06.007>.
- 122 Vivero-Escoto, J.L., Slowing, I.I., Trewyn, B.G. and Lin, V.S.-Y. (2010) Mesoporous Silica Nanoparticles for Intracellular Controlled Drug Delivery. *Small*, **6**, 1952–1967. <https://doi.org/10.1002/sml.200901789>.
- 123 Herd, H., Daum, N., Jones, A.T., Huwer, H., Ghandehari, H. and Lehr, C.M. (2013) Nanoparticle Geometry and Surface Orientation Influence Mode of Cellular Uptake. *ACS Nano*, **7**, 1961–1973. <https://doi.org/10.1021/nn304439f>.
- 124 Akinc, A., Zumbuehl, A., Goldberg, M., Leshchiner, E.S., Busini, V., Hossain, N., Bacallado, S.A., Nguyen, D.N., Fuller, J., Alvarez, R., Borodovsky, A., Borland, T., Constien, R., de Fougères, A., Dorkin, J.R., Narayanannair Jayaprakash, K., Jayaraman, M., John, M., Kotliansky, V., Manoharan, M., Nechev, L., Qin, J., Racie, T., Raitcheva, D., Rajeev, K.G., Sah, D.W.Y., Soutschek, J., Toudjarska, I., Vornlocher, H.-P., Zimmermann, T.S., Langer, R. and Anderson, D.G. (2008) A Combinatorial Library of Lipid-like Materials for Delivery of RNAi Therapeutics. *Nature biotechnology*, **26**, 561–569. <https://doi.org/10.1038/nbt1402>.
- 125 Soutschek, J., Akinc, A., Bramlage, B., Charisse, K., Constien, R., Donoghue, M., Elbashir, S., Geick, A., Hadwiger, P., Harborth, J., John, M., Kesavan, V., Lavine, G., Pandey, R.K., Racie, T., Rajeev, K.G., Röhl, I., Toudjarska, I., Wang, G., Wuschko, S., Bumcrot, D., Kotliansky, V., Limmer, S., Manoharan, M. and Vornlocher, H.-P. (2004) Therapeutic Silencing of an Endogenous Gene by Systemic Administration of Modified SiRNAs. *Nature*, **432**, 173–178. <https://doi.org/10.1038/nature03121>.
- 126 Ulvila, J., Parikka, M., Kleino, A., Sormunen, R., Ezekowitz, R.A., Kocks, C. and Ramet, M. (2006) Double-Stranded RNA Is Internalized by Scavenger Receptor-Mediated Endocytosis in *Drosophila* S2 Cells. *Journal of Biological Chemistry*, **281**, 14370–14375. <https://doi.org/10.1074/jbc.M513868200>.
- 127 Inoue, Y., Kurihara, R., Tsuchida, A., Hasegawa, M., Nagashima, T., Mori, T., Niidome, T., Katayama, Y. and Okitsu, O. (2008) Efficient Delivery of SiRNA Using Dendritic Poly(l-Lysine) for Loss-of-Function Analysis. *Journal of Controlled Release*, **126**, 59–66. <https://doi.org/10.1016/j.jconrel.2007.10.022>.
- 128 Breunig, M., Hozsa, C., Lungwitz, U., Watanabe, K., Umeda, I., Kato, H. and Goepferich, A. (2008) Mechanistic Investigation of Poly(Ethylene Imine)-Based SiRNA Delivery: Disulfide Bonds Boost Intracellular Release of the Cargo. *Journal of Controlled Release*, **130**, 57–63. <https://doi.org/10.1016/j.jconrel.2008.05.016>.
- 129 McNaughton, B.R., Cronican, J.J., Thompson, D.B. and Liu, D.R. (2009) Mammalian Cell Penetration, SiRNA Transfection, and DNA Transfection by Supercharged Proteins. *Proceedings of the National Academy of Sciences of the United States of America*, **106**, 6111–6116. <https://doi.org/10.1073/pnas.0807883106>.

- 130 Engels, J.W. (2013) Gene Silencing by Chemically Modified SiRNAs. *New Biotechnology*, Elsevier B.V., **30**, 302–307. <https://doi.org/10.1016/j.nbt.2012.07.002>.
- 131 Stephen, S.L., Freestone, K., Dunn, S., Twigg, M.W., Homer-Vanniasinkam, S., Walker, J.H., Wheatcroft, S.B. and Ponnambalam, S. (2010) Scavenger Receptors and Their Potential as Therapeutic Targets in the Treatment of Cardiovascular Disease. *International journal of hypertension*, **2010**, 646929. <https://doi.org/10.4061/2010/646929>.
- 132 Jones, N.L. and Willingham, M.C. (1999) Modified LDLs Are Internalized by Macrophages in Part via Macropinocytosis. *The Anatomical Record*, **255**, 57–68. [https://doi.org/10.1002/\(SICI\)1097-0185\(19990501\)255:1<57::AID-AR7>3.0.CO;2-Z](https://doi.org/10.1002/(SICI)1097-0185(19990501)255:1<57::AID-AR7>3.0.CO;2-Z).
- 133 Canton, J., Neculai, D. and Grinstein, S. (2013) Scavenger Receptors in Homeostasis and Immunity. *Nature reviews. Immunology*, Nature Publishing Group, **13**, 621–34. <https://doi.org/10.1038/nri3515>.
- 134 Murshid, A., Gong, J., Prince, T., Borges, T.J. and Calderwood, S.K. (2015) Scavenger Receptor SREC-I Mediated Entry of TLR4 into Lipid Microdomains and Triggered Inflammatory Cytokine Release in RAW 264.7 Cells upon LPS Activation. Kim, C.H., Ed., *PLOS ONE*, **10**, e0122529. <https://doi.org/10.1371/journal.pone.0122529>.
- 135 Miller, D.K. (1983) Cell Killing by Lysosomotropic Detergents. *The Journal of Cell Biology*, **97**, 1841–1851. <https://doi.org/10.1083/jcb.97.6.1841>.
- 136 Huang, H.W., Chen, F.-Y. and Lee, M.-T. (2004) Molecular Mechanism of Peptide-Induced Pores in Membranes. *Physical Review Letters*, **92**, 198304. <https://doi.org/10.1103/PhysRevLett.92.198304>.
- 137 Chendrimada, T.P., Finn, K.J., Ji, X., Baillat, D., Gregory, R.I., Liebhaber, S.A., Pasquinelli, A.E. and Shiekhattar, R. (2007) MicroRNA Silencing through RISC Recruitment of EIF6. *Nature*, **447**, 823–828. <https://doi.org/10.1038/nature05841>.
- 138 Vocelle, D., Chan, C. and Walton, S.P. (2019) Endocytosis Controls Small Interfering RNA Efficiency: Implications for Small Interfering RNA Delivery Vehicle Design and Cell-Specific Targeting. *Nucleic Acid Therapeutics*, **00**, nat.2019.0804. <https://doi.org/10.1089/nat.2019.0804>.
- 139 Sandvig, K., Pust, S., Skotland, T. and van Deurs, B. (2011) Clathrin-Independent Endocytosis: Mechanisms and Function. *Current Opinion in Cell Biology*, Elsevier Ltd, **23**, 413–420. <https://doi.org/10.1016/j.ceb.2011.03.007>.
- 140 El-Sayed, A. and Harashima, H. (2013) Endocytosis of Gene Delivery Vectors: From Clathrin-Dependent to Lipid Raft-Mediated Endocytosis. *Molecular Therapy*, **21**, 1118–1130. <https://doi.org/10.1038/mt.2013.54>.
- 141 Smart, E.J. and Anderson, R.G.W. (2002) Alterations in Membrane Cholesterol That Affect Structure and Function of Caveolae. *Methods in Enzymology*, 131–139. [https://doi.org/10.1016/S0076-6879\(02\)53043-3](https://doi.org/10.1016/S0076-6879(02)53043-3).

- 142 Cooper, J.A. (1987) Effects of Cytochalasin and Phalloidin on Actin. *The Journal of Cell Biology*, **105**, 1473–1478. <https://doi.org/10.1083/jcb.105.4.1473>.
- 143 Langhorst, M.F., Solis, G.P., Hannbeck, S., Plattner, H. and Stuermer, C.A.O. (2007) Linking Membrane Microdomains to the Cytoskeleton: Regulation of the Lateral Mobility of Reggie-1/Flotillin-2 by Interaction with Actin. *FEBS Letters*, **581**, 4697–4703. <https://doi.org/10.1016/j.febslet.2007.08.074>.
- 144 Solis, G.P., Hülsbusch, N., Radon, Y., Katanaev, V.L., Plattner, H. and Stuermer, C.A.O. (2013) Reggies/Flotillins Interact with Rab11a and SNX4 at the Tubulovesicular Recycling Compartment and Function in Transferrin Receptor and E-Cadherin Trafficking. Gruenberg, J.E., Ed., *Molecular Biology of the Cell*, **24**, 2689–2702. <https://doi.org/10.1091/mbc.e12-12-0854>.
- 145 Macia, E., Ehrlich, M., Massol, R., Boucrot, E., Brunner, C. and Kirchhausen, T. (2006) Dynasore, a Cell-Permeable Inhibitor of Dynamin. *Developmental Cell*, **10**, 839–850. <https://doi.org/10.1016/j.devcel.2006.04.002>.
- 146 Sandvig, K., Torgersen, M.L., Raa, H.A. and Deurs, B. (2008) Clathrin-Independent Endocytosis: From Nonexisting to an Extreme Degree of Complexity. *Histochemistry and Cell Biology*, **129**, 267–276. <https://doi.org/10.1007/s00418-007-0376-5>.
- 147 Kleyman, T.R. and Cragoe, E.J. (1988) Amiloride and Its Analogs as Tools in the Study of Ion Transport. *The Journal of Membrane Biology*, **105**, 1–21. <https://doi.org/10.1007/BF01871102>.
- 148 Yao, D., Ehrlich, M., Henis, Y.I. and Leof, E.B. (2002) Transforming Growth Factor- β Receptors Interact with AP2 by Direct Binding to B2 Subunit. Heldin, C.-H., Ed., *Molecular Biology of the Cell*, **13**, 4001–4012. <https://doi.org/10.1091/mbc.02-07-0104>.
- 149 Portis, A.M., Carballo, G., Baker, G.L., Chan, C. and Walton, S.P. (2010) Confocal Microscopy for the Analysis of SiRNA Delivery by Polymeric Nanoparticles. *Microscopy Research and Technique*, **73**, 878–885. <https://doi.org/10.1002/jemt.20861>.
- 150 Dalby, B., Cates, S., Harris, A., Ohki, E.C., Tilkins, M.L., Price, P.J. and Ciccarone, V.C. (2004) Advanced Transfection with Lipofectamine 2000 Reagent: Primary Neurons, SiRNA, and High-Throughput Applications. *Methods*, **33**, 95–103. <https://doi.org/10.1016/j.ymeth.2003.11.023>.
- 151 Cui, S., Zhang, S., Chen, H., Wang, B., Zhao, Y. and Zhi, D. (2012) The Mechanism of Lipofectamine 2000 Mediated Transmembrane Gene Delivery. *Engineering*, **04**, 172–175. <https://doi.org/10.4236/eng.2012.410B045>.
- 152 Lazebnik, M., Keswani, R.K. and Pack, D.W. (2016) Endocytic Transport of Polyplex and Lipoplex SiRNA Vectors in HeLa Cells. *Pharmaceutical Research*, Pharmaceutical Research, **33**, 2999–3011. <https://doi.org/10.1007/s11095-016-2022-1>.
- 153 Pichon, C., Billiet, L. and Midoux, P. (2010) Chemical Vectors for Gene Delivery: Uptake

- and Intracellular Trafficking. *Current Opinion in Biotechnology*, Elsevier Ltd, **21**, 640–645. <https://doi.org/10.1016/j.copbio.2010.07.003>.
- 154 Billiet, L., Gomez, J.P., Berchel, M., Jaffrès, P.A., Le Gall, T., Montier, T., Bertrand, E., Cheradame, H., Guégan, P., Mével, M., Pitard, B., Benvegna, T., Lehn, P., Pichon, C. and Midoux, P. (2012) Gene Transfer by Chemical Vectors, and Endocytosis Routes of Polyplexes, Lipoplexes and Lipopolyplexes in a Myoblast Cell Line. *Biomaterials*, Elsevier Ltd, **33**, 2980–2990. <https://doi.org/10.1016/j.biomaterials.2011.12.027>.
- 155 Ming, X., Sato, K. and Juliano, R.L. (2011) Unconventional Internalization Mechanisms Underlying Functional Delivery of Antisense Oligonucleotides via Cationic Lipoplexes and Polyplexes. *Journal of Controlled Release*, Elsevier B.V., **153**, 83–92. <https://doi.org/10.1016/j.jconrel.2011.04.029>.
- 156 Vercauteren, D., Vandenbroucke, R.E., Jones, A.T., Rejman, J., Demeester, J., De Smedt, S.C., Sanders, N.N. and Braeckmans, K. (2010) The Use of Inhibitors to Study Endocytic Pathways of Gene Carriers: Optimization and Pitfalls. *Molecular Therapy*, Nature Publishing Group, **18**, 561–569. <https://doi.org/10.1038/mt.2009.281>.
- 157 Ivanov, A.I. (2008) Exocytosis and Endocytosis. Ivanov, A.I., Ed., *Methods in Molecular Biology*, Humana Press, Totowa, NJ, **440**, 15–33. <https://doi.org/10.1007/978-1-59745-178-9>.
- 158 Rodal, S.K., Skretting, G., Garred, Ø., Vilhardt, F., van Deurs, B. and Sandvig, K. (1999) Extraction of Cholesterol with Methyl- β -Cyclodextrin Perturbs Formation of Clathrin-Coated Endocytic Vesicles. Krieger, M., Ed., *Molecular Biology of the Cell*, **10**, 961–974. <https://doi.org/10.1091/mbc.10.4.961>.
- 159 Elkin, S.R., Bendris, N., Reis, C.R., Zhou, Y., Xie, Y., Huffman, K.E., Minna, J.D. and Schmid, S.L. (2015) A Systematic Analysis Reveals Heterogeneous Changes in the Endocytic Activities of Cancer Cells. *Cancer Research*, **75**, 4640–4650. <https://doi.org/10.1158/0008-5472.CAN-15-0939>.
- 160 Saslowsky, D.E., Cho, J.A., Chinnapen, H., Massol, R.H., Chinnapen, D.J.F., Wagner, J.S., De Luca, H.E., Kam, W., Paw, B.H. and Lencer, W.I. (2010) Intoxication of Zebrafish and Mammalian Cells by Cholera Toxin Depends on the Flotillin/Reggie Proteins but Not Derlin-1 or -2. *Journal of Clinical Investigation*, **120**, 4399–4409. <https://doi.org/10.1172/JCI42958>.
- 161 Howes, M.T., Kirkham, M., Riches, J., Cortese, K., Walser, P.J., Simpson, F., Hill, M.M., Jones, A., Lundmark, R., Lindsay, M.R., Hernandez-Deviez, D.J., Hadzic, G., McCluskey, A., Bashir, R., Liu, L., Pilch, P., McMahon, H., Robinson, P.J., Hancock, J.F., Mayor, S. and Parton, R.G. (2010) Clathrin-Independent Carriers Form a High Capacity Endocytic Sorting System at the Leading Edge of Migrating Cells. *The Journal of Cell Biology*, **190**, 675–691. <https://doi.org/10.1083/jcb.201002119>.
- 162 dos Santos, T., Varela, J., Lynch, I., Salvati, A. and Dawson, K.A. (2011) Effects of Transport Inhibitors on the Cellular Uptake of Carboxylated Polystyrene Nanoparticles in

- Different Cell Lines. Schnur, J.M., Ed., *PLoS ONE*, **6**, e24438.
<https://doi.org/10.1371/journal.pone.0024438>.
- 163 Guo, Z., Li, S., Wang, C., Xu, J., Kirk, B., Wu, J., Liu, Z. and Xue, W. (2017) Biocompatibility and Cellular Uptake Mechanisms of Poly(N -Isopropylacrylamide) in Different Cells. *Journal of Bioactive and Compatible Polymers*, **32**, 17–31.
<https://doi.org/10.1177/0883911516648969>.
- 164 Al Soraj, M., He, L., Peynshaert, K., Cousaert, J., Vercauteren, D., Braeckmans, K., De Smedt, S.C. and Jones, A.T. (2012) SiRNA and Pharmacological Inhibition of Endocytic Pathways to Characterize the Differential Role of Macropinocytosis and the Actin Cytoskeleton on Cellular Uptake of Dextran and Cationic Cell Penetrating Peptides Octaarginine (R8) and HIV-Tat. *Journal of Controlled Release*, **161**, 132–141.
<https://doi.org/10.1016/j.jconrel.2012.03.015>.
- 165 Miller, C.M., Tanowitz, M., Donner, A.J., Prakash, T.P., Swayze, E.E., Harris, E.N. and Seth, P.P. (2018) Receptor-Mediated Uptake of Phosphorothioate Antisense Oligonucleotides in Different Cell Types of the Liver. *Nucleic Acid Therapeutics*, **28**, 119–127. <https://doi.org/10.1089/nat.2017.0709>.
- 166 Arkhipova, K.A., Sheyderman, A.N., Laktionov, K.K., Mochalnikova, V. V. and Zborovskaya, I.B. (2014) Simultaneous Expression of Flotillin-1, Flotillin-2, Stomatin and Caveolin-1 in Non-Small Cell Lung Cancer and Soft Tissue Sarcomas. *BMC Cancer*, **14**, 100. <https://doi.org/10.1186/1471-2407-14-100>.
- 167 Lisanti, M.P., Lodish, H.F., Schnitzer, J.E., Oh, P., Scherer, P.E. and Bickel, P.E. (2002) Flotillin and Epidermal Surface Antigen Define a New Family of Caveolae-Associated Integral Membrane Proteins. *Journal of Biological Chemistry*, **272**, 13793–13802.
<https://doi.org/10.1074/jbc.272.21.13793>.
- 168 Donaldson, J.G. (2003) Multiple Roles for Arf6: Sorting, Structuring, and Signaling at the Plasma Membrane. *Journal of Biological Chemistry*, **278**, 41573–41576.
<https://doi.org/10.1074/jbc.R300026200>.
- 169 Watson, P., Jones, A.T. and Stephens, D.J. (2005) Intracellular Trafficking Pathways and Drug Delivery: Fluorescence Imaging of Living and Fixed Cells. *Advanced Drug Delivery Reviews*, **57**, 43–61. <https://doi.org/10.1016/j.addr.2004.05.003>.
- 170 Vermeulen, L.M.P., Brans, T., De Smedt, S.C., Remaut, K. and Braeckmans, K. (2018) Methodologies to Investigate Intracellular Barriers for Nucleic Acid Delivery in Non-Viral Gene Therapy. *Nano Today*, Elsevier Ltd, **21**, 74–90.
<https://doi.org/10.1016/j.nantod.2018.06.007>.
- 171 Peters, J. (2008) Nikon Instruments TiE-PFS Dynamic Focusing System. *Nature Methods / Application Notes*. <https://doi.org/10.1038/an6676>.
- 172 Claxton, N.S., Fellers, T.J. and Davidson, M.W. (2006) Laser Scanning Confocal Microscopy. *Encyclopedia of Medical Devices and Instrumentation*, **1979**, 1–37.

- <https://doi.org/10.1002/0471732877.emd291>.
- 173 Hutagalung, A.H. and Novick, P.J. (2011) Role of Rab GTPases in Membrane Traffic and Cell Physiology. *Physiological Reviews*, **91**, 119–149.
<https://doi.org/10.1152/physrev.00059.2009>.
- 174 Stenmark, H. (2009) Rab GTPases as Coordinators of Vesicle Traffic. *Nature reviews. Molecular cell biology*, Nature Publishing Group, **10**, 513–525.
<https://doi.org/10.1038/nrm2728>.
- 175 Sönnichsen, B., De Renzis, S., Nielsen, E., Rietdorf, J. and Zerial, M. (2000) Distinct Membrane Domains on Endosomes in the Recycling Pathway Visualized by Multicolor Imaging of Rab4, Rab5, and Rab11. *Journal of Cell Biology*, **149**, 901–913.
<https://doi.org/10.1083/jcb.149.4.901>.
- 176 McCaffrey, M.W., Bielli, A., Cantalupo, G., Mora, S., Roberti, V., Santillo, M., Drummond, F. and Bucci, C. (2001) Rab4 Affects Both Recycling and Degradative Endosomal Trafficking. *FEBS Letters*. [https://doi.org/10.1016/S0014-5793\(01\)02359-6](https://doi.org/10.1016/S0014-5793(01)02359-6).
- 177 Hales, C.M., Vaerman, J.P. and Goldenring, J.R. (2002) Rab11 Family Interacting Protein 2 Associates with Myosin Vb and Regulates Plasma Membrane Recycling. *Journal of Biological Chemistry*. <https://doi.org/10.1074/jbc.M209270200>.
- 178 Jordens, I., Fernandez-Borja, M., Marsman, M., Dusseljee, S., Janssen, L., Calafat, J., Janssen, H., Wubbolts, R. and Neefjes, J. (2001) The Rab7 Effector Protein RILP Controls Lysosomal Transport by Inducing the Recruitment of Dynein-Dynactin Motors. *Current Biology*. [https://doi.org/10.1016/S0960-9822\(01\)00531-0](https://doi.org/10.1016/S0960-9822(01)00531-0).
- 179 Rojas, R., Van Vlijmen, T., Mardones, G.A., Prabhu, Y., Rojas, A.L., Mohammed, S., Heck, A.J.R., Raposo, G., Van Der Sluijs, P. and Bonifacino, J.S. (2008) Regulation of Retromer Recruitment to Endosomes by Sequential Action of Rab5 and Rab7. *Journal of Cell Biology*. <https://doi.org/10.1083/jcb.200804048>.
- 180 Eskelinen, E.L. (2006) Roles of LAMP-1 and LAMP-2 in Lysosome Biogenesis and Autophagy. *Molecular Aspects of Medicine*. <https://doi.org/10.1016/j.mam.2006.08.005>.
- 181 Krause, K. and Michalak, M. (1997) Calreticulin Meeting Review. *Cell*, **88**, 439–443.
- 182 Stöber, W., Fink, A. and Bohn, E. (1968) Controlled Growth of Monodisperse Silica Spheres in the Micron Size Range. *Journal of Colloid and Interface Science*, **26**, 62–69.
[https://doi.org/10.1016/0021-9797\(68\)90272-5](https://doi.org/10.1016/0021-9797(68)90272-5).
- 183 Huang, M., Khor, E. and Lim, L.Y. (2004) Uptake and Cytotoxicity of Chitosan Molecules and Nanoparticles: Effects of Molecular Weight and Degree of Deacetylation. *Pharmaceutical Research*, **21**, 344–353.
<https://doi.org/10.1023/B:PHAM.0000016249.52831.a5>.
- 184 Mahmoodi, N.M., Khorramfar, S. and Najafi, F. (2011) Amine-Functionalized Silica

- Nanoparticle: Preparation, Characterization and Anionic Dye Removal Ability. *Desalination*, **279**, 61–68. <https://doi.org/10.1016/j.desal.2011.05.059>.
- 185 Zhang, M., Liu, J., Kuang, Y., Li, Q., Zheng, D.W., Song, Q., Chen, H., Chen, X., Xu, Y., Li, C. and Jiang, B. (2017) Ingenious PH-Sensitive Dextran/Mesoporous Silica Nanoparticles Based Drug Delivery Systems for Controlled Intracellular Drug Release. *International Journal of Biological Macromolecules*, Elsevier B.V., **98**, 691–700. <https://doi.org/10.1016/j.ijbiomac.2017.01.136>.
- 186 Lin, Y.S., Abadeer, N. and Haynes, C.L. (2011) Stability of Small Mesoporous Silica Nanoparticles in Biological Media. *Chemical Communications*. <https://doi.org/10.1039/c0cc02923h>.
- 187 Rasband, W. ImageJ. *U. S. National Institutes of Health, Bethesda, Maryland, USA*, <http://imagej.nih.gov/ij/>.
- 188 Liu, X., Howard, K. a., Dong, M., Andersen, M.Ø., Rahbek, U.L., Johnsen, M.G., Hansen, O.C., Besenbacher, F. and Kjems, J. (2007) The Influence of Polymeric Properties on Chitosan/SiRNA Nanoparticle Formulation and Gene Silencing. *Biomaterials*, **28**, 1280–1288. <https://doi.org/10.1016/j.biomaterials.2006.11.004>.
- 189 Kaufman, W.L., Kocman, I., Agrawal, V., Rahn, H.-P., Besser, D. and Gossen, M. (2008) Homogeneity and Persistence of Transgene Expression by Omitting Antibiotic Selection in Cell Line Isolation. *Nucleic Acids Research*, **36**, e111–e111. <https://doi.org/10.1093/nar/gkn508>.
- 190 Rappoport, J.Z. (2003) Real-Time Analysis of Clathrin-Mediated Endocytosis during Cell Migration. *Journal of Cell Science*, **116**, 847–855. <https://doi.org/10.1242/jcs.00289>.
- 191 Gaidarov, I., Santini, F., Warren, R.A. and Keen, J.H. (1999) Spatial Control of Coated-Pit Dynamics in Living Cells. *Nature Cell Biology*, **1**, 1–7. <https://doi.org/10.1038/8971>.
- 192 Meister, M. and Tikkanen, R. (2014) Endocytic Trafficking of Membrane-Bound Cargo: A Flotillin Point of View. *Membranes*, **4**, 356–371. <https://doi.org/10.3390/membranes4030356>.
- 193 Schindelin, J., Arganda-Carreras, I., Frise, E., Kaynig, V., Longair, M., Pietzsch, T., Preibisch, S., Rueden, C., Saalfeld, S., Schmid, B., Tinevez, J.Y., White, D.J., Hartenstein, V., Eliceiri, K., Tomancak, P. and Cardona, A. (2012) Fiji: An Open-Source Platform for Biological-Image Analysis. *Nature Methods*, **9**, 676–682. <https://doi.org/10.1038/nmeth.2019>.
- 194 Bolte, S. and Cordelières, F.P. (2006) A Guided Tour into Subcellular Colocalization Analysis in Light Microscopy. *Journal of Microscopy*, **224**, 213–232. <https://doi.org/10.1111/j.1365-2818.2006.01706.x>.
- 195 Platt, N., Suzuki, H., Kurihara, Y., Kodama, T. and Gordon, S. (1996) Role for the Class A Macrophage Scavenger Receptor in the Phagocytosis of Apoptotic Thymocytes in

Vitro. *Proceedings of the National Academy of Sciences*, **93**, 12456–12460.
<https://doi.org/10.1073/pnas.93.22.12456>.